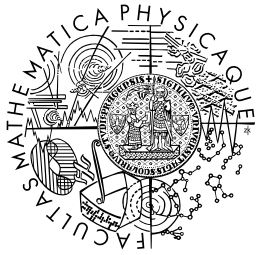

FACULTY
OF MATHEMATICS
AND PHYSICS
Charles University

DOCTORAL THESIS

Kateřina Jarkovská

Quantum aspects of particle physics models with extended gauge symmetries

Institute of Particle and Nuclear Physics

Supervisor of the doctoral thesis: doc. Ing. Michal Malinský, Ph.D.

Study programme: Particle and Nuclear Physics

Study branch: Physics

Prague 2023

I declare that I carried out this doctoral thesis independently, and only with the cited sources, literature and other professional sources. It has not been used to obtain another or the same degree.

I understand that my work relates to the rights and obligations under the Act No. 121/2000 Sb., the Copyright Act, as amended, in particular the fact that the Charles University has the right to conclude a license agreement on the use of this work as a school work pursuant to Section 60 subsection 1 of the Copyright Act.

In Prague, July 11, 2023 .....

Author's signature

I would like to express my gratitude to my supervisor Michal Malinský for his patience, guidance and support. Special thanks also belong to my collaborators Vasja Susič and Timon Mede, without whose help this work would never have been written. I would like to take this opportunity to also acknowledge V. Susič for being the inspiration behind the derivation in the Appendix C.

I am grateful to all my colleagues Martin Krivoš, Ingrid Knapová, Tomáš Kadavý, Hedvika Gedeonová and Matěj Hudec from our institute for being great companions during our concurrent PhD adventures, and to other fellow physicists Lýdia Štofanová, Abhijeet Borkar and Pavel Soldán for expanding my horizons outside particle physics.

Last but not least, I would like to thank my family, who supported me during every step of my life, especially my soon-to-be husband Martin Sýkora who was there for me whenever I needed it and who made my days enjoyable with his humour.

Title: Quantum aspects of particle physics models with extended gauge symmetries

Author: Kateřina Jarkovská

Department: Institute of Particle and Nuclear Physics

Supervisor: doc. Ing. Michal Malinský, Ph.D., Institute of Particle and Nuclear Physics

Abstract: In this thesis, we study quantum aspects of the minimal renormalizable SO(10) Grand Unified Theory with the scalar sector consisting of $\mathbf{45} \oplus \mathbf{126} \oplus \mathbf{10}_{\mathbb{C}}$. It is an interesting candidate for a theory describing physics beyond the Standard model which has the potential to allow for proton lifetime prediction with Plank-scale-physics-induced theoretical uncertainties confined within the expected one-order-of-magnitude experimental proton lifetime improvement window.

With the complete information about the numerical one-loop scalar mass spectrum and analytical one-loop beta functions of all the dimensionless scalar couplings, we formulate consistency criteria that every viable region of the parameter space must satisfy; namely, we require the existence of a stable Standard-model-like vacuum, unification of gauge couplings and robustness of perturbative calculations.

Only narrow parameter space regions around symmetry breaking chains with $\mathrm{SU}(4)_C \times \mathrm{SU}(2)_L \times \mathrm{U}(1)_R$ or $\mathrm{SU}(3)_c \times \mathrm{SU}(2)_L \times \mathrm{SU}(2)_R \times \mathrm{U}(1)_{B-L}$ intermediate stages are demonstrated to be potentially realistic. Detailed analysis of the SO(10) Higgs model with $\mathbf{45} \oplus \mathbf{126}$ scalar sector indicates a preference for the former option, mainly due to increased perturbative instability and phenomenologically unsuitable values of energy scales predicted in the latter symmetry breaking case. Moreover, we calculate partial proton decay rates for two channels $p \to \pi^+ \overline{\nu}$ and $p \to K^+ \overline{\nu}$ with antineutrinos in the final states.

Afterwards the analysis is repeated in case of the full SO(10) Grand Unified Theory with the $\mathbf{45} \oplus \mathbf{126} \oplus \mathbf{10}_{\mathbb{C}}$ scalar sector in the symmetry breaking regime with $\mathrm{SU}(4)_C \times \mathrm{SU}(2)_L \times \mathrm{U}(1)_R$ intermediate stage. The existence of a realistic Yukawa sector is discussed. We identify the inability of the model to successfully accommodate Standard-Model-like low-energy Higgs boson in the perturbatively stable parts of the parameter space. Hence perturbativity criteria turn out to be a powerful tool to constrain viable regimes of the minimal SO(10) Grand Unified Theory.

Keywords: quantum field theory, particle physics, Standard Model, gauge field theory, extended gauge symmetries, grand unification

Contents

Preface

With the advent of the next generation large-volume neutrino experiments [1–4] testing, among other things, stability of the baryonic matter, we expect at least one order of magnitude improvement of the experimental lower bounds on rates of the baryon number violating proton decays. Such experimental advancement is however not followed by the corresponding progress on the theory side; even in the Grand Unified Theories (GUTs), the most popular models predicting baryon number violation, the theoretical uncertainties of proton lifetime predictions usually span over several orders of magnitude [5] and hence do not reach the necessary level of theoretical precision to fully benefit from the experimental progress.

The most problematic theoretical proton lifetime uncertainties originate from the proximity of the unification scale to the Planck scale [6]. The Planck-scale-suppressed non-renormalizable operators can generate corrections to quantities relevant for proton lifetime calculations (gauge matching scale, flavour structure), which are typically not under control. Fortunately, this issue can be satisfactorily addressed in the framework of the minimal renormalizable SO(10) GUT with the **45** scalar representation triggering the SO(10) symmetry breaking and the $\mathbf{126} \oplus \mathbf{10}_{\mathbb{C}}$ accommodating scalars that account for the Yukawa sector, where the most severe Planck-scale induced theoretical uncertainties are not present or they have very reduced influence [7]. This intriguing model in which theoretical proton lifetime uncertainties can be in principle confined within the one-order-of-magnitude experimental window was however discarded in the past due to the presence of notorious tachyonic instabilities in the tree-level scalar mass spectrum that cannot be avoided in potentially realistic breaking patterns [8–10]. Only in 2010 it was recognized [11] that the tree-level vacuum instability is an artefact of the leading order calculations and the theory can be fully consistent at the quantum level when at least one-loop scalar mass corrections are invoked.

The first attempts to study the $\mathbf{45} \oplus \mathbf{126}$ SO(10) Higgs model at one-loop level in the two phenomenologically favoured symmetry breaking regimes with the $\mathrm{SU}(4)_C \times \mathrm{SU}(2)_L \times \mathrm{U}(1)_R$ or $\mathrm{SU}(3)_c \times \mathrm{SU}(2)_L \times \mathrm{SU}(2)_R \times \mathrm{U}(1)_{B-L}$ intermediate stages were accomplished in [12–14] and they demonstrated that once beyond-the-leading-order scalar mass corrections are engaged, a big part of the parameter space opens for non-tachyonic scalar spectrum. In the follow-up of these studies [15], the analytical expressions for the prominent one-loop corrections to all potentially problematic scalar states were calculated.

This thesis provides the ultimate self-consistent study of the minimal renormalizable SO(10) Grand Unified Theory at the quantum level and it is based on the results of papers [16, 17]. We numerically calculate the one-loop mass corrections to the whole scalar sector, including potentially problematic states suffering from the tree-level tachyonicity, and analytically derive a full set of one-loop scalar beta functions of all scalar dimensionless couplings. This allows us to not only address the existence of a stable Standard-model-like vacuum but also assess the perturbative stability of the model by constraining the relative size of one-loop and tree-level mass corrections and by controlling their stability under the change of the renormalization scale. In addition, we study the implications of the requirement of a low-energy Standard-model-like Higgs doublet in the scalar

sector.

The thesis is organised in the following way: in Sec. 1 we review the motivation for considering the minimal SO(10) GUT as an intriguing candidate for a theory beyond the Standard Model and the preceding theoretical development that lead to this conclusion. In Sec. 2 we recapitulate all the important features of the model under consideration with more emphasis put on aspects concerning the proton decay. In Sec. 3 we present the results of the model analysis. First, in Sec. 3.1 we clearly define theoretical and phenomenological constraints that any viable part of the parameter space must satisfy. Then in Sec. 3.2 we provide numerical analysis of the parameter space of the $\mathbf{45} \oplus \mathbf{126}$ SO(10) Higgs model in the two consistent breaking chains with $\mathrm{SU}(4)_C \times \mathrm{SU}(2)_L \times \mathrm{U}(1)_R$ or $\mathrm{SU}(3)_c \times \mathrm{SU}(2)_L \times \mathrm{SU}(2)_R \times \mathrm{U}(1)_{B-L}$ intermediate symmetry stages, where the preference is identified for the former regime. Proton lifetime predictions for dimension $d = 6$ channels with antineutrinos in the final states are determined. In Sec. 3.3 we perform the numerical analysis of the full $\mathbf{45} \oplus \mathbf{126} \oplus \mathbf{10}_{\mathbb{C}}$ SO(10) GUT with the symmetry breaking pattern featuring the $\mathrm{SU}(4)_C \times \mathrm{SU}(2)_L \times \mathrm{U}(1)_R$ intermediate symmetry stage, including discussion of the fine-tuning in the scalar sector to acquire Standard-Model-like Higgs boson. Finally, we conclude in Sec. 4. All the technical details are deferred to set of Appendices.

1. Road to the minimal SO(10) GUT

1.1 Classical era and gauge invariance

The journey to the *gauge symmetries* as model-building tools began in the old days of classical electromagnetism when it was noticed that applying a certain set of local transformations on vector and scalar electromagnetic potentials did not change the measurable quantities (see [18] and references in it). This invariance under local transformations was later called the *principle of gauge symmetry*, and although it was observed already at the turn of the 19th and 20th centuries, the gauge invariance principle was not properly appreciated as a model-building tool back then.

The change came after H. Weyl first used gauge invariance as a guiding principle in his attempts to unify electromagnetism and gravity [19, 20]. Even though his theory did not manage to successfully describe the physical world, he was able to show that the gauge invariance implied the conservation of electric charge. With the advent of quantum mechanics, V. Fock demonstrated that the quantum system of a charged particle interacting with the electromagnetic field is also symmetric with respect to the gauge transformations [21]. Weyl subsequently revisited his previous attempts of using gauge invariance in model building [22], now in the context of electromagnetically interacting quantum system of charged particles, and he significantly contributed to the principle of gauge invariance becoming the foundation stone of modern particle physics.

1.2 Arrival of the Standard Model

Foundations of the quantum electrodynamics (QED) as a theory of electromagnetically interacting systems which employs the assumption of Abelian gauge invariance were laid in the late 1920s by P. Dirac [23] and later fully developed in the 1940s by incorporating the renormalization procedure [24–27]. Quantum electrodynamics turned out to be very successful in predicting the quantum behaviour of charged particles and electromagnetic fields with anomalous electron magnetic moment $g - 2$ measurement remaining the most accurate test of QED validity to date [28]. Later, the principle of non-Abelian gauge invariance was used to unite descriptions of strong, weak and electromagnetic interactions [29–33]. It started the modern era of gauge theories which engaged Lagrangians invariant with respect to non-Abelian gauge groups.

However, there was one riddle that needed to be solved. Weak-interactions-mediating gauge bosons had non-zero masses, but the explicit gauge boson mass term in the Lagrangian was forbidden by gauge invariance [34, 35]. Such a complication was eventually bypassed by employing the so-called *Higgs mechanism* [36–38] in which the field content of the gauge-symmetric theory involves an additional scalar Higgs field whose vacuum expectation value (VEV) does not exhibit

the same gauge invariance.[1] The aforementioned situation when the Lagrangian obeys gauge symmetries which are not manifest in the physical spectrum is referred to as *spontaneous symmetry breaking* (SSB).

Finally, the concepts of renormalizability, gauge invariance and spontaneous symmetry breaking were put together to formulate the Standard Model (SM) of Particle Physics that describes strong, weak and electromagnetic interactions of all known elementary particles. The dynamics of the SM is determined by the underlying $\mathrm{SU}(3)_c \times \mathrm{SU}(2)_L \times \mathrm{U}(1)_Y$ gauge symmetry where the hypercharge obeys $Y = Q - T_L^{(3)}$ with Q standing for an electromagnetic charge and T_L^3 being the 3rd component of weak isospin. The SM field content consists of three generations of spin-$\frac{1}{2}$ fermionic matter fields

$$Q_L \equiv \begin{pmatrix} u_L \\ d_L \end{pmatrix} \sim (3, 2, +\tfrac{1}{6}), \qquad L_L \equiv \begin{pmatrix} \nu_L \\ e_L \end{pmatrix} \sim (1, 2, -\tfrac{1}{2}),$$

$$u_R \sim (\bar{3}, 1, -\tfrac{2}{3}),\ d_R \sim (\bar{3}, 1, +\tfrac{1}{3}), \qquad e_R \sim (1, 1, +1),$$

where L/R marks left-handed/right-handed Weyl spinors, a set of spin-1 bosonic gauge fields

$$G_\mu \sim (8, 1, 0), \qquad A_\mu \sim (1, 3, 0), \qquad B_\mu \sim (1, 2, 0),$$

corresponding to the $\mathrm{SU}(3)_c$, $\mathrm{SU}(2)_L$ and $\mathrm{U}(1)_Y$ gauge factors, respectively, and one spin-0 scalar Higgs field

$$\Phi_H \sim (1, 2, +\tfrac{1}{2}).$$

The Higgs field Φ_H acquires the non-zero VEV $\langle \Phi_H \rangle \equiv v_{SM} \doteq 174\,\mathrm{GeV}$, and consequently triggers spontaneous symmetry breaking of the SM gauge symmetry down to the $\mathrm{SU}(3)_c \times \mathrm{U}(1)_Q$. For every aforementioned field, we indicated its transformation properties with respect to the $\mathrm{SU}(3)_c \times \mathrm{SU}(2)_L \times \mathrm{U}(1)_Y$. Let us emphasise that in such a setting the neutrinos are by construction massless.

1.3 Beyond the Standard Model

Although the Standard Model proved to be an incredibly successful theory describing elementary particle interactions over many orders of magnitude in energy, the observation of neutrino flavour oscillations [41–43] provided definitive demand for massive neutrinos, which necessitated going beyond the SM framework.

1.3.1 Neutrino mass generation

The easiest way how to introduce non-zero neutrino masses is by adding three Weyl spinors playing the role of right-handed neutrinos ν_R (one per generation), in general transforming as $\mathrm{SU}(3)_c$ and $\mathrm{SU}(2)_L$ singlets, and appropriate Yukawa

[1] Although the Higgs mechanism is the canonical tool for generating gauge boson masses, alternative mechanisms can be found in the literature, such as dynamical spontaneous breaking in which the Higgs field is replaced by a composite field [39, 40].

interactions between the SM Higgs and neutrinos, analogously to the charged fermions.

There are, however, issues with such a simplified approach that arise only at the quantum level. Let us recall that the quantization of the hypercharge of the SM fields is enforced by requiring the cancellation of the so-called *chiral anomalies* [44, 45], which ensures that no physical amplitude depends on the selection of gauge. In practice, the chiral anomaly cancellation boils down to the set of algebraic equations [46]

$$\mathrm{Tr}_L\left(\{T^a,T^b\}T^c\right)-\mathrm{Tr}_R\left(\{T^a,T^b\}T^c\right)=0 \tag{1.1}$$

with T^a being the gauge symmetry generators and traces are taken over representations of all left-handed (L) or right-handed (R) Weyl spinors in the theory. In the SM, Eqns. (1.1) lead to the hypercharge quantization [47–50]

$$\frac{Y_{Q_L}}{Y_{\Phi_H}}=+\frac{1}{3},\quad \frac{Y_{L_L}}{Y_{\Phi_H}}=-1,\quad \frac{Y_{u_R}}{Y_{\Phi_H}}=+\frac{4}{3},\quad \frac{Y_{d_R}}{Y_{\Phi_H}}=-\frac{2}{3},\quad \frac{Y_{e_R}}{Y_{\Phi_H}}=-2, \tag{1.2}$$

which is modified by right-handed neutrino to

$$\frac{Y_{Q_L}}{Y_{\Phi_H}}=+\frac{1}{3}\left(1-\frac{Y_{\nu_R}}{Y_{\Phi_H}}\right),\qquad \frac{Y_{L_L}}{Y_{\Phi_H}}=-1\left(1-\frac{Y_{\nu_R}}{Y_{\Phi_H}}\right), \tag{1.3}$$

$$\frac{Y_{u_R}}{Y_{\Phi_H}}=+\frac{4}{3}\left(1-\frac{Y_{\nu_R}}{4Y_{\Phi_H}}\right),\qquad \frac{Y_{d_R}}{Y_{\Phi_H}}=-\frac{2}{3}\left(1+\frac{Y_{\nu_R}}{2Y_{\Phi_H}}\right), \tag{1.4}$$

$$\frac{Y_{e_R}}{Y_{\Phi_H}}=-2\left(1+\frac{Y_{\nu_R}}{2Y_{\Phi_H}}\right). \tag{1.5}$$

Since the ratio Y_{ν_R}/Y_{Φ_H} is not restricted by anomaly cancellation, there is no a priori reason for the hypercharge to be quantized and the Standard Model with right-handed neutrinos loses part of its predictive power.

Hypercharge quantization can be reestablished by requiring the three copies of the right-handed neutrinos to be Majorana and, thus, transforming as full SM singlets, i.e.

$$\nu_R\sim(1,1,0).$$

In such a case, $Y_{\nu_R}=0$ and the hypercharge relations of Eq. (1.2) get reinstated. Neutrino masses are then extracted from the relevant part of the Lagrangian

$$\mathcal{L}_{\nu_R}=-Y_\nu\overline{L_L}\nu_R\Phi_H-\frac{1}{2}M_\nu^M\nu_R^TC\nu_R+h.c., \tag{1.6}$$

where M_ν^M is the Majorana mass matrix and the Dirac mass contribution is defined as $M_\nu^D=Y_\nu v_{SM}$. In the broken phase,

$$\mathcal{L}_{\nu_R}=-\frac{1}{2}n_L^TC\mathcal{M}_\nu n_L+h.c+\cdots. \tag{1.7}$$

with $n_L^T=(\nu_L,\nu_R^c)$ and 6×6 neutrino mass matrix

$$\mathcal{M}_\nu=\begin{pmatrix}0 & M_\nu^D\\ M_\nu^D & M_\nu^M\end{pmatrix}. \tag{1.8}$$

In the case of $|M_\nu^D| \ll |M_\nu^M|$, diagonalization of $\mathcal{M}_\nu$ yields the light neutrino mass matrix

$$m_\nu \approx -M_\nu^D \left(M_\nu^M\right)^{-1} M_\nu^{D\,T} \tag{1.9}$$

and the heavy neutrino mass matrix

$$M_\nu \approx M_\nu^M \tag{1.10}$$

with the corresponding mass eigenstates dominated by the ν_L and the ν_R components, respectively. Note that the above-described mechanism of generating the light neutrino masses by invoking inverse proportionality of m_ν to the Majorana mass term M_ν^M is commonly called "type-I seesaw" [51–54]. Numerically, if no suppression is imposed upon Yukawa couplings, i.e. $Y_\nu \sim \mathcal{O}(1)$, and $m_\nu \lesssim 1\,\text{eV}$, the Majorana mass term is expected to be in the energy range of

$$M_\nu^M \sim 10^{12-13}\,\text{GeV}. \tag{1.11}$$

1.3.2 Models with extended gauge symmetry

Neutrino mass generation via type-I seesaw introduces Majorana mass M_ν^M in the energy range (1.11) far beyond any typical mass scale of the SM fields, thus hinting at the existence of a new dynamics governing quantum field interactions at energies $\gtrsim 10^{12}\,\text{GeV}$. Such a physics at high energy scales can be naturally realized by considering gauge symmetry extensions of the SM whose underlying gauge groups spontaneously break down to the $\text{SU}(3)_c \times \text{SU}(2)_L \times \text{U}(1)_Y$ at energies much larger than v_{SM}.

Left-right symmetric model

The Standard Model with three right-handed Majorana neutrinos provides two hints that can guide us in selecting promising gauge symmetry extensions of the SM.

- The presence of the right-handed neutrinos restores "left-right" symmetry in the fermionic spectrum. Therefore one can introduce the "right-handed" weak isospin charge $T_R^{(3)}$ that takes on $\pm\frac{1}{2}$ values only for u_R, d_R and ν_R, e_R, c.f. Table 1.1, analogously to the weak isospin charge which acquires the $T_L^{(3)} = \pm\frac{1}{2}$ solely for the components of the $\text{SU}(2)_L$ doublet, and therefore acts non-trivially only on the left-handed Weyl spinors. Pairs of right-handed spinors $(u_R\ d_R)^T$, $(\nu_R\ e_R)^T$ would possess $T_R^{(3)}$ charges as if they were doublets with respect to an $\text{SU}(2)_R$ underlying gauge symmetry, which acts non-trivially solely on the right-handed fermionic fields.

- Baryon $\mathcal{B}$ and lepton $\mathcal{L}$ numbers[2] are charges corresponding to accidental global symmetries of the SM. The value of their difference $\mathcal{B} - \mathcal{L}$ can be assigned for all fields by introducing $(B-L)$ charge [55–58] defined as $(B-$

[2]Non-zero baryon numbers are assigned only to quarks and antiquarks which carry $\mathcal{B} = +\frac{1}{3}$ and $\mathcal{B} = -\frac{1}{3}$, respectively. Analogously, the non-vanishing lepton number is attributed only to leptons and antileptons which have $\mathcal{L} = +1$ and $\mathcal{L} = -1$, respectively.

$L) = 2(Y - T_R^{(3)})$, which satisfies relation $(B-L)_f = (\mathcal{B}-\mathcal{L})_f$ for fermionic fields, c.f. Table 1.1. Corresponding $U(1)_{B-L}$ symmetry can be promoted to the local symmetry in the case of the SM with three Dirac neutrinos. In the Majorana case, $U(1)_{B-L}$ is explicitly broken by the Majorana mass term (1.6) in the Lagrangian.

We can thus consider enlarging the underlying gauge symmetry of the SM to the

$$\mathrm{SU}(3)_c \times \mathrm{SU}(2)_L \times \mathrm{SU}(2)_R \times \mathrm{U}(1)_{B-L}$$

to restore the "left-right" symmetry [53, 59, 60]. Consequently, the electromagnetic charge can be expressed in the "left-right" symmetric form

$$Q = T_L^{(3)} + T_R^{(3)} + \frac{1}{2}(B-L). \tag{1.12}$$

The spontaneous symmetry breaking of the $\mathrm{SU}(3)_c \times \mathrm{SU}(2)_L \times \mathrm{SU}(2)_R \times \mathrm{U}(1)_{B-L}$ down to the $\mathrm{SU}(3)_c \times \mathrm{SU}(2)_L \times \mathrm{U}(1)_Y$ at the energy scale $\sim M_\nu^M$ naturally gives rise to Majorana mass term in $\mathcal{L}_{\nu_R}$ of Eq. (1.6), thus dynamically explaining its origin.

Pati-Salam model

Continuing in the line of gauge group enlarging and possible additional "unification" of certain model aspects, analogously to the "unification" of the treatment of the left-handed and right-handed fermions discussed in the left-right symmetric model, we can group quarks and leptons into common fermionic multiplets as it was first done by J. Pati and A. Salam [61]. On the gauge group level, the unification of quarks and leptons consists of extending the $\mathrm{SU}(3)_c$ gauge symmetry to $\mathrm{SU}(4)_C \supset \mathrm{SU}(3)_c$ with fermions being accommodated in its vector representations **4** in the following way:

$$F_L = \begin{pmatrix} Q_L^a \\ L_L \end{pmatrix}, \qquad F_{R,u} = \begin{pmatrix} u_R^a \\ \nu_R \end{pmatrix}, \qquad F_{R,d} = \begin{pmatrix} d_R^a \\ e_R \end{pmatrix},$$

where $a = 1, 2, 3$ denotes the colour index. We have thus arrived at the Pati-Salam

$$\mathrm{SU}(4)_C \times \mathrm{SU}(2)_L \times \mathrm{SU}(2)_R$$

extension of the Standard Model that incorporates the right-handed neutrinos and "unifies" the description of the right-handed and left-handed spinors, as well as leptons and quarks.

1.4 Arrival of the Grand Unified Theories

In the previous section, the origin of the seesaw scale M_ν^M was explained by introducing gauge symmetry extensions of the SM that lead to the "unification" of certain model aspects. We can take one step further and consider the Grand Unified Theories (GUTs) in which the Lagrangian is symmetric under a "unifying" simple gauge group G. Such group G drives model dynamics at high energies and it is subsequently spontaneously broken down to the SM $\mathrm{SU}(3)_c \times \mathrm{SU}(2)_L \times \mathrm{U}(1)_Y$.

Table 1.1: Charges of the Standard Model fermionic fields from one generation with the right-handed neutrino. The hypercharge Y and $(B-L)$ charge are normalized in accordance with Appendix F.

fermion	Y	Q	$T_L^{(3)}$	$T_R^{(3)}$	$(B-L)$
u_L	$+\frac{1}{6}$	$+\frac{2}{3}$	$+\frac{1}{2}$	0	$+\frac{1}{3}$
d_L	$+\frac{1}{6}$	$-\frac{1}{3}$	$-\frac{1}{2}$	0	$+\frac{1}{3}$
u_R	$+\frac{2}{3}$	$+\frac{2}{3}$	0	$+\frac{1}{2}$	$+\frac{1}{3}$
d_R	$-\frac{1}{3}$	$-\frac{1}{3}$	0	$-\frac{1}{2}$	$+\frac{1}{3}$
ν_L	$-\frac{1}{2}$	0	$+\frac{1}{2}$	0	-1
e_L	$-\frac{1}{2}$	-1	$-\frac{1}{2}$	0	-1
ν_R	0	0	0	$+\frac{1}{2}$	-1
e_R	-1	-1	0	$-\frac{1}{2}$	-1

Unlike in the left-right symmetric and Pati-Salam models, the SSB energy scale cannot be chosen arbitrarily, but it is rather fixed by the position of the gauge coupling unification, thus enhancing the overall predictive power of the GUTs. The point of gauge coupling unification can be assessed by examining the one-loop running of the SM gauge couplings [62, 63]. The SM gauge couplings corresponding to the non-Abelian factors[3] $\mathrm{SU}(3)_c$, $\mathrm{SU}(2)_L$ unify at scale $\mu = M_{GUT} \sim 10^{17}\,\mathrm{GeV}$, dubbed the GUT scale, see Fig. 1.1 — close to the energy scale that is currently probed by the proton decay searches [1, 2, 64, 65]. Let us also note that spontaneous breaking of the unified group G to the Standard Model can happen via two or more stages, thus allowing for the option to include an intermediate symmetry stage at $M_{Inter} < M_{GUT}$ in the energy ballpark $\sim 10^{12-13}\,\mathrm{GeV}$ preferred by the see-saw mechanism with heavy right-handed neutrinos, c.f. Eq. (1.11).

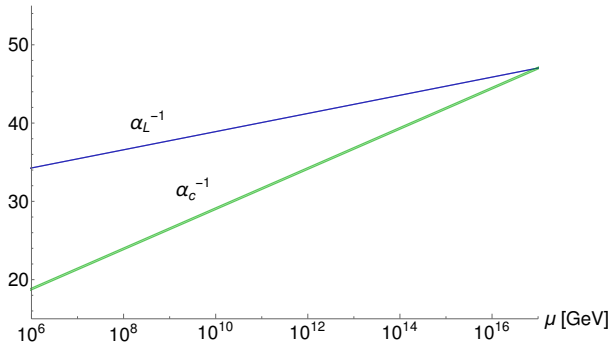

Figure 1.1: The one-loop running of the SM gauge couplings corresponding to the $\mathrm{SU}(3)_c$ and $\mathrm{SU}(2)_L$ non-Abelian group factors.

[3]The gauge factor α_Y^{-1} corresponding to the Abelian $\mathrm{U}(1)_Y$ group factor is deliberately excluded from the one-loop gauge coupling unification analysis as the α_Y can be arbitrarily rescaled in the SM as long as the product $g_Y Y$ stays constant. The proper hypercharge normalization is typically fixed in the GUTs by considering group-theoretical embedding of the $\mathrm{SU}(3)_c \times \mathrm{SU}(2)_L \times \mathrm{U}(1)_Y$ into the G [46].

The Grand Unified Theories bring with them interesting aspects of the beyond the SM physics. All the charges corresponding to its U(1) sub-groups are quantized, thus the hypercharge quantization condition is automatically satisfied [66]. New interaction vertices typically allow for perturbative lepton number violation (LNV)[4] and baryon number violation (BNV). The most prominent such signal in the GUTs is the hypothetical proton decay, which is BNV process that violates the Standard Model prediction of baryonic matter stability. Moreover, one of the inevitable consequences of the Grand Unified Theories is the existence of topologically stable magnetic monopoles [67, 68] in whose presence the cross sections of the BNV and LNV processes are enhanced [69–71]. (Non-)observation of magnetic monopole flux can therefore impose further phenomenological constraints upon GUTs.

Let us now briefly comment on several different Grand Unified Theories. From the group-theoretical point of view, the underlying unified gauge group G has to allow for complex representations and have a rank bigger or equal to 4 with the $\mathrm{SU}(3) \times \mathrm{SU}(2) \times \mathrm{U}(1)$ as its sub-group [46].

1.4.1 Rank= 4 GUTs

At rank 4, there is only one such option [46, 66] — the SU(5) with the Standard Model gauge group as its substructure. In the minimal scenario [72, 73], SM fermionic fields are accommodated in three copies of the 5-dimensional fundamental and 10-dimensional antisymmetric tensor representations of SU(5):

$$\overline{\mathbf{5}}_F = d^c_R \oplus L_L, \qquad \mathbf{10}_F = u^c_R \oplus e^c_R \oplus Q_L.$$

In addition, the SU(5) is spontaneously broken to the Standard model gauge group by the scalar 24-dimensional adjoint representation and the $\mathrm{SU}(3)_c \times \mathrm{SU}(2)_L \times \mathrm{U}(1)_Y$ is subsequently broken down to $SU(3)_c \times U(1)_Q$ via the scalar 5-dimensional representation that contains the SM Higgs field. Both of them decompose into the SM irreducible representations as

$$\begin{aligned} \mathbf{24} &= (8,1,0) \oplus (1,3,0) \oplus (1,1,0) \oplus (3,2,-\tfrac{5}{6}) \oplus (\overline{3},2,+\tfrac{5}{6}), \\ \mathbf{5} &= (1,2,+\tfrac{1}{2}) \oplus (3,1,-\tfrac{1}{3}). \end{aligned}$$

Neutrinos in the minimal SU(5) GUT are massless at renormalizable level[5] unless additional fields are introduced to the spectrum, namely SU(5) spin-$\frac{1}{2}$ singlets identified with right-handed Majorana neutrinos in case of type-I seesaw, or non-trivial SU(5) spin-0 or spin-$\frac{1}{2}$ multiplets containing $(1,3,+1)$ (type-II seesaw [74–76]) or $(1,3,0)$ (type-III seesaw [77]) SM-transforming representations, respectively. Moreover, the model's weak mixing angle prediction turns out to be inconsistent with the SPS $W^{\pm}/Z$ mass ratio measurements [78, 79], thus ruling out the viability of the minimal SU(5) GUT. Hence, realistic SU(5) GUTs have to involve extended scalar and/or fermion sector [80–89].

[4] Perturbative lepton number violation was already present in the SM extended by Majorana neutrinos discussed in Sec. 1.3.1 as the second term in the Lagrangian 1.6 explicitly breaks lepton number.

[5] The SU(5) gauge model in principle allows for neutrino-mass-generating non-renormalizable dimension $d = 5$ operator of the type $\frac{1}{\Lambda}\,\overline{\mathbf{5}}_F\,\overline{\mathbf{5}}_F\,\mathbf{5}\,\mathbf{5}$, with Λ being the SU(5) cutoff scale.

1.4.2 Rank> 4 GUTs

The failure of the minimal SU(5) GUT motivates searches for a unified theory with an underlying gauge group of rank > 4 whose minimal version accommodates additional fields to generate neutrino masses and correctly predict low-energy quantities, including the weak mixing angle. At rank 5, two simple gauge groups meet the group-theoretical criteria of the GUT hypothesis [46]: SU(6) and SO(10). As the former one inevitably enforces the addition of new, presumably heavy, fermionic matter [90–92], the latter option is more interesting. The SO(10) Grand Unified Theory [93], studied almost simultaneously with the Georgi-Glashow SU(5), allows for even greater "unification" as a single 16-dimensional spinorial representation of SO(10) can accommodate one generation of the SM fermions. Moreover, this representation also contains one fermionic singlet, which can play the role of the right-handed neutrino. The SO(10) symmetry is typically spontaneously broken in two stages due to its rank, c.f. Fig. 1.2, with intermediate stages being, for instance, the Georgi-Glashow SU(5) or the Pati-Salam $\mathrm{SU}(4)_C \times \mathrm{SU}(2)_L \times \mathrm{SU}(2)_R$. Although the minimal realization of the SO(10) faces notorious tachyonic instabilities in the tree-level scalar mass spectrum [8–10] that can be remedied only by introducing loop corrections [11], it remains intensively studied theory [7, 11–17]. Hence, from now on, we shall focus solely on the minimal SO(10) GUT.

Finally, remark that the rank 5 groups are not the only ones that can be used to construct a Grand Unified Theory. The honourable mention deserves the rank-6 exceptional $E(6)$ group [94–102] as one of the even larger beyond-the-SM gauge groups with SO(10) being its potential intermediate symmetry stage.

1.5 The SO(10) gauge model as a realistic GUT

In the general SO(10) Grand Unified Theory, the gauge sector is accommodated in the adjoint 45-dimensional representation. It decomposes into the following SM irreducible representations [46]:

$$\begin{aligned}
\mathbf{45}_G = {} & (8,1,0) \oplus (1,3,0) \oplus (1,1,0) \oplus (1,1,0) \oplus \\
& \downarrow \qquad \downarrow \qquad \downarrow \\
& G_\mu \qquad A_\mu \qquad B_\mu \\
\\
& \oplus (\overline{3},2,+\tfrac{5}{6}) \oplus (3,2,-\tfrac{5}{6}) \oplus (\overline{3},2,-\tfrac{1}{6}) \oplus (3,2,+\tfrac{1}{6}) \oplus (3,1,+\tfrac{2}{3}) \oplus (1,1,+1) + h.c. \\
& \qquad\qquad \downarrow \qquad\qquad\qquad\qquad \downarrow \\
& X_\mu \oplus \overline{X}_\mu \qquad\qquad Y_\mu \oplus \overline{Y}_\mu
\end{aligned} \tag{1.13}$$

The presence of the additional X_μ, Y_μ gauge fields allows for the gauge boson-mediated proton decay, which is the smoking gun signal of the vast majority of GUTs, c.f. Sec. 2.5.

As we already mentioned in Sec. 1.4.2, one of the most remarkable aspects of the minimal SO(10) GUT is the fact that the whole generation of the SM fermionic matter fields can be accommodated into a 16-dimensional irreducible

spinorial representation. Specifically,

$$\mathbf{16}_F = (3,2,+\tfrac{1}{6}) \oplus (1,2,-\tfrac{1}{2}) \oplus (\overline{3},1,-\tfrac{2}{3}) \oplus (\overline{3},1,+\tfrac{1}{3}) \oplus (1,1,0) \oplus (1,1,+1). \quad (1.14)$$
$$\downarrow \qquad \downarrow \qquad \downarrow \qquad \downarrow \qquad \downarrow \qquad \downarrow$$
$$Q_L \qquad L_L \qquad \overline{u_R} \qquad \overline{d_R} \qquad \overline{\nu_R} \qquad \overline{e_R}$$

All fermionic hypercharges are properly quantized and, at the same time, all chiral anomalies get automatically cancelled. Furthermore, the neutrino masses can be generated via the type-I seesaw mechanism by employing the right-handed neutrino ν_R.

The different scalar sector configurations typically distinguish realizations of the SO(10) GUT with distinctive phenomenological implications. Fig. 1.2 shows all possible symmetry breaking chains with SO(10) representations of dimension less than 300 which can be employed to spontaneously break simple group SO(10) to the $\mathrm{SU}(3)_c \times \mathrm{SU}(2)_L \times \mathrm{U}(1)_Y$, and subsequently even further to the $\mathrm{SU}(3)_c \times \mathrm{U}(1)_Q$. We shall identify the minimal potentially realistic renormaliz-

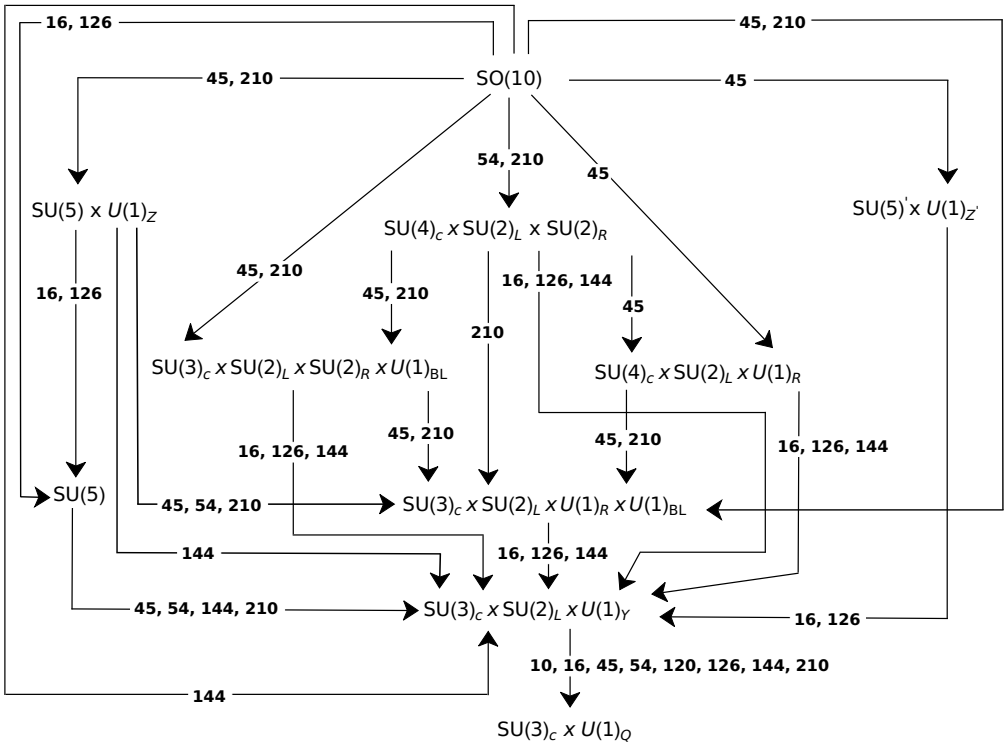

Figure 1.2: Symmetry breaking chains [103–105] of the SO(10) GUT which lead to the $\mathrm{SU}(3)_c \times \mathrm{SU}(2)_L \times \mathrm{U}(1)_Y$, and subsequently to the $SU(3)_c \times U(1)_Q$, with representations of dimension less than 300 employed.

able realisation of the SO(10) GUT, i.e. the renormalizable realization which still has a chance to be viable and contains the smallest number of field degrees of freedom.[6] The scalar content of such a scenario can be determined by considering

[6]There are two perspectives on how to assess the minimality of a given model — either by the number of field degrees of freedom or by the number of independent parameters of the Lagrangian. The SO(10) GUT studied in this thesis is minimal only concerning the former criterion as there exist alternative SO(10) GUT realizations which are determined by an even smaller number of lagrangian parameters, see for example [106].

restrictions coming from the Yukawa sector and from the successful SSB of the SO(10) down to the SM gauge group.

The SO(10) decomposition of the spinor bilinear [103]

$$\mathbf{16} \otimes \mathbf{16} = \mathbf{10} \oplus \mathbf{126} \oplus \mathbf{120} \tag{1.15}$$

dictates that any renormalizable Yukawa Lagrangian engages only **10**, **126** and **120** scalar representations of SO(10) (see studies [106–119]). The minimal renormalizable Yukawa sector that can support viable fermion mass fits [109] consists of the 126-dimensional tensor and the complexified 10-dimensional vector representations of SO(10).[7]

The scalar **10** does not contain any SM singlet and thus cannot contribute to the SSB of the SO(10) down to the SM gauge group, c.f. Fig. 1.2. The **126** accommodates one complex SM singlet, which, however, breaks SO(10) only to SU(5). Hence it is necessary to employ yet additional scalar irreducible representation to spontaneously break SO(10) to the $\mathrm{SU}(3)_c \times \mathrm{SU}(2)_L \times \mathrm{U}(1)_Y$ and to avoid phenomenologically disfavoured breaking chain containing SU(5) intermediate stage. The smallest such representation is the adjoint **45**.

In total, the scalar sector of the minimal renormalizable SO(10) GUT consists of

$$\mathbf{45} \oplus \mathbf{126} \oplus \mathbf{10}_{\mathbb{C}}, \tag{1.16}$$

where **45** is real and **126**, $\mathbf{10}_{\mathbb{C}}$ are complex representations.

[7] It is necessary to consider at least two different scalar representations employed in the Yukawa Lagrangian to avoid undesirable correlations between quark and lepton masses. Moreover, the realization with the **126** and the real **10** SO(10) representations likewise leads to a contradiction with the fermion mass and mixing data [108]. For further details, see Sec. 2.1.3.

2. Structure and phenomenology of the minimal SO(10) GUT

Let us reiterate that the gauge fields of the SO(10) GUT reside in the adjoint $\mathbf{45}_G$ representation. The fermionic fields including right-handed neutrinos are accommodated in three copies of the 16-dimensional spinorial representation. We parametrize the bispinor $(\mathbf{16}_F, \overline{\mathbf{16}}_F)^T$ by

$$\Omega^p_x, x = 1, \ldots, 32, \tag{2.1}$$

where $p = 1, 2, 3$ denotes family index. The decomposition of $\mathbf{16}_F$ spinors into various subgroups can be found in Appendix F.4. The scalar sector consists of

$$\mathbf{45} \oplus \mathbf{126} \oplus \mathbf{10}_{\mathbb{C}}.$$

In what follows, we write $\mathbf{45}$ as a set of 2-index real antisymmetric components

$$\phi_{ij},\ i, j = 1, \ldots, 10, \qquad\qquad \phi_{ji} = -\phi_{ij}. \tag{2.2}$$

The $\mathbf{126}$ is represented by a 5-index self-dual antisymmetric tensor with complex components

$$\Sigma_{ijklm},\ i, j, k, l, m = 1, \ldots, 10, \qquad \Sigma_{ijklm} = -\frac{i}{5!}\epsilon_{ijklmnopqr}\Sigma_{nopqr}, \tag{2.3}$$

where the totally antisymmetric Levi-Civita tensor convention is

$$\epsilon_{12345678910} = +1. \tag{2.4}$$

Last, but not least, we write the $\mathbf{10_C}$ as a vector with complex components[1]

$$H_i,\ i = 1, \ldots, 10. \tag{2.5}$$

Since Σ and H are complex, we denote the corresponding complex conjugated components as Σ^* and H^*, respectively. For more details, see Appendix A of [120].

Decomposition of the $\mathbf{45} \oplus \mathbf{126} \oplus \mathbf{10}_{\mathbb{C}}$ into several physically relevant SO(10) subgroups can be found in Appendix F.4. The model's scalar content in terms of the irreducible $\mathrm{SU}(3)_c \times \mathrm{SU}(2)_L \times \mathrm{U}(1)_Y$ representations is gathered in Table 2.1. Every SM representation is accompanied by information about its reality/complexity, multiplicity, SO(10) origin and the number of would-be Goldstone modes.

2.1 Lagrangian

The most general form of the renormalizable Lagrangian $\mathcal{L}$ in an unbroken phase can be written as

$$\mathcal{L} = \mathcal{L}_{kin} - V_0 + \mathcal{L}_Y. \tag{2.6}$$

It consists of the kinetic part $\mathcal{L}_{kin}$, the scalar potential V_0 and the Yukawa interactions $\mathcal{L}_Y$.

[1]The 10-dimensional vector representation of SO(10) is real, however, we work with its complexified version, and hence the components H_i are complex.

Table 2.1: Scalar content of the $\mathbf{45} \oplus \mathbf{126} \oplus \mathbf{10}_{\mathbb{C}}$ SO(10) GUT in terms of the $\mathrm{SU}(3)_c \times \mathrm{SU}(2)_L \times \mathrm{U}(1)_Y$ irreducible representations. Each SM representation R has its reality/complexity, multiplicity # and SO(10) origins indicated. The column labeled "WGB" indicates the number of massless would-be Goldstone modes that transform as a given SM representation.

$R \sim G_{\mathrm{SM}}$	$\mathbb{R}/\mathbb{C}$	#	WGB	$\subseteq$ SO(10)
$(1,1,0)$	$\mathbb{R}$	4	1	ϕ, ϕ, Σ, Σ^*
$(1,1,+1)$	$\mathbb{C}$	2	1	ϕ, Σ
$(1,1,+2)$	$\mathbb{C}$	1	0	Σ
$(1,2,+\frac{1}{2})$	$\mathbb{C}$	4	0	Σ, Σ^*, H, H^*
$(1,3,-1)$	$\mathbb{C}$	1	0	Σ
$(1,3,0)$	$\mathbb{R}$	1	0	ϕ
$(3,2,-\frac{5}{6})$	$\mathbb{C}$	1	1	ϕ
$(3,2,+\frac{1}{6})$	$\mathbb{C}$	3	1	ϕ, Σ, Σ^*
$(3,2,+\frac{7}{6})$	$\mathbb{C}$	2	0	Σ, Σ^*
$(3,3,-\frac{1}{3})$	$\mathbb{C}$	1	0	Σ
$(\bar{3},1,-\frac{2}{3})$	$\mathbb{C}$	2	1	ϕ, Σ
$(\bar{3},1,+\frac{1}{3})$	$\mathbb{C}$	5	0	Σ, Σ, Σ^*, H, H^*
$(\bar{3},1,+\frac{4}{3})$	$\mathbb{C}$	1	0	Σ
$(6,3,+\frac{1}{3})$	$\mathbb{C}$	1	0	Σ
$(\bar{6},1,-\frac{4}{3})$	$\mathbb{C}$	1	0	Σ
$(\bar{6},1,-\frac{1}{3})$	$\mathbb{C}$	1	0	Σ
$(\bar{6},1,+\frac{2}{3})$	$\mathbb{C}$	1	0	Σ
$(8,1,0)$	$\mathbb{R}$	1	0	ϕ
$(8,2,+\frac{1}{2})$	$\mathbb{C}$	2	0	Σ, Σ^*

2.1.1 Kinetic part

The kinetic part is

$$\mathcal{L}_{kin} = \frac{1}{4}\left(F_{\mu\nu}\right)_{ij}\left(F^{\mu\nu}\right)_{ij} + i\overline{\Omega_x^p}\gamma_\mu D^\mu \Omega_x^p + \frac{1}{4}\left(D_\mu\phi_{ij}\right)^*\left(D^\mu\phi_{ij}\right) + \\ + \frac{1}{5!}\left(D_\mu\Sigma_{ijklm}\right)^*\left(D^\mu\Sigma_{ijklm}\right) + \left(D_\mu H_i\right)^*\left(D^\mu H_i\right), \quad (2.7)$$

where γ_μ are the Dirac gamma matrices and [11, 15]

$$(F^{\mu\nu})_{ij} = \partial^\mu A^\nu_{ij} - \partial^\nu A^\mu_{ij} - i\, g\, [A^\mu, A^\nu]_{ij}\,, \tag{2.8}$$

$$D^\mu \phi_{ij} = \partial^\mu \phi_{ij} - ig\, [A^\mu, \phi]_{ij}, \tag{2.9}$$

$$\begin{aligned} D^\mu \Sigma_{ijklm} = \partial^\mu \Sigma_{ijklm} - ig(&A^\mu_{in}\Sigma_{njklm} + A^\mu_{jn}\Sigma_{inklm} + \\ &+ A^\mu_{kn}\Sigma_{ijnlm} + A^\mu_{ln}\Sigma_{ijknm} + A^\mu_{mn}\Sigma_{ijkln}) \end{aligned} \tag{2.10}$$

$$D^\mu H_i = \partial^\mu H_i - ig\, (A^\mu H)_i\,, \tag{2.11}$$

$$D_\mu \Omega^p_x = \partial^\mu \Omega^p_x - ig \frac{1}{4} \left(\tilde{A}_\mu \Omega\right)^p_x. \tag{2.12}$$

The contribution of gauge vector fields is conveniently described in terms of

$$A^\mu = A^\mu_{(ij)} T_{(ij)} \tag{2.13}$$

with $T_{(ij)}$ being SO(10) generators in the 10-dimensional vector representation and

$$\tilde{A}^\mu = A^\mu_{(ij)} \tilde{S}_{(ij)}, \tag{2.14}$$

where $\tilde{S}_{(ij)}$ are SO(10) generators in the 32-dimensional reducible spinorial representation. For their explicit forms, see Appendix F. The indices $i, j \in \{1, \ldots, 10\}$; $x \in \{1, \ldots, 32\}$ and the subscript (ij) stands for 45 ordered pairs of indices i, j. Three fermion families are distinguished by $p \in \{1, 2, 3\}$. As usual, summation over repeated indices is assumed.

2.1.2 Scalar potential

The most general tree-level renormalizable scalar potential can be expressed as

$$V_0 = V_{45} + V_{126} + V_{10} + V_{\rm mix} \tag{2.15}$$

with

$$V_{45} = -\frac{\mu^2}{4}(\phi\phi)_0 + \frac{a_0}{4}\,(\phi\phi)_0(\phi\phi)_0 + \frac{a_2}{4}(\phi\phi)_2(\phi\phi)_2, \tag{2.16}$$

$$\begin{aligned} V_{126} = &-\frac{\nu^2}{5!}(\Sigma\Sigma^*)_0 + \frac{\lambda_0}{(5!)^2}\,(\Sigma\Sigma^*)_0(\Sigma\Sigma^*)_0 + \frac{\lambda_2}{(4!)^2}(\Sigma\Sigma^*)_2(\Sigma\Sigma^*)_2 + \\ &+ \frac{\lambda_4}{(3!)^2(2!)^2}(\Sigma\Sigma^*)_4(\Sigma\Sigma^*)_4 + \frac{\lambda'_4}{(3!)^2}(\Sigma\Sigma^*)_{4'}(\Sigma\Sigma^*)_{4'} + \\ &+ \frac{\eta_2}{(4!)^2}(\Sigma\Sigma)_2(\Sigma\Sigma)_2 + \frac{\eta_2^*}{(4!)^2}(\Sigma^*\Sigma^*)_2(\Sigma^*\Sigma^*)_2, \end{aligned} \tag{2.17}$$

$$V_{10} = -\xi^2(H^*H)_0 - \xi'^2(HH)_0 - \xi'^{*2}(H^*H^*)_0 +$$

$$
\begin{aligned}
&+ h_4\,(HH)_0(HH)_0 + h_4^*\,(H^*H^*)_0(H^*H^*)_0 + \\
&+ h_3\,(HH)_0(HH^*)_0 + h_3^*\,(H^*H^*)_0(H^*H)_0 + \\
&+ h_2\,(H^*H)_0(H^*H)_0 + h_2'\,(H^*H^*)_0(HH)_0,
\end{aligned}
\tag{2.18}
$$

$$
\begin{aligned}
V_{\rm mix} = &\frac{\kappa_0}{2}\,(H^*H)_0(\phi\phi)_0 + \kappa_2\,(H^*H)_2(\phi\phi)_2 + \\
&+ \frac{\kappa_0'}{2}\,(HH)_0(\phi\phi)_0 + \frac{\kappa_0'^*}{2}\,(H^*H^*)_0(\phi\phi)_0 + \\
&+ \kappa_2'\,(HH)_2(\phi\phi)_2 + \kappa_2'^*\,(H^*H^*)_2(\phi\phi)_2 + \\
&+ \frac{\zeta}{4}(\phi\phi)_4(H\Sigma)_4 + \frac{\zeta^*}{4}(\phi\phi)_4(H^*\Sigma^*)_4 + \\
&+ \frac{\zeta'}{4}(\phi\phi)_4(H^*\Sigma)_4 + \frac{\zeta'^*}{4}(\phi\phi)_4(H\Sigma^*)_4 + \\
&+ \frac{\rho_0}{5!}(H^*H)_0(\Sigma\Sigma^*)_0 + \frac{\rho_2}{4!}(H^*H)_2(\Sigma\Sigma^*)_2 + \\
&+ \frac{\rho_0'}{5!}(HH)_0(\Sigma\Sigma^*)_0 + \frac{\rho_0'^*}{5!}(H^*H^*)_0(\Sigma\Sigma^*)_0 + \\
&+ \frac{\psi_2}{4!}(HH)_2(\Sigma\Sigma)_2 + \frac{\psi_2^*}{4!}(H^*H^*)_2(\Sigma^*\Sigma^*)_2 + \\
&+ + \frac{\psi_1}{4!}(HH^*)_2(\Sigma\Sigma)_2 + \frac{\psi_1^*}{4!}(H^*H)_2(\Sigma^*\Sigma^*)_2 + \\
&+ \frac{\psi_0}{4!}(H^*H^*)_2(\Sigma\Sigma)_2 + \frac{\psi_0^*}{4!}(HH)_2(\Sigma^*\Sigma^*)_2 + \\
&+ \frac{\varphi}{3!}(H\Sigma)_4(\Sigma\Sigma^*)_4 + \frac{\varphi^*}{3!}(H^*\Sigma^*)_4(\Sigma\Sigma^*)_4 + \\
&+ \frac{\varphi'}{3!}(H^*\Sigma)_4(\Sigma\Sigma^*)_4 + \frac{\varphi'^*}{3!}(H\Sigma^*)_4(\Sigma\Sigma^*)_4 + \\
&+ \frac{i\tau}{4!}(\phi)_2(\Sigma\Sigma^*)_2 + i\tau'(\phi)_2(HH^*)_2 + \\
&+ \frac{\gamma_2}{4!}(\phi\phi)_2(\Sigma\Sigma)_2 + \frac{\gamma_2^*}{4!}(\phi\phi)_2(\Sigma^*\Sigma^*)_2 + \\
&+ \frac{\alpha}{2\cdot 5!}(\phi\phi)_0(\Sigma\Sigma^*)_0 + \frac{\beta_4}{4\cdot 3!}(\phi\phi)_4(\Sigma\Sigma^*)_4 + \\
&+ \frac{\beta_4'}{3!}(\phi\phi)_{4'}(\Sigma\Sigma^*)_{4'}.
\end{aligned}
\tag{2.19}
$$

The following abbreviated notation of invariant contractions is used:

$$
\begin{aligned}
(HH)_0 &= H_iH_i, \\
(HH)_2 &= H_iH_j, \\
(\phi\phi)_0 &= \phi_{ij}\phi_{ij}, \\
(\phi\phi)_2 &= (\phi\phi)_{jk} = \phi_{ij}\phi_{ik}, \\
(\phi\phi)_4 &= \phi_{ij}\phi_{kl}, \\
(\Sigma\Sigma^*)_0 &= \Sigma_{ijklm}\Sigma^*_{ijklm}, \\
(\Sigma\Sigma^*)_2 &= (\Sigma\Sigma^*)_{mn} = \Sigma_{ijklm}\Sigma^*_{ijkln}, \\
(\Sigma\Sigma^*)_4 &= (\Sigma\Sigma^*)_{lmno} = \Sigma_{ijklm}\Sigma^*_{ijkno}, \\
(H\Sigma)_4 &= (H\Sigma)_{ijklm} = H_i\Sigma_{ijklm},
\end{aligned}
$$

$$
\begin{aligned}
(\phi)_2\,(HH^*)_2 &= \phi_{ij}H_iH_j^*,\\
(\phi\phi)_2\,(HH)_2 &= (\phi\phi)_{jk}\,H_jH_k,\\
(\phi\phi)_4\,(H\Sigma)_4 &= \phi_{ij}\phi_{kl}\,(H\Sigma)_{ijkl}\,,\\
(\phi)_2\,(\Sigma\Sigma^*)_2 &= \phi_{mn}\,(\Sigma\Sigma^*)_{mn}\,,\\
(\phi\phi)_2\,(\Sigma\Sigma)_2 &= (\phi\phi)_{jk}\,(\Sigma\Sigma)_{jk}\,,\\
(\phi\phi)_4\,(\Sigma\Sigma^*)_4 &= \phi_{lm}\phi_{no}\,(\Sigma\Sigma^*)_{lmno}\,,\\
(\phi\phi)_{4'}\,(\Sigma\Sigma^*)_{4'} &= \phi_{lm}\phi_{no}\,(\Sigma\Sigma^*)_{lnmo}\,,\\
(\Sigma\Sigma^*)_2\,(\Sigma\Sigma^*)_2 &= (\Sigma\Sigma^*)_{mn}\,(\Sigma\Sigma^*)_{mn}\,,\\
(\Sigma\Sigma^*)_4\,(\Sigma\Sigma^*)_4 &= (\Sigma\Sigma^*)_{lmno}\,(\Sigma\Sigma^*)_{lmno}\,,\\
(\Sigma\Sigma^*)_{4'}\,(\Sigma\Sigma^*)_{4'} &= (\Sigma\Sigma^*)_{lmno}\,(\Sigma\Sigma^*)_{lnmo}\,,\\
(HH)_2\,(\Sigma\Sigma)_2 &= H_mH_n\,(\Sigma\Sigma)_{mn}\,,\\
(H\Sigma)_4\,(\Sigma\Sigma^*)_4 &= (H\Sigma)_{lmno}\,(\Sigma\Sigma^*)_{lmno}\,.
\end{aligned}
\tag{2.20}
$$

The normalization of the scalar potential terms was chosen in such a way that it compensates for the combinatorical factors appearing once the abbreviated invariants are expanded. In addition to that, this normalization ensures that expressions μ^2 and ν^2 represent the mass-squares of the fields in **45** and **126** in the unbroken phase, respectively.

The scalar potential contains 30 dimensionless parameters, out of which 15 are real

$$
\{a_0, a_2, \lambda_0, \lambda_2, \lambda_4, \lambda_4', \alpha, \beta_4, \beta_4', h_2, h_2', \kappa_0, \kappa_2, \rho_0, \rho_2\} \tag{2.21}
$$

and the remaining 15 couplings are complex

$$
\{\gamma_2, \eta_2, h_3, h_4, \kappa_0', \kappa_2', \zeta, \zeta', \rho_0', \rho_2', \psi_0, \psi_1, \psi_2, \phi, \phi'\}. \tag{2.22}
$$

These are accompanied by 5 real

$$
\{\mu, \nu, \xi, \tau, \tau'\} \tag{2.23}
$$

and one complex dimensionfull parameter

$$
\{\xi'\}. \tag{2.24}
$$

2.1.3 Yukawa interactions

Last, but not least, the tree-level Yukawa interaction Lagrangian can be schematically sketched as

$$
\mathcal{L}_Y = -\mathbf{16}_F^p \left[(Y_{10})^{pq}\,\mathbf{10}_{\mathbb{C}} + \left(\tilde{Y}_{10}\right)^{pq}\mathbf{10}_{\mathbb{C}}^* + (Y_{126})^{pq}\,\overline{\mathbf{126}} \right] \mathbf{16}_F^q + h.c., \tag{2.25}
$$

where Y_{10}, $\tilde{Y}_{10}$ and Y_{126} are 3×3 complex Yukawa matrices that are symmetric in the generation space over which the indices p, q get summed.

The Lagrangian $\mathcal{L}_Y$ is rather complicated with three Yukawa matrices determining Yukawa interactions, thus it is typically subject to additional constraints that increase the predictive power of the model [108], such as extra global symmetry of the Peccei-Quinn type or demanding **10** is real. Let us discuss in brief

the former option and postpone the discussion of the latter one to Sec. 2.4.3.The global Peccei-Quinn $\mathrm{U}(1)_{PQ}$ symmetry [106–114] assigns charges to all SO(10) representations:

$$[\mathbf{16}_F]_{PQ} = +1, \qquad [\mathbf{45}]_{PQ} = 0, \qquad [\mathbf{126}]_{PQ} = +2, \qquad [\mathbf{10}_{\mathbb{C}}]_{PQ} = -2. \tag{2.26}$$

Consequently, the $\mathbf{16}_F\mathbf{10}^*_{\mathbb{C}}\mathbf{16_F}$ term in $\mathcal{L}_Y$ is not $\mathrm{U}(1)_{PQ}$ symmetric and thus the Yukawa couplings $\tilde{Y}_{10}$ must vanish. This greatly improves the predictive power of the model as it reduces the number of free parameters that have to be determined. At the same time, a number of scalar couplings has to vanish to make V_0 symmetric with respect to the $\mathrm{U}(1)_{PQ}$, which leads to even greater model simplification. One such parameter is γ_2 of V_{mix} and it is forbidden for any non-trivial assignment of the PQ charges, see Appendix C in [17]. Since the γ_2 coupling turns out to be crucial in fixing the tree-level tachyonicity of the pseudo-Goldstone masses, c.f. Sec. 3.2.1, its value cannot vanish in the minimal renormalizable SO(10) theory. Hence the PQ symmetry cannot be imposed as the theory would run into issues with tachyonicity of its spectrum.

The non-viability of the alternative scenario with the real **10** is discussed in Sec. 2.4.3. Therefore the $\mathcal{L}_Y$ of Eq. (2.25) is the minimal Yukawa Lagrangian that can be written with a chance of satisfying all phenomenological requirements.

2.2 VEVs and Symmetry breaking

The scalar spectrum of the minimal SO(10) GUT contains three SM singlets: the **45** accommodates two real ones and an additional complex SM singlet resides in the **126**. Their vacuum expectation values can be parameterized as

$$\langle(1,1,1,0)_\phi\rangle \equiv \sqrt{3}\omega_{BL}, \tag{2.27}$$

$$\langle(1,1,3,0)_\phi\rangle \equiv \sqrt{2}\omega_R, \tag{2.28}$$

$$\langle(1,1,3,2)_\Sigma\rangle \equiv \sqrt{2}\sigma. \tag{2.29}$$

For unambiguous identification of these fields, in parentheses it is referred to their $\mathrm{SU}(3)_c \times \mathrm{SU}(2)_L \times \mathrm{SU}(2)_R \times \mathrm{U}(1)_{B-L}$ transformational properties. The lower indices of ϕ and Σ indicate that these fields belong to the **45** and **126**, respectively. In general, one can always redefine the overall phase of Σ in such a way that σ is real and positive. A similar transformation can be performed on ϕ allowing one of ω's values to be positive. Although this simplification is utilized in our scans in Sec. 3, all analytical expressions onward are written without capitalizing on the freedom in choosing phases and signs of σ and ω's.

As sugested by their names, the ω_{BL} VEV preserves the $\mathrm{U}(1)_{B-L}$ symmetry and the ω_R VEV, on the other hand, conserves $\mathrm{U}(1)_R$ symmetry. The residual gauge symmetries in all relevant symmetry-breaking chains are summarized in Table 2.2.

The SO(10) gauge symmetry of the minimal model is assumed to be spontaneously broken down to the $\mathrm{SU}(3)_c \times \mathrm{SU}(2)_L \times \mathrm{U}(1)_Y$ of the SM in two stages with separate energy scales as the single-stage symmetry breaking does not lead to a successful gauge coupling unification due to heavy part of the spectrum being clustered around the unification scale. Hence the GUT symmetry is broken

Table 2.2: Residual gauge symmetries for various VEV configurations. The abbreviated notation $n \equiv \mathrm{SU}(n)$ is introduced. The penultimate column corresponds to the flipped SU(5) intermediate symmetry stage [121, 122], see Appendix F.3 for SM embedding details. The SU(5) symmetry in the last column remains unbroken due to the SU(5)-singlet nature of σ.

	$\omega_{BL} \neq 0$	$\omega_{BL} = 0$	$\omega_{BL} \neq 0$	$\omega_{BL} \neq 0$	$\omega_{BL} \neq 0$
	$\omega_R \neq 0$	$\omega_R \neq 0$	$\omega_R = 0$	$\omega_R = -\omega_{BL}$	$\omega_R = \omega_{BL}$
$\sigma = 0$	$3_c\, 2_L\, 1_R\, 1_{B-L}$	$4_C\, 2_L\, 1_R$	$3_c\, 2_L\, 2_R\, 1_{B-L}$	$5'\, 1_{Z'}$	$5\, 1_Z$
$\sigma \neq 0$	$3_c\, 2_L\, 1_Y$	$3_c\, 2_L\, 1_Y$	$3_c\, 2_L\, 1_Y$	$3_c\, 2_L\, 1_Y$	5

down by the larger of the ω VEVs down to a rank-5 subgroup. Subsequently, this intermediate symmetry is broken by the rank reducing σ VEV down to the $\mathrm{SU}(3)_c \times \mathrm{SU}(2)_L \times \mathrm{U}(1)_Y$. The $\max[|\omega_{BL}|, |\omega_R|]$ plays the role of the GUT unification scale ($\max[|\omega_{BL}|, |\omega_R|] \sim M_{GUT}$) and σ determines the seesaw scale. The seesaw-compatible regime implies the scale hierarchy

$$|\sigma| \ll \max[|\omega_{BL}|, |\omega_R|], \tag{2.30}$$

which is confirmed by results in Sec. 3.

Last, but not least, a fully realistic symmetry breaking chain has to involve spontaneous symmetry breaking of the $\mathrm{SU}(3)_c \times \mathrm{SU}(2)_L \times \mathrm{U}(1)_Y$ down to the $\mathrm{SU}(3)_c \times \mathrm{U}(1)_Q$. Hence at least some of the $\mathrm{SU}(3)_c \times \mathrm{U}(1)_Q$ neutral components of scalar fields must acquire a non-zero expectation value. However, the SM symmetry breaking does not affect the preceding step of the SO(10) breaking to the $\mathrm{SU}(3)_c \times \mathrm{SU}(2)_L \times \mathrm{U}(1)_Y$, thus it will be mostly omitted from the following considerations. The interested reader is kindly deferred to Sec. 2.4.3, which contemplates on some explicit implications of the $\mathrm{SU}(3)_c \times \mathrm{SU}(2)_L \times \mathrm{U}(1)_Y$ symmetry breaking for the flavour sector.

2.3 Vacuum stability conditions

The presence of three non-zero vacuum expectation values entails the existence of three non-trivial vacuum stationarity conditions

$$\frac{\partial V(\langle\phi\rangle, \langle\Sigma\rangle, \langle H\rangle)}{\partial \omega_{BL}} = 0, \tag{2.31}$$

$$\frac{\partial V(\langle\phi\rangle, \langle\Sigma\rangle, \langle H\rangle)}{\partial \omega_{R}} = 0, \tag{2.32}$$

$$\frac{\partial V(\langle\phi\rangle, \langle\Sigma\rangle, \langle H\rangle)}{\partial \sigma} = 0, \tag{2.33}$$

where $V(\langle\phi\rangle, \langle\Sigma\rangle, \langle\Omega\rangle)$ denotes the effective scalar potential with all the fields evaluated in a vacuum.

Eqns. (2.31)-(2.33) are used to relate the dimensionfull scalar parameters $\{\mu, \nu, \tau\}$ with the VEVs $\{\omega_{BL}, \omega_R, \sigma\}$. Let us note that if there were any non-trivial relations between VEVs, the number of non-trivial vacuum stationarity

conditions would reduce and some of the $\{\mu, \nu, \tau\}$ parameters could not be expressed as a function of VEVs and dimensionless scalar couplings. For example, if $\omega_R = \omega_{BL}$, Eqns. (2.31) and (2.32) are identical and a certain combination of $\{\mu, \nu\}$ becomes an independent structure whose value is not restricted by vacuum stability conditions (2.31)-(2.33).

By inserting the tree-level scalar potential V_0 into Eqns. (2.31)-(2.33), one obtains the following tree-level relations

$$\mu^2 = (12a_0 + 2a_2)\omega_{BL}^2 + (8a_0 + 2a_2)\omega_R^2 + 2a_2\omega_{BL}\omega_R + 4(\alpha + \beta_4')|\sigma|^2, \quad (2.34)$$

$$\begin{aligned}\nu^2 = {} & 3(\alpha + 4\beta_4')\omega_{BL}^2 + 2(\alpha + 3\beta_4')\omega_R^2 + 12\beta_4'\omega_{BL}\omega_R + 4\lambda_0|\sigma|^2 + \\ & + a_2\frac{\omega_{BL}\omega_R}{|\sigma|^2}(\omega_{BL} + \omega_R)(3\omega_{BL} + 2\omega_R),\end{aligned} \quad (2.35)$$

$$\tau = 2\beta_4'(3\omega_{BL} + 2\omega_R) + a_2\frac{\omega_{BL}\omega_R}{|\sigma|^2}(\omega_{BL} + \omega_R). \quad (2.36)$$

Notice that expressions (2.35) and (2.36) contain a peculiar VEV structure accommodating the σ VEV in the denominator. This structure will become important in the considerations about perturbativity of Sec. 3.1.3 and it will help narrow down a set of viable symmetry breaking patterns, see Sec. 3.1.3. For later convenience, we will define the dimensionless universal VEV ratio as

$$\chi = \frac{\omega_{BL}\omega_R}{|\sigma|^2}. \quad (2.37)$$

2.4 Tree-level spectrum

Let us determine the full tree-level mass spectrum of the scalar, vector and fermionic fields.

2.4.1 Tree-level gauge masses

Gauge mass-squared matrix $\mathbf{M}_G^2$ originates from the scalar-field-dependent part of $\mathcal{L}_{kin}$ of Eq. (2.7), which contains the gauge mass term

$$\mathcal{L} \supset \frac{1}{2}\mathbf{M}^2_{G(ij)(kl)}A^{\mu}_{(ij)}A_{\mu(kl)}, \quad (2.38)$$

where

$$\begin{aligned}\frac{2}{g^2}\mathbf{M}^2_{G(mn)(op)} = {} & \delta^{mo}\langle\Sigma^*_{n(jklm)}\rangle\langle\Sigma_{p(jklm)}\rangle + \delta^{np}\langle\Sigma^*_{m(jklm)}\rangle\langle\Sigma_{o(jklm)}\rangle - \\ & - \delta^{mp}\langle\Sigma^*_{n(jklm)}\rangle\langle\Sigma_{o(jklm)}\rangle - \delta^{no}\langle\Sigma^*_{m(jklm)}\rangle\langle\Sigma_{p(jklm)}\rangle + \\ & + \langle\Sigma^*_{mp(klm)}\rangle\langle\Sigma_{no(klm)}\rangle + \langle\Sigma^*_{no(klm)}\rangle\langle\Sigma_{mp(klm)}\rangle - \\ & - \langle\Sigma^*_{mo(klm)}\rangle\langle\Sigma_{np(klm)}\rangle - \langle\Sigma^*_{np(klm)}\rangle\langle\Sigma_{mo(klm)}\rangle + \\ & + \frac{1}{2}\left[T_{(mn)}, \langle\phi\rangle\right]_{ij}\left[T_{(op)}, \langle\phi\rangle\right]_{ji} + \begin{pmatrix} m \leftrightarrow o \\ n \leftrightarrow p \end{pmatrix}\end{aligned} \quad (2.39)$$

is 45×45 dimensional Hermitian matrix [15]. All the Latin indices $j, \ldots, p$ run over $\{1, \ldots, 10\}$ and the superscripts $(i_1, \ldots, i_n)$ denote $\binom{10}{n}$ ordered pairs of n indices. As before, $\langle\Sigma\rangle$ and $\langle\phi\rangle$ stand for fields Σ and ϕ evaluated in the vacuum, respectively. Let us note that $\mathbf{10}_{\mathbb{C}}$ does not contribute to $\mathbf{M}_G^2$ as it acquires zero vacuum expectation value unless $\mathrm{SU}(3)_c \times \mathrm{SU}(2)_L \times \mathrm{U}(1)_Y$ symmetry breaking is considered.

The tree-level gauge mass-squared matrix eigenvalues at the GUT scale are

$$M_G^2(1,1,0) = 10g^2|\sigma|^2, \tag{2.40}$$
$$M_G^2(1,1,+1) = 2g^2\left(|\sigma|^2 + \omega_R^2\right), \tag{2.41}$$
$$M_G^2(3,1,+\tfrac{2}{3}) = 2g^2\left(|\sigma|^2 + \omega_{BL}^2\right), \tag{2.42}$$
$$M_G^2(3,2,+\tfrac{1}{6}) = 2g^2\left(|\sigma|^2 + \tfrac{1}{4}\left(\omega_R + \omega_{BL}\right)^2\right), \tag{2.43}$$
$$M_G^2(3,2,-\tfrac{5}{6}) = \tfrac{1}{2}g^2\left(\omega_R - \omega_{BL}\right)^2, \tag{2.44}$$

where the $\mathrm{SU}(3)_c \times \mathrm{SU}(2)_L \times \mathrm{U}(1)_Y$ transformation properties of the corresponding gauge fields are written in parentheses. The remaining 12 zero modes correspond to 12 generators of the unbroken SM gauge group.

2.4.2 Tree-level scalar masses

The tree-level scalar mass-squared matrix $\mathbf{M}_S^2$ is obtained by taking second derivatives of the scalar potential V_0:

$$\mathbf{M}_S^2 = \left.\frac{\partial^2 V_0}{\partial\Phi\partial\Phi^*}\right|_{\Phi=\langle\Phi\rangle}, \tag{2.45}$$

where $\Phi \in \{\phi, \Sigma, H\}$ and $\langle\Phi\rangle$ denotes a scalar field evaluated in the vacuum. Eq. (2.45) implicitly assumes that stationarity conditions (2.34)-(2.36) are employed. In general, $\mathbf{M}_S^2$ is the 317×317 dimensional[2] Hermitian matrix. As the eigenstates belonging to different $\mathrm{SU}(3)_c \times \mathrm{SU}(2)_L \times \mathrm{U}(1)_Y$ representations do not mix, there exists a basis in which the scalar mass-squared matrix takes a block diagonal structure with every block corresponding to a separate SM representation. The collection of scalar mass-squares associated with distinct $\mathrm{SU}(3)_c \times \mathrm{SU}(2)_L \times \mathrm{U}(1)_Y$ representations, without considering $\mathbf{10}_{\mathbb{C}}$, is presented in Appendix E.1 in several VEV limits.

The minimal renormalizable SO(10) model is known to be suffering from the presence of tachyonic tree-level states in the scalar spectrum [8, 9]. Observe that the scalar masses of the fields transforming as $(8,1,0)$ and $(1,3,0)$ under the SM $\mathrm{SU}(3)_c \times \mathrm{SU}(2)_L \times \mathrm{U}(1)_Y$ gauge group have the form

$$M_S^2(8,1,0) = 2a_2(\omega_R - \omega_{BL})(\omega_{BL} + 2\omega_R), \tag{2.46}$$
$$M_S^2(1,3,0) = 2a_2(\omega_{BL} - \omega_R)(\omega_R + 2\omega_{BL}), \tag{2.47}$$

which can be simultaneously made non-tachyonic if and only if

$$a_2 > 0, \qquad -2 < \frac{\omega_{BL}}{\omega_R} < -\frac{1}{2}. \tag{2.48}$$

[2]It spans over the 45 real fields ϕ_{ij} together with the 126 and 10 complex fields Σ_{ijklm} and H_i, respectively.

the VEV configuration in Eq. (2.48) directly corresponds to the vicinity of the scenario with flipped-SU(5) intermediate symmetry stage, c.f. Table 2.2. Such a breaking scheme, however, inevitably runs into issues with phenomenological requirements — either one respects the seesaw-compatible hierarchy between VEVs $|\sigma| \ll \max[|\omega_R|, |\omega_{BL}|]$ in the flipped-SU(5)-compatible regime $\omega_{BL} \approx -\omega_R$, causing the mass of the proton mediating gauge boson $M_G^2(3, 2, +\frac{1}{6})$ to be suppressed well below the GUT scale, c.f. Eq. (2.43), which leads to violating current proton lifetime limits, or one performs flipped-SU(5) and SO(10) symmetry breakings close to each other by lifting σ to be right below the GUT scale (almost one-stage symmetry breaking pattern), which inevitably spoils successful gauge coupling unification [104, 123]. Thus no phenomenologically viable scenario allows for a non-tachyonic tree-level scalar spectrum. As a consequence, the minimal renormalizable SO(10) model had been regarded as non-viable for almost 30 years [8, 11]. Fortunately, it was resurrected by invoking radiative corrections [11] — if the a_2 parameter is artificially set to be small, i.e. $|a_2| \ll 1$, then the tree-level masses (2.46)-(2.47) are accidentally suppressed and one-loop mass corrections may remedy undesirable tree-level tachyonicities along potentially viable breaking schemes outside the problematic flipped-SU(5) scenario (2.48).

Let us note that it was shown recently [15] that the tree-level scalar mass spectrum accommodates another state that is prone to tachyonic instabilities outside of the regime (2.48). This scalar field is transforming as a singlet with respect to the $\mathrm{SU}(3)_c \times \mathrm{SU}(2)_L \times \mathrm{U}(1)_Y$ gauge group and its mass acquires the following form

$$M_S^2(1,1,0)_3 = a_2(\omega_{BL} - \omega_R)^2 + 4a_0\left(3\omega_{BL}^2 + 2\omega_R^2\right)\left(1 - \sqrt{1 + \left(\frac{a_2}{a_0}\right)\frac{3(3\omega_{BL}^2 - 2\omega_R^2)(\omega_{BL}^2 - \omega_R^2)}{2\,(3\omega_{BL}^2 + 2\omega_R^2)^2} + \left(\frac{a_2}{a_0}\right)^2 \frac{9\,(\omega_{BL}^2 - \omega_R^2)^2}{16\,(3\omega_{BL}^2 + 2\omega_R^2)^2}}\right) + \mathcal{O}\left(\frac{|\sigma|^2}{\max[|\omega_R|, |\omega_{BL}|]^2}\right), \quad (2.49)$$

assuming the seesaw-compatible regime $|\sigma| \ll \max[|\omega_R|, |\omega_{BL}|]$. The subscripts denote the multiplicity index in the presence of more fields with the same SM quantum numbers in ascending mass ordering. Note that four scalar fields are transforming as singlets with respect to the SM: one is the would-be Goldstone boson, one is the intermediate symmetry breaking Higgs field and the remaining two correspond to the state (2.49) and its companion with the mass $M_S^2(1,1,0)_4$, which is the same as (2.49), but with the opposite sign in front of the square root.

In the well-motivated regime $|a_2| \ll |a_0|$, stemming from the requirement $|a_2| \ll 1$, the expression (2.49) can be approximated as

$$M_S^2(1,1,0)_3 \approx a_2\left(-\frac{45\,\omega_{BL}^4}{3\,\omega_{BL}^2 + 2\,\omega_R^2} + 13\,\omega_{BL}^2 - 2\,\omega_{BL}\omega_R - 2\,\omega_R^2\right) + \mathcal{O}\left(\frac{a_2^2}{a_0^2}, \frac{|\sigma|^2}{\max[|\omega_R|, |\omega_{BL}|]^2}\right). \quad (2.50)$$

In the opposite regime $|a_0| \ll |a_2|$, the masses $M_S^2(1,1,0)_3$ and $M_S^2(1,1,0)_4$ are approximately equal to the octet and triplet masses (2.46)-(2.47).

Assuming $a_2 > 0$, the expression (2.50) is positive if and only if $\omega_{BL} \approx -\omega_R$. Hence we demonstrated again that tachyonic instabilities in the tree-level scalar

mass spectrum can be avoided only in the regime (2.48), which is in the proximity of the troublesome breaking chain with the flipped-SU(5) intermediate symmetry. Thus the radiative mass corrections have to be invoked and the minimal renormalizable SO(10) GUT has to be treated on the quantum level.

Pseudo-Goldstone nature of the tachyonic states

Observe that the tree-level masses of the scalar fields $(8,1,0)$, $(1,3,0)$ and $(1,1,0)$, whose masses are prone to tachyonic instabilities, are determined by one scalar parameter — a_2. Let us show that these fields are pseudo-Goldstone bosons corresponding to a symmetry explicitly broken by the a_2 term in the scalar potential.

We consider the case of an exactly vanishing VEV $\sigma = 0$, which is the limiting case of the phenomenologically motivated seesaw-compatible VEV regime $|\sigma| \ll \max[|\omega_{BL}|, |\omega_R|]$. We can thus focus solely on the **45**-dependent part of the scalar sector and neglect any mixing between **45** and $\mathbf{126}\oplus\mathbf{10}_{\mathbb{C}}$. The relevant part of the scalar potential becomes V_{45} defined in Eq. (2.16). It possesses extra global O(45) symmetry for $a_2 = 0$ [11]. However, once **45** acquires a nonzero VEV in the direction of the SM singlet, the O(45) gets broken to O(44) and 44 massless fields corresponding to the 44 generators of the O(45)/O(44) coset space are expected to appear in the scalar spectrum. As the SO(10) part of the O(45) is gauged and the general alignment of the ω_{BL}, ω_R VEVs in **45** triggers spontaneous symmetry breaking of the SO(10) to the $\mathrm{SU}(3)_c \times \mathrm{SU}(2)_L \times \mathrm{U}(1)_R \times \mathrm{U}(1)_{B-L}$, c.f. Table 2.2, 32 out of these 44 massless modes coincide with would-be Goldstone bosons associated with this local symmetry breaking. The remaining 12 physical massless fields residing in $(8,1,0)$, $(1,3,0)$ and $(1,1,0)$ SM respresentations become true Goldstone bosons.

For non-zero values of a_2, the O(45) breaking term $(\phi\phi)_2\,(\phi\phi)_2$ in V_{45} is reinstated. Hence the Goldstone bosons $(8,1,0)$, $(1,3,0)$ and $(1,1,0)$ can receive only a_2-proportional tree-level contribution, which can be verified by looking at Eqns. (2.46), (2.47) and (2.50). Therefore, from now on, we will refer to these states as pseudo-Goldstone bosons (PGBs).

Thus, to this end, one distinguishes four types of scalar fields:

1. The *would-be Goldstones* have zero mass and get absorbed into longitudinal components of the corresponding massive gauge boson companions. These transform as $(3,2,-\frac{5}{6})$, $(1,1,+1)_1$, $(\bar{3},1,-\frac{2}{3})$, $(3,2,+\frac{1}{6})$, $(1,1,0)_1$ SM multiplets.

2. The *heavy scalars* are defined as having masses that are well estimated by the dominant $M^2_{GUT}-$proportional contributions.

3. The *pseudo-Goldstone bosons* are scalars with accidentally suppressed tree-level $a_2 \cdot M^2_{GUT}$-proportional mass-squares, assuming $|a_2| \ll 1$, whose corresponding one-loop mass corrections can be of the comparable size or dominate over the tree level.

4. The *intermediate-scale scalars* have masses that are $|\sigma|-$proportional to all orders in the perturbative expansion as this property is protected by symmetry, see [124] and Appendix E.2.

2.4.3 Fermion spectrum

The fermion masses can be derived from the Yukawa part $\mathcal{L}_Y$ (2.25) of the Lagrangian by inserting scalar fields evaluated in the vacuum after the SM gauge symmetry $\mathrm{SU}(3)_c \times \mathrm{SU}(2)_L \times \mathrm{U}(1)_Y$ is broken down to the $\mathrm{SU}(3) \times \mathrm{U}(1)_Q$. The complex representations **126** and $\mathbf{10}_{\mathbb{C}}$ contain two complex weak doublets each so four corresponding $\mathrm{SU}(3)_c \times \mathrm{U}(1)_Q$ neutral components can obtain non-zero VEVs,[3] c.f. Tables F.1 and F.4. The projections of the SM Higgs VEV v_{SM} onto these four individual weak doublets are labeled

$$v_{10}^u = \left\langle (1,2,+\tfrac{1}{2})_{10} \right\rangle, \qquad v_{10}^d = \langle (1,2,-\tfrac{1}{2})_{10} \rangle, \tag{2.51}$$

$$v_{126}^u = \left\langle (1,2,+\tfrac{1}{2})_{\overline{126}} \right\rangle, \qquad v_{126}^d = \langle (1,2,-\tfrac{1}{2})_{\overline{126}} \rangle, \tag{2.52}$$

where we refer to the $\mathrm{SU}(3)_c \times \mathrm{SU}(2)_L \times \mathrm{U}(1)_Y$ transformation properties of the fields and the subscripts mark their SO(10) origin. Nonzero VEVs are acquired by $\mathrm{SU}(2)_L$ doublet components with either positive $+\frac{1}{2}$ (denoted u) or negative $-\frac{1}{2}$ (denoted d) hypercharge. Notice that the $\mathrm{SU}(3)_c \times \mathrm{U}(1)_Q$ neutral component of the $\mathrm{SU}(2)_L$ triplet in **126** will also obtain the non-zero induced VEV

$$w = \langle (1,3,+1)_{\overline{126}} \rangle \,. \tag{2.53}$$

Hence the tree-level quark and lepton mass matrices at the GUT scale have the following form [12, 108]:

$$M_U = Y_{10} v_{10}^u + \tilde{Y}_{10} v_{10}^{d\,*} + Y_{126} v_{126}^u, \tag{2.54}$$

$$M_D = Y_{10} v_{10}^d + \tilde{Y}_{10} v_{10}^{u\,*} + Y_{126} v_{126}^d, \tag{2.55}$$

$$M_E = Y_{10} v_{10}^d + \tilde{Y}_{10} v_{10}^{u\,*} - 3 Y_{126} v_{126}^d, \tag{2.56}$$

$$M_\nu^D = Y_{10} v_{10}^u + \tilde{Y}_{10} v_{10}^{d\,*} - 3 Y_{126} v_{126}^u \tag{2.57}$$

with U, D and E subscripts referring to the up, down and charged lepton sectors, respectively, and

$$M_\nu^{M,\text{type I}} = c^I Y_{126}\ \sigma, \qquad M_\nu^{M,\text{type II}} = c^{II} Y_{126}\ w, \tag{2.58}$$

where the superscripts D and M denote the Dirac and (type-I and type-II see-saw) Majorana neutrino mass contributions, respectively. The coefficients c^I, c^{II} include extra numerical factors, such as Clebsch-Gordan coefficients. Note that the presence of Majorana neutrino mass contributions (2.58) directly implies that the Yukawa Lagrangian (2.25) $\mathcal{L}_Y$ evaluated in the SM broken phase explicitly violates lepton number conservation [125]. The light neutrino mass can then be written as

$$m_\nu = M_\nu^{M,typeII} - M_\nu^D \left(M_\nu^{M,typeI} \right)^{-1} M_\nu^D. \tag{2.59}$$

There are several comments to be made concerning the v-VEVs in this minimal realization of the SO(10) GUT:

[3] For the sake of completeness, let us mention that there are three additional $\mathrm{SU}(3)_c \times \mathrm{U}(1)_Q$ singlets residing in **45**, two of which are also SM singlets which obtain ω_{BL} and ω_R proportional VEVs, c.f. Table F.3

- Non-trivial relations between the VEVs (2.51)–(2.53) can be derived by looking at mass ratio $\varrho_0 \equiv \frac{m_W^2}{m_Z^2 \cos^2\theta_W}$, which acquires the following tree-level form [126]

$$\varrho_0 = \frac{|v_{10}^u|^2 + |v_{10}^d|^2 + |v_{126}^u|^2 + |v_{126}^d|^2 + 2|w|^2}{|v_{10}^u|^2 + |v_{10}^d|^2 + |v_{126}^u|^2 + |v_{126}^d|^2 + 4|w|^2}. \tag{2.60}$$

  Thus the w VEV is expected to be much smaller than the other v-VEVs as it explicitly violates the measured relation $\varrho_0 = 1.00030 \pm 0.00020$ [127], i.e.

$$|w|^2 \ll |v_{10}^u|^2 + |v_{10}^d|^2 + |v_{126}^u|^2 + |v_{126}^d|^2. \tag{2.61}$$

  Consequently,

$$|v_{10}^u|^2 + |v_{10}^d|^2 + |v_{126}^u|^2 + |v_{126}^d|^2 \simeq v_{SM}^2. \tag{2.62}$$

  Let us point out that the smallness of w VEV is simultaneously enforced by the requirement $m_\nu \lesssim 1$ eV [127], see Eq. (2.59), if no cancellations between type-I and type-II neutrino mass contributions are assumed.

- The predictive power of the fermion mass relations (2.54)-(2.57) can be increased by considering the non-complexified 10-dimensional representation. In such a case, the real **10** contains only one complex weak doublet; thus

$$v_{10}^u = v_{10}^d, \tag{2.63}$$

  which significantly reduces the complexity of a flavour fit. However, the relation (2.63) is in direct contradiction with the phenomenological requirement [108]

$$\left|\frac{v_{10}^u}{v_{10}^d}\right| \approx \frac{m_t}{m_b} \gg 1. \tag{2.64}$$

  Hence a realistic Yukawa sector is supported only if **10** is complexified.

- A phenomenologically viable flavour fit obtained with tree-level fermion mass relations (2.54)-(2.57) enforces the SM Higgs VEV v_{SM} to be an admixture of the v-VEVs from $\mathbf{10}_{\mathbb{C}}$ as well as **126**. If the SM Higgs VEV projections v_{126}^u, v_{126}^d vanish, the SU(5)−like correlation

$$M_D \approx M_E \tag{2.65}$$

  is recovered at the GUT scale. On the other hand, if v_{10}^u, v_{10}^d are zeroed out, the relation

$$M_D \approx -3M_E \tag{2.66}$$

  holds at the GUT scale. Such correlations are, however, not phenomenologically viable [128].

  By employing the fermion fit results from [113], we can further estimate the amount of the **126** component in the v_{SM} by evaluating the size of the ratio

$$\sqrt{\frac{|v_{126}^u|^2 + |v_{126}^d|^2}{v_{SM}^2}} = \frac{1}{4}\frac{|\mathrm{Tr}M_D - \mathrm{Tr}M_E|}{v_{SM}}\frac{\sqrt{1+|r|^2|s|^2}}{|\mathrm{Tr}Y_{126}|}, \tag{2.67}$$

where

$$r = \frac{v^u_{10}}{v^d_{10}}, \qquad\qquad s = \frac{v^u_{126}}{v^d_{126}}\frac{v^d_{10}}{v^u_{10}}. \tag{2.68}$$

As the Yukawa matrix Y_{126} is typically subject to perturbativity constraints $\mathrm{Tr}\,[Y_{126}] \lesssim 1$, the ratio (2.67) can be restricted from below

$$\sqrt{\frac{|v^u_{126}|^2 + |v^d_{126}|^2}{v^2_{SM}}} \gtrsim \frac{\sqrt{1+|r|^2|s|^2}}{4}\frac{|\mathrm{Tr}M_D - \mathrm{Tr}M_E|}{v_{SM}}. \tag{2.69}$$

Plugging in numerical values from [113], we obtain

$$\sqrt{\frac{|v^u_{126}|^2 + |v^d_{126}|^2}{v^2_{SM}}} \gtrsim 3\times 10^{-2}. \tag{2.70}$$

This demonstrates that the SM Higgs VEV v_{SM} and, consequently, the SM Higgs field $\Phi_H \sim (1,2,+\frac{1}{2})$ has to contain a non-zero admixture of **126** component in a successful fermion mass fit.

Let us note that the numerical fermion fit results used to make the estimate (2.70) assumed the Peccei-Quinn-like symmetry. However, the size of $\mathrm{Tr}M_D - \mathrm{Tr}M_E$ in Eq. (2.69) is fixed by the difference between the SM Yukawas $y_b - y_\tau$ at the GUT scale, irrespective of the Y_{10} and $\tilde{Y}_{10}$. Similarly, the appropriately large top Yukawa from M_U and a small Dirac neutrino mass contribution M^D_ν is achieved only with large $|rs|$ as $M_U - M^D_\nu = (M_D - M_E)rs$. Hence the 2-Yukawa-case fermion fit [113] is applicable for estimating the ratio (2.70) even in the general scenario with 3 Yukawa matrices.

2.5 Proton decay

The Standard Model of Particle Physics possesses accidental global symmetries which manifest themselves in the conservation of baryon $\mathcal{B}$ and lepton $\mathcal{L}$ numbers [129]. Thus one cannot write any SM renormalizable-level Lagrangian operators that would directly lead to the perturbative $\mathcal{B}$ and $\mathcal{L}$ violation. However, such a restriction is lifted in the renormalizable SO(10) GUTs due to the presence of additional gauge and scalar fields.

The aforementioned feature of the SO(10) GUTs opens the door for possible experimental searches for baryon and lepton number violating processes that could test the viability of the model under consideration. Let us focus solely on the proton decay, BNV process which will be further probed by the upcoming large-volume neutrino experiments (DUNE [1], Hyper-K [3], JUNO [2], Theia [4]) that aim to improve nucleon lifetime lower bounds by one order of magnitude with respect to the current limits.

2.5.1 $d = 4$ BNV operators

Let us go back to the SM framework for a moment. As we mentioned earlier, there are no dimension $d \leq 4$ baryon and lepton number violating operators that one

can write into the SM Lagrangian. Since proton decay is mediated by operators with non-zero baryon number, we have to look at the SM Lagrangian beyond the renormalizable level. Suitable non-renormalizable operators, containing at least three quarks that conceive a colour singlet, are composed of at least four fermionic fields.Hence the dimension of BNV operators in the SM is at least six [130].

There are four classes of $d = 6$ BNV operators, which can be schematically written as [130–133]:

$$O^{(1)} = \frac{1}{\Lambda^2}(d_R u_R)(Q_L L_L), \tag{2.71}$$

$$O^{(2)} = \frac{1}{\Lambda^2}(Q_L Q_L)(u_R e_R), \tag{2.72}$$

$$O^{(3)} = \frac{1}{\Lambda^2}(Q_L Q_L)(Q_L L_L), \tag{2.73}$$

$$O^{(4)} = \frac{1}{\Lambda^2}(d_R u_R)(u_R e_R), \tag{2.74}$$

where all $\mathrm{SU}(2)_L$ and $\mathrm{SU}(3)_c$ indices were suppressed, Λ is the SM cutoff scale and, for simplicity, only first-family fermions were used. It turns out that these operators also violate lepton number, but conserve $\mathcal{B} - \mathcal{L}$ as there is exactly one lepton present in every expressions (2.71)–(2.72). In proton decay, $\Delta\mathcal{B} = -1$, and therefore $\Delta\mathcal{L} = -1$, which implies that the final states of the $d = 6$ proton decay processes always contain an antilepton.

Now let us come back to the framework of the minimal SO(10) GUT. The presence of additional scalar and gauge fields allows one to write renormalizable-level operators that directly break baryon number. Consequently, the effective operators (2.71)-(2.74) of four-fermion interactions in the SM correspond to tree-level processes in the SO(10) mediated by heavy gauge or scalar bosons with mass $\Lambda \sim \max[|\omega_R|, |\omega_{BL}|]$, where the heavy field was integrated out. This situation is schematically depicted in Fig. 2.1 for case of the $O^{(1)}$ operator.

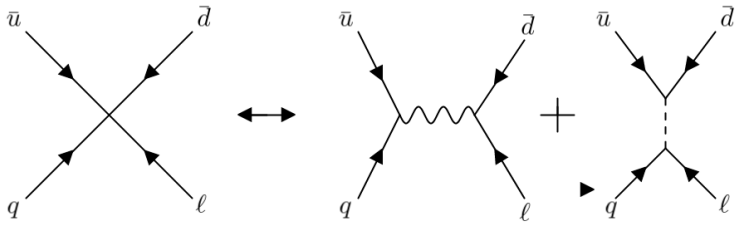

Figure 2.1: Schematic depiction of the relation between the effective SM four-fermion non-renormalizable interaction described by the $O^{(1)}$ operator and the corresponding tree-level renormalizable SO(10) processes mediated by heavy gauge and scalar bosons.

All possible proton decay mediators in the minimal SO(10) and the corresponding effective SM non-renormalizable operators are summarized in Table 2.3. We have already met some of these fields when discussing the gauge sector of SO(10), see Sec. 1.5.

The gauge-boson-mediated proton decay processes often dominate since the tree-level interaction vertices of the scalar mediated decays are suppressed by the

Table 2.3: Proton decay mediators in the minimal SO(10). We present their SM transformation properties, gauge or scalar bosonic type (G or S, respectively) and effective SM non-renormalizable operators they give rise to.

label	$3_c 2_L 1_Y$ representation	G/S	effective operator
X_μ	$(\overline{3}, 2, +\frac{5}{6})$	G	$O^{(1)}$, $O^{(2)}$
Y_μ	$(\overline{3}, 2, -\frac{1}{6})$	G	$O^{(1)}$
Δ_c	$(3, 1, +\frac{1}{3})$	S	$O^{(1)}$, $O^{(2)}$, $O^{(3)}$, $O^{(4)}$
$\tilde{\Delta}_c$	$(3, 1, -\frac{4}{3})$	S	$O^{(4)}$
Δ_{cT}	$(3, 3, -\frac{1}{3})$	S	$O^{(3)}$

numerical smallness of the fist generation Yukawa couplings. Therefore, from now on we will focus solely on the gauge-boson-mediated proton decay.

2.5.2 Partial proton decay widths and experimental limits

All the relevant $d = 6$ proton decay channels are summarized in Table 2.4 together with the corresponding 90% confidence level exclusion bounds. In what follows, we will assume that the neutrino flavour and the chirality of charged leptons cannot be distinguished by proton decay experiments.

Table 2.4: Proton decay channels and the corresponding 90% confidence level exclusion bounds, where τ is the total proton lifetime and $\mathcal{B}$ is the branching ratio of a proton decay channel. The numerical values were taken from the Super-Kamiokande experimental results [134–139].

proton decay channel	$\frac{\tau}{\mathcal{B}}$ [years]
$p \to \pi^0 e^+$	$> 2.4 \cdot 10^{34}$
$p \to \pi^0 \mu^+$	$> 1.6 \cdot 10^{34}$
$p \to K^0 e^+$	$> 1.1 \cdot 10^{33}$
$p \to K^0 \mu^+$	$> 3.6 \cdot 10^{33}$
$p \to \eta^0 e^+$	$> 4.1 \cdot 10^{33}$
$p \to \eta^0 \mu^+$	$> 1.2 \cdot 10^{33}$
$p \to \pi^+ \overline{\nu}$	$> 3.9 \cdot 10^{32}$
$p \to K^+ \overline{\nu}$	$> 6.6 \cdot 10^{33}$

A detailed compilation of $d = 6$ partial proton decay width formulae can be found in [140, 141]. Let us focus on proton decay channels with antineutrinos in the final state:

$$p \to \pi^+ \overline{\nu}, \tag{2.75}$$

$$p \to K^+ \overline{\nu}. \tag{2.76}$$

as the corresponding partial decay widths take on a simple form which does not depend on the flavour structure of the SO(10) GUT due to the symmetric nature

of the Yukawa matrices, c.f. Section. Hence,

$$\Gamma\left(p \to \pi^+ \overline{\nu}\right) = C_\pi \left[k_1^4 |(V_{CKM})_{11}|^2 + k_2^4 + 2k_1^2 k_2^2 |(V_{CKM})_{11}|^2\right], \tag{2.77}$$

$$\Gamma\left(p \to K^+ \overline{\nu}\right) = C_K k_1^4 \left(B_2^2 |(V_{CKM})_{11}|^2 + B_3^2 |(V_{CKM})_{12}|^2\right), \tag{2.78}$$

where we adhered to the notation of [6]. The V_{CKM} is the CKM quark mixing matrix,

$$k_1 = \frac{g}{\sqrt{2} M_G(3,2,-\frac{5}{6})} = \frac{1}{|\omega_R - \omega_{BL}|}, \tag{2.79}$$

$$k_2 = \frac{g}{\sqrt{2} M_G(3,2,+\frac{1}{6})} = \frac{1}{2\sqrt{|\sigma|^2 + \frac{1}{4}(\omega_R + \omega_{BL})^2}} \tag{2.80}$$

with mass relations (2.43)–(2.44) inserted in, and g is the unified gauge coupling at the GUT scale. The prefactors are defined as

$$C_\pi = \frac{(m_p^2 - m_{\pi\pm}^2)^2}{8\pi m_p^3 f_\pi^2} A_L^2 \left(A_S^{(1)}\right)^2 |\tilde{\alpha}|^2 (1 + D + F)^2, \tag{2.81}$$

$$C_K = \frac{(m_p^2 - m_{K\pm}^2)^2}{8\pi m_p^3 f_\pi^2} A_L^2 \left(A_S^{(1)}\right)^2 |\tilde{\alpha}|^2 \tag{2.82}$$

and

$$B_2 = \frac{2m_N}{3m_B} D, \tag{2.83}$$

$$B_3 = 1 + \frac{m_N}{3m_B}(D + 3F). \tag{2.84}$$

The proton, pion and kaon masses are denoted by m_p, $m_{\pi\pm}$ and $m_{K\pm}$, respectively; $m_N \approx m_p$, m_B stands for an average baryon mass ($m_B \approx m_\Sigma \approx m_\Lambda$) and f_π labels the pion decay constant. The proton decay constant $\tilde{\alpha}$ and the coefficients D, F are the chiral Lagrangian parameters evaluated at the μ_{had} scale. The factor

$$A_L = \left(\frac{\alpha_S(\mu_{had})}{\alpha_S(m_b)}\right)^{\frac{6}{25}} \left(\frac{\alpha_S(m_b)}{\alpha_S(M_Z)}\right)^{\frac{6}{23}} \tag{2.85}$$

governs the running effects of the one-loop evolution of the effective four-fermion BNV operators from μ_{had} to M_Z; α_S and m_b are the strong gauge coupling and the bottom quark mass, respectively. The coefficient

$$A_S^{(1)} = \Pi_{i=1}^3 \Pi_I^{M_Z < M_I < M_{GUT}} \left[\frac{\alpha_i(M_{I+1})}{\alpha_i(M_I)}\right]^{\frac{\gamma_i^{(1)}}{b_{Ii}}} \tag{2.86}$$

takes care of the RGE running effects from M_Z to the GUT scale M_{GUT}. It depends on the SM gauge coupling factors $\alpha_i = \frac{g_i^2}{4\pi}$; b_{Ii} are one-loop beta coefficients of α_i in the effective theory between the scales M_I and M_{I+1}, and

$$\gamma^{(1)} = \left(\tfrac{11}{20}, \tfrac{9}{4}, 2\right). \tag{2.87}$$

A detailed derivation of the expression (2.86) can be found in Appendix C.

2.5.3 Theoretical uncertainties

As we already mentioned, the upcoming new experiments [1–4] will further improve the exclusion bounds on partial widths of various proton decay channels. However, such advancement will typically reach a maximal proton decay width improvement rate of one order of magnitude per decade of experimental measurements. Hence the community would benefit the most from the aforementioned experimental progress if the theoretical uncertainties of proton lifetime predictions were confined within the one-order-of-magnitude window. Unfortunately, that is not the case as proton lifetime theoretical uncertainties typically span several orders of magnitude, c.f. Table II in [142] or Figure 2 in [5].

The proton lifetime theoretical uncertainties [6] come from the ambiguities in measurements and/or calculations of quantities entering the partial decay width formulae such as Eqns. 2.77-(2.78). They can be divided into two main categories, resulting either from insufficient experimental data at low energies or from purely theoretical uncertainties originating from perturbative expansion and Planck-scale physics.

Purely theoretical uncertainties

Purely theoretical uncertainties are *reducible* or *irreducible*. *Reducible* theoretical uncertainties typically stem from the finite perturbative order calculations, the *irreducible* theoretical uncertainties arise from Planck-scale effects:

- Reducible uncertainties: As we have mentioned before, the reducible uncertainties come from the fact that proton lifetime calculations are typically performed at a fixed order in perturbation theory. These uncertainties can be improved by adding higher-order corrections.

  It turns out that the proton lifetime calculations are most affected by the accuracy of the perturbative computation of proton decay mediator masses since they enter $d = 6$ partial decay widths as inverse fourth powers through the k_i dependence, c.f. Eqns. (2.77)-(2.78). Hence, even small perturbative uncertainty in k_i can result in huge ambiguity in the final proton lifetime prediction.

  The values of M_{GUT}, unified gauge coupling g and, consequently, the k_i quantities are determined by the gauge coupling unification constraints. The difference between proton decay widths obtained by employing one-loop or two-loop gauge beta functions can be estimated by [6]

$$\frac{\Gamma^{2-loop}}{\Gamma^{1-loop}} \approx \exp\left(4k \log \frac{M_{GUT}}{M_Z}\right), \tag{2.88}$$

  where

$$\log \frac{M_{GUT}}{M_Z} \approx 34.5 \tag{2.89}$$

  for $M_{GUT} \approx 10^{15}\,\text{GeV}$ and k is the typical size of the ratio between two-loop corrections of beta coefficients and their one-loop values. Expression (2.88) potentially exceeds several orders of magnitude even for $|k| \approx \mathcal{O}(1)\%$ and

therefore every perturbatively robust proton lifetime calculation requires at least two-loop gauge coupling RGE analysis. Let us note that the requirement of the two-loop gauge unification goes hand in hand with the need for proper high-energy scalar spectrum analysis to account for threshold corrections.

- Irreducible uncertainties: Irreducible uncertainties stem from the effects of the Planck-scale physics and thus there are typically no means to control them. However, we can estimate their effect by considering Planck-scale suppressed non-renormalizable operators. The biggest impact on proton lifetime prediction have $d = 5$ operators

$$\mathcal{O}_1 = \kappa_1 F^{\mu\nu} F_{\mu\nu} \frac{\phi}{M_{Pl}}, \tag{2.90}$$

$$\mathcal{O}_2 = \kappa_2^{pq} \Omega^p \Omega^q H_{SM} \frac{\phi}{M_{Pl}}, \tag{2.91}$$

where $\kappa_1, \kappa_2 \in \mathcal{O}(1)$ are unknown couplings, $H_{SM} \in \{\Sigma, H\}$ contains the SM Higgs doublet, $p, q = 1, \ldots, 3$ are family indices and we suppressed the spinorial structure of $\mathcal{O}_2$. Expressions (2.90)-(2.91) form a complete set of $d = 5$ structures which contain SO(10) symmetry breaking field ϕ.[4]

The $\mathcal{O}_1$ operator alters the gauge-kinetic part of the Lagrangian in the broken phase and thus introduces inhomogeneous shifts in the gauge coupling values at high-energy scales. This can dramatically modify the determination of the GUT scale and, consequently, the proton lifetime predictions through the k_i dependence, c.f. discussion about *reducible* uncertainties. The $\mathcal{O}_2$ operator affects Yukawa matching conditions between the SO(10) GUT at high energies and the SM at low energies. Such Planck-scale-induced modifications directly alter flavour-dependent parts of the proton decay width.

Let us emphasise that the minimal SO(10) GUT under out to be robust with respect to both aforementioned irreducible uncertainties. The $\mathcal{O}_1$ operator can be formed if and only if the scalar **45** is contained in the symmetric product of two adjoint representations. Since the product decomposition [103]

$$(\mathbf{45} \otimes \mathbf{45})_{sym} = \mathbf{1}_{sym} \oplus \mathbf{54}_{sym} \oplus \mathbf{210}_{sym} \oplus \mathbf{770}_{sym} \tag{2.94}$$

does not contain **45** of SO(10), the $\mathcal{O}_1$ vanishes identically. Moreover, the numerical study [7] showed that the flavour effects induced by the $\mathcal{O}_2$ oper-

[4] In principle, the aforementioned set of operators can be accompanied by two additional operators

$$\mathcal{O}_3 = \kappa_3^{pq} \Omega^p \not{D} \Omega^q \frac{\phi}{M_{Pl}}, \tag{2.92}$$

$$\mathcal{O}_4 = \kappa_4 D_\mu \Phi D^\mu \Phi \frac{\phi}{M_{Pl}}, \tag{2.93}$$

where $\kappa_3, \kappa_4 \in \mathcal{O}(1)$ are unknown couplings, $\Phi \in \{\phi, \Sigma, H\}$, $p, q = 1, \ldots, 3$ are family indices and spinorial structure of $\mathcal{O}_3$ was suppressed. However, these can be removed by using equations of motion and integration by parts [143].

ator are not spoiling the desired one-order-of-magnitude window of theoretical uncertainties in proton decay channels (2.75)–(2.76) with antineutrino final states.

Low-energy uncertainties

Low-energy uncertainties come from the limited information available in the low-energy data — either for hadronic matric elements or for flavour fits.

- Uncertainties in hadronic matrix elements: An integral part of the proton decay predictions is the knowledge of hadronic matrix elements which provide translation between hadronic initial/final states and quark-level processes. They are computed on lattice and/or by using chiral perturbation theory [144]. Luckily, the accuracy of their determination has greatly improved over the last decades [6, 144–146] and the errors introduced by hadronic matrix elements are no longer obstructing relatively good proton lifetime predictions [6].

- Flavour structure uncertainties: Successful determination of partial decay widths involves the matching of the GUT-scale Yukawa matrices with the low-energy flavour data. Such a task is complicated by the insufficient amount of available experimental observables (lepton and quark masses, PMNS and CKM mixing parameters), which typically do not admit a full recontruction of the GUT-scale Yukawa matrices. Fortunately, the symmetric nature of the minimal SO(10) Yukawa matrices yields great simplification in proton width formulae for channels with antineutrinos in the final state [140], c.f. Eqns. (2.77)-(2.78).

We have shown that the proton lifetime predictions are typically plagued by many theoretical uncertainties that are not always under control. In the minimal SO(10) GUT framework, it turns out that the calculation of partial proton decay widths with antineutrinos in the final state is robust with respect to the irreducible uncertainties coming from the flavour fits as well as the Planck-scale physics. Such observation implies that for these decay channels, it is, in principle, possible to carry out partial proton decay width analysis in the minimal SO(10) GUT with theoretical uncertainties confined within the one-order-of-magnitude window.

3. Analysis of the minimal SO(10) GUT

Motivated by the possibility to achieve proton lifetime prediction with theoretical uncertainty confined within the one-order-of-magnitude window, we perform a thorough analysis of the minimal SO(10) GUT under consideration.

The analysis of the minimal SO(10) GUT is presented in the following steps: In Sec. 3.1, various theoretical and phenomenological consistency constraints applied to the allowed parameter space are introduced at the conceptual level. We show that only two breaking chains with the $\mathrm{SU}(4)_C \times \mathrm{SU}(2)_L \times \mathrm{U}(1)_R$ and $\mathrm{SU}(3)_c \times \mathrm{SU}(2)_L \times \mathrm{SU}(2)_R \times \mathrm{U}(1)_{B-L}$ intermediate symmetries lead to potentially realistic scenarios. In Sec. 3.2, we provide the numerical model analysis of these two fully consistent breaking chains in the simplified $\mathbf{45} \oplus \mathbf{126}$ SO(10) Higgs model where details of the Yukawa sector are neglected. A clear preference for the former symmetry breaking pattern is identified. Therefore in Sec. 3.3 we carry out the full analysis of the $\mathbf{45} \oplus \mathbf{126} \oplus \mathbf{10}_{\mathbb{C}}$ SO(10) theory in case of the breaking chain with a well-pronounced $\mathrm{SU}(4)_C \times \mathrm{SU}(2)_L \times \mathrm{U}(1)_R$ intermediate symmetry.

Let us stress that we present only a streamlined version of both model analyses. The interested reader is deferred to articles [16, 17] to account for all details.

3.1 Viability constraints

We provide an overview of the *viability* constraints that have to be satisfied by the minimal SO(10) theory. All the criteria are considered for any given point in the parameter space and they include non-tachyonicity of the mass spectrum (Sec. 3.1.1), SM gauge coupling unification (Sec. 3.1.2) and perturbativity (Sec. 3.1.3). These can be imposed upon the $\mathbf{45} \oplus \mathbf{126} \oplus \mathbf{10}_{\mathbb{C}}$ SO(10) GUT as well as the simplified $\mathbf{45} \oplus \mathbf{126}$ SO(10) Higgs model.

3.1.1 Non-tachyonicity of the scalar spectrum

The perturbative expansion in the broken phase has to be developed around a vacuum that corresponds to the minimum of the scalar potential in which all physical scalar masses are non-tachyonic.

At the tree level, the $(8,1,0)$, $(1,3,0)$, $(1,1,0)$ scalar SM multiplets suffer from tachyonic mass instabilities in realistic symmetry breaking scenarios, c.f. Sec. 2.4. Hence radiative corrections have to be invoked to correct for these undesirable tree-level tachyonicities. For that purpose, we developed a numerical procedure to calculate the full one-loop effective masses to all scalar states in the simplified $\mathbf{45} \oplus \mathbf{126}$ SO(10) Higgs model as well as in the $\mathbf{45} \oplus \mathbf{126} \oplus \mathbf{10}_{\mathbb{C}}$ SO(10) GUT, c.f. Appendix D for definition of the one-loop effective mass. Let us emphasize that this is a significant improvement from the partial one-loop calculations in [11, 13–15].

There are several conceptual remarks to be made:

- One-loop corrections do not significantly alter masses, and consequently the tree-level non-tachyonicity, of the *heavy scalars* whose tree-level masses are dominated by the M_{GUT}-proportional contributions.

- One-loop corrections to the *intermediate-scale scalars* with σ-proportional masses should be calculated in the intermediate-stage effective field theory, which typically has a much smaller number of field degrees of freedom than the full SO(10) model and thus the σ-proportional masses are expected to obtain only small one-loop corrections. We therefore simplify the analysis by considering such *intermediate-scale masses* only at the tree level.

- In the simplified $\mathbf{45} \oplus \mathbf{126}$ SO(10) Higgs model we have only partial information about the mass matrices of the SM scalar multiplets $(\bar{3}, 1, +\frac{1}{3})$ and $(1, 2, +\frac{1}{2})$ as they will eventually mix with additional pair of doublets $(1, 2, +\frac{1}{2})$ and two triplets $(\bar{3}, 1, +\frac{1}{3})$ from $\mathbf{10}_{\mathbb{C}}$.[1] In such a case, we have access only to the full 3×3 (triplet) or 2×2 (doublet) sub-blocks of the 5×5 and 4×4 full mass matrices, respectively, c.f. Eqns.(3.58) and (3.61). Still, it is possible to formulate the necessary, but not sufficient, non-tachyonicity condition on the sub-blocks of the mass matrices corresponding to these SM multiplets by invoking Sylvester's criterion [147] and requiring positivity of all their leading principal minors (i.e. determinants of the $1 \times 1, 2 \times 2, \ldots$ upper-left matrix sub-blocks).

Finally, let us stress that the one-loop effective mass is not physical since it lacks contributions from the momentum-dependent part of the field self-energy [148]. As such it is prone to large logarithmic contributions of the form

$$\log\left[\frac{m_l^2}{\mu_R^2}\right], \tag{3.1}$$

where $m_l^2 \ll \mu_R^2$ is the mass of a scalar or a gauge field which is much lighter than the rest of the spectrum and appears in the loop of a Feynman diagram contributing to the relevant one-loop effective mass. By studying the Abelian Higgs model. c.f. Appendix D, it is suggested to replace the unphysically large logarithm (3.1) by

$$\log\left[\frac{m_l^2}{\mu_R^2}\right] \mapsto \log\left[\frac{m_S^2}{\mu_R^2}\right] + \log[c] + I(c) \tag{3.2}$$

with m_S^2 being the tree-level mass of the field we calculate the one-loop effective mass to, $c = \frac{m_l^2}{m_S^2}$ and $I(c) = \int_0^1 dx \log\left|1 - \frac{x(1-x)}{c}\right|$. Since the numerical evaluation of $I(c)$ for every effective mass contribution would be time-consuming, and the behaviour of $\log[c] + I[c]$ and $\log[c]$ does not differ much for most values of c, see Figure 3.1, we simplify the replacement rule (3.2) by following $\log[c]$ (**blue** curve) for $c > c_0 \approx 0.0763$ with c_0 being determined by $I(c_0) = 0$ and then using constant value $\log[c_0]$ for $c \leq c_0$.

[1] Notice that in the minimal SO(10) Higgs model we also neglect the one-loop scalar mass corrections originating from $\mathbf{10}_{\mathbb{C}}$. These, however, are likely to be insignificant due to the small number of additional scalar fields in loops.

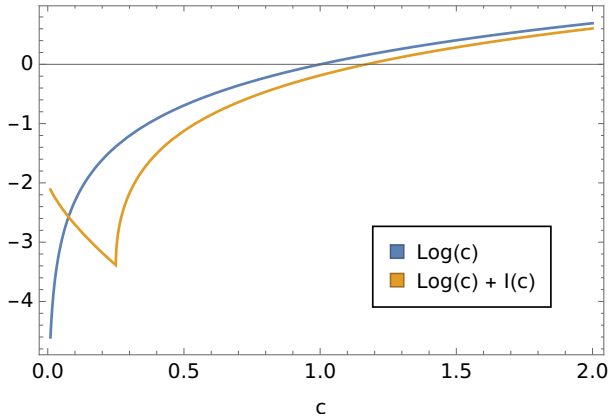

Figure 3.1: The behaviour of logarithmic contributions to the one-loop effective scalar masses without (**blue** curve, $\log[c]$) and with (**orange** curve, $\log[c]+I(c)$) taming of the large logarithms. The ratio $c = \frac{m_l^2}{m_S^2}$ relates the tree-level scalar masses m_l^2 and m_S^2 of fields in the loop and on the outer legs of a Feynman diagram contributing to the one-loop effective mass.

Therefore we define the *regularized one-loop effective scalar mass* as an improved version of the one-loop effective mass with all logarithmic terms (3.1) replaced by

$$\log\left[\frac{m_l^2}{\mu_R^2}\right] \mapsto \begin{cases} \log\left[\frac{|m_l^2|}{\mu_R^2}\right] & \text{if } |c| > c_0, \\ \log\left[c_0 \cdot \frac{|m_S^2|}{\mu_R^2}\right] & \text{if } |c| \leq c_0. \end{cases} \tag{3.3}$$

The ratio c and all the arguments of the logs are taken in absolute values to avoid computational issues with potentially tachyonic contributions. This procedure is referred to as *taming of the logs*. It can be shown that in the perturbative regime, non-tachyonicity of the regularized one-loop effective mass implies non-tachyonicity of the physical mass; for details see Appendix A of [16]. Hence we use the regularized one-loop effective masses to assess the non-tachyonicity of the scalar spectrum.

3.1.2 Gauge coupling unification

In consistent Grand Unified Theory the SM gauge couplings are expected to unify at M_{GUT}. We employ the top-down approach, where the value of the SO(10) unified gauge coupling g is run from M_{GUT} down to the Z-boson mass scale by using gauge coupling RGEs to properly fit the EW-scale experimental values [149–153]

$$\alpha_c^{-1}(M_Z) = 8.550 \pm 0.065, \tag{3.4}$$
$$\alpha_L^{-1}(M_Z) = 29.6261 \pm 0.0051, \tag{3.5}$$
$$\alpha_1^{-1}(M_Z) = 59.1054 \pm 0.0031, \tag{3.6}$$

c.f. Appendix A.

Gauge unification in the $\mathbf{45} \oplus \mathbf{126}$ SO(10) Higgs model

For the purposes of the $\mathbf{45} \oplus \mathbf{126}$ SO(10) Higgs model study, the gauge coupling unification is examined at the one-loop level, despite proper proton decay analysis requiring implementation at least at two loops, c.f. Sec. 2.5. The gauge coupling unification is performed in the SM effective theory complemented by the information about the full SO(10) mass spectrum. However, in the simplified Higgs model, we have access only to part of the mass matrices of the SM multiplets $(\bar{3}, 1, +\frac{1}{3})$ and $(1, 2, +\frac{1}{2})$, and hence their eigenvalues $M_S^2(\bar{3}, 1, +\frac{1}{3})_{1,2,3}$ and $M_S^2(2, 1, +\frac{1}{2})_{1,2}$ (see Table E.1 for their tree-level form) are not the proper eigenvalues of the corresponding full mass matrices. We mimic the realistic situation with an extra $\mathbf{10}_{\mathbb{C}}$ scalar representation in the following way:

- One of the doublets $(1, 2, +\frac{1}{2})$ is set to play the role of the SM Higgs and its mass is fixed to be 125 GeV. The mass of another doublet is assigned to be equal to the geometric mean of $M_S^2(2, 1, +\frac{1}{2})_{1,2}$.
- Masses $M_S^2(\bar{3}, 1, +\frac{1}{3})_{1,2,3}$ are used as an approximation of three eigenvalues of the full triplet mass matrix.
- Remaining two doublet $(1, 2, +\frac{1}{2})$ and two triplet $(\bar{3}, 1, +\frac{1}{3})$ eigenstates stemming from an extra $\mathbf{10}_{\mathbb{C}}$ are assumed to have masses exactly equal to M_{GUT} and thus they induce only negligible shift in the position of g and no change in the unification scale. In the realistic case with the minimal survival hypothesis invoked, these doublets and triplets cluster around M_{GUT} and their masses deviate from the degenerate scenario only minimally.

For every parameter point, the positions of M_{GUT} and σ scales, as well as gauge coupling g at the point of unification, are analytically determined to exactly fit the experimental values (3.4)-(3.6). For further details, the interested reader is deferred to Appendix B 1 b of [16].

Gauge unification in the $\mathbf{45} \oplus \mathbf{126} \oplus \mathbf{10}_{\mathbb{C}}$ SO(10) GUT

Fully-fledged two-loop gauge coupling unification analysis with one-loop threshold corrections is applied in case of the $\mathbf{45} \oplus \mathbf{126} \oplus \mathbf{10}_{\mathbb{C}}$ SO(10) model study. It is carried out by considering a sequence of two effective theories

$$\mathrm{SO}(10) \to G \to \mathrm{SU}(3)_c \times \mathrm{SU}(2) \times \mathrm{U}(1)$$

with G being the intermediate gauge symmetry. The procedure assumes a spectrum with one of the doublets identified with the SM Higgs. This requires that two remaining doublets have masses around M_{GUT} and one doublet mass resides around σ scale, c.f. Sec. 3.3.2. Unlike in the one-loop case, the gauge coupling g and the scales M_{GUT}, σ cannot be determined analytically; hence they are taken as input parameters of the numerical two-loop gauge RGE analysis, and we constrain their values by requiring the computed SM gauge couplings to be within $\chi^2 < 9$ of the experimental values (3.4)-(3.6). Further details can be found in Appendix B of [17].

3.1.3 Perturbativity

All one-loop mass computations implicitly assume that the use of a perturbation expansion is justified. However, the presence of $\mathcal{O}(100)$ quantum fields contributing to the loop corrections raises concerns about the robustness of the perturbative calculations. Therefore we introduce several perturbativity criteria which ensure that our computations remain self-consistent. Let us note that the following perturbativity constraints are discussed here only conceptually and technical details can be found in Appendix B 1 c of [16]. Perturbativity constraints imposed upon *viable* parameter points are deliberately chosen to be rather mild and thus we discard only severely non-perturbative points.

Perturbative VEV configurations

First perturbativity constraint stems from the potentially large VEV structure

$$\frac{\omega_{BL}\omega_R}{|\sigma|^2}\left(\omega_{BL}+\omega_R\right) \tag{3.7}$$

appearing in stationarity conditions and consequently in scalar masses. At the tree level, the structure (3.7) is always accompanied by the a_2 scalar parameter, c.f. (2.35)-(2.36), and thus all possible divergencies for $|\sigma| \ll |\omega_{BL}|, |\omega_R|$ can be tamed by imposing $a_2 \ll 1$, which is precisely the limit suitable for solving the PGB tree-level tachyonicity issue. However, the VEV structure (3.7) occurs not only at the tree level but also in the (polynomial part of the) one-loop corrections with several dimensionless parameters other then a_2 as prefactors. Let us explicitly demonstrate this on the one-loop stationarity condition for τ :

$$\begin{aligned}\tau_{1-loop} = \frac{1}{64\pi^2}\Big(&64\pi^2 a_2 - 288 a_0 a_2 - 228 a_2^2 + 24\alpha a_2 - 48 a_2\beta_4 - 480 a_2\beta_4' + \\ &+2a_2\lambda_0 - 492 a_2\lambda_2 - 708 a_2\lambda_4 + 48 a_2\lambda_4' + 15\beta_4^2 - 180\beta_4\beta_4' + \\ &+300\beta_4'^2 - 1680|\gamma|^2 - 5g^4\Big)\frac{\omega_{BL}\omega_R(\omega_{BL}+\omega_R)}{|\sigma|^2} + \cdots\end{aligned} \tag{3.8}$$

It is difficult to keep τ_{1-loop} perturbative by suppressing the coupling-dependent prefactor due to the presence of relatively large gauge coupling ($g \sim 0.5$). Moreover, if the scalar coupling values were fine-tuned so that they compensate for the effect of g, the prefactor cancellation would eventually be disrupted even by a small change in the renormalization scale due to the non-negligible RGE running of all scalar parameters. Thus we deal with problematic VEV structure (3.7) by restricting possible VEV configurations, i.e. we require

$$\frac{|\omega_{BL}\omega_R(\omega_{BL}+\omega_R)|}{|\sigma|^2} \lesssim \max\left[|\omega_{BL}|, |\omega_R|\right]. \tag{3.9}$$

There are only four possible distinctive breaking chains corresponding to four perturbative VEV combinations in which the structure (3.7), omnipresent at the quantum level, is tamed:

1. $|\sigma| \approx \max\left[|\omega_{BL}|, |\omega_R|\right]$ inducing approximate single-stage spontaneous symmetry breaking of SO(10) to the SM $\mathrm{SU}(3)_c \times \mathrm{SU}(2)_L \times \mathrm{U}(1)_Y$,

2. $\omega_{BL} \approx -\omega_R$ inducing two-stage spontaneous symmetry breaking with the flipped-SU(5) intermediate-symmetry stage,

3. $|\omega_{BL}| \ll |\sigma| \ll |\omega_R|$ inducing two-stage spontaneous symmetry breaking with the $\mathrm{SU}(4)_C \times \mathrm{SU}(2)_L \times \mathrm{U}(1)_R$ intermediate-symmetry stage,

4. $|\omega_R| \ll |\sigma| \ll |\omega_{BL}|$ inducing two-stage spontaneous symmetry breaking with the $\mathrm{SU}(3)_c \times \mathrm{SU}(2)_L \times \mathrm{SU}(2)_R \times \mathrm{U}(1)_{B-L}$ intermediate-symmetry stage.

As we already mentioned in Sec. 2.4.2, single-stage spontaneous symmetry breaking is not compatible with gauge coupling unification and the scenario with the flipped-SU(5) intermediate-symmetry stage violates current proton lifetime limits. Therefore the first two cases are phenomenologically disfavoured and we are left with only two viable scenarios corresponding to the $|\omega_{BL}| \ll |\sigma| \ll |\omega_R|$ (referred to as $\omega_{BL} \to 0$) and the $|\omega_R| \ll |\sigma| \ll |\omega_{BL}|$ (referred to as $\omega_R \to 0$) limits with $\mathrm{SU}(4)_C \times \mathrm{SU}(2)_L \times \mathrm{U}(1)_R$ and $\mathrm{SU}(3)_c \times \mathrm{SU}(2)_L \times \mathrm{SU}(2)_R \times \mathrm{U}(1)_{B-L}$ intermediate breaking stages, respectively. Let us note that in both of these scenarios, the subdominant ω plays a role of an induced VEV and it influences our computation only through the universal VEV ratio χ defined in Eq. (2.37). Consequently the criterion (3.9) implies

$$|\chi| \lesssim 1. \tag{3.10}$$

Global mass perturbativity

Let us now introduce the global mass perturbativity criterion which restricts the relative size of one-loop corrections with respect to the tree-level masses. In practice, we define the quantity $\overline{\Delta}$ to measure overall mass shifts

$$\overline{\Delta} := \frac{\max_{i,j \in \text{heavy fields}} \left[\left| M^2_{ij,\text{one-loop}} - M^2_{ij,\text{tree}} \right| \right]}{\overline{M^2_{\text{heavy}}}}, \tag{3.11}$$

where $M^2_{ij,\text{tree}}$ and $M^2_{ij,\text{one-loop}}$ are tree-level and regularized one-loop effective scalar masses, c.f. Sec. 3.1.1, respectively; $\overline{M^2_{\text{heavy}}}$ denotes the average of the *heavy* tree-level scalar masses over real degrees of freedom. Observe that $\overline{\Delta}$ includes only one-loop corrections to *heavy* masses as *intermediate-scale* masses are taken at tree-level and for the one-loop shifts of the PGBs it is even desirable that they are larger than the corresponding accidentally light tree-level masses. All the *viable* points in the parameter space then have to satisfy

$$\overline{\Delta} < 1. \tag{3.12}$$

Stability under RG running

Regularized one-loop effective masses discussed in Sec. 3.1.1, and consequently global mass perturbativity criterion (3.12), possess residual renormalization scale dependence, c.f. the Abelian Higgs model study in Appendix D. Hence we demand loop corrections to be under control even if the renormalization scale is changed, which is not always easy to accomplish in the environment of GUTs with many field degrees of freedom contributing to loops.

Potential pathologies stemming from the renormalization scale dependence technically manifest themselves by the presence of a Landau pole in the RG flow of a coupling. To avoid such scenarios, the full set of one-loop beta functions of all dimensionless scalar couplings was derived, see Appendix B, and it was used to impose stability under the RG running. We define the following perturbativity measures:

$$t_{\pm} := \log_{10} \left| \frac{\mu_{R\pm}}{\mu_R} \right| \tag{3.13}$$

and

$$\bar{t} := \sqrt{t_+ t_-}, \tag{3.14}$$

where μ_R labels the initial choice of the renormalization scale and $\mu_{R\pm}$ are upper/lower renormalization scale limits at which the system of dimensionless couplings' RGEs blows up. Quantities t_+ and t_- determine how many orders of magnitude the scalar couplings can run above and below the initial μ_R value before encountering a Landau pole, respectively, whereas $\bar{t}$ is interpreted as the averaged amount of RGE running up and down before the RGE system blows up. The larger the $t_{\pm}$ and/or $\bar{t}$, the more numerically robust our loop calculations are with respect to the RG running. We impose

$$t_+ > 0.5 \tag{3.15}$$

to ensure that one can safely run the *viable* points at least half-an-order magnitude up in the renormalization scale.

Vacuum position stability

Another perturbativity criterion concerns the stability of the position of the broken-phase vacuum in the VEV space. In practice, we require that the one-loop $\{\mu^2, \nu^2, \tau\}$-values are not "too far" from their tree-level positions, c.f. point 3 in Appendix B 1 c of [16]. The vacuum position stability test is repeated also after the running of the dimensionless scalar couplings half an order of magnitude up in the renormalization scale, thus further establishing the robustness of our numerical calculations with respect to the RG running.

Such perturbativity constraint may seem rather arbitrary as it depends on the rescaling of the non-physical quantities $\{\mu^2, \nu^2, \tau\}$ whose normalization was chosen in such a way that $-\mu^2$ and $-\nu^2$ are masses of the scalar fields in the unbroken phase. However, stationarity conditions, and consequently $\{\mu^2, \nu^2, \tau\}$, are an integral part of the scalar effective mass calculations and a big shift in the one-loop vacuum position typically induces large one-loop mass corrections. Moreover, the vacuum position stability is easier to computationally verify than the preceeding two perturbativity constraints and thus it is therefore used as the first fast criterion to discard badly non-perturbative patches of the parameter space.

Iterative PGB masses

The last perturbativity constraint we implement emerges from the technical aspects of the taming of the logs (3.2), due to which the one-loop calculation of the

regularized effective masses is prone to being non-reliable for pseudo-Goldstone bosons. In practice, a one-loop regularized effective mass of a PGB scalar can be schematically written as

$$M^2_{PBG,1-loop} = C_1 + C_2 \log \frac{M^2_{PGB,tree}}{\mu^2_R}, \tag{3.16}$$

where C_1 and C_2 are coefficients independent of the PGB mass M^2_{PGB}. Logarithmic dependence in (3.16) originates from contributions of Feynman diagrams with pseudo-Goldstone fields in the loop or from the replacement rule (3.3) in case of one-loop mass corrections involving lighter (*intermediate-scale*) fields. Since the PGB tree-level mass $M^2_{PGB,tree}$ is accidentally suppressed, the log contribution in (3.16) is artificially enhanced and the C_2-proportional term might dominate over C_1. This situation is undesirable because the C_2 contribution stems from the mere approximations introduced in the taming of the logs and hence the computationally stable loop calculation should not be overly sensitive to $\log \frac{M^2_{PGB,tree}}{\mu^2_R}$-proportional terms.

We test for such ill-behaved cases by carrying out iterative PGB mass computation according to the prescription

$$M^2_{PGB,(i+1)} = C_1 + C_2 \log \frac{|M^2_{PGB,(i)}|}{\mu^2_R} \tag{3.17}$$

with the starting values $M^2_{PGB,(0)} = M^2_{PGB,tree}$, $M^2_{PGB,(1)} = M^2_{PGB,1-loop}$ and $i \leq 30$. Ultimately, the one-loop calculations are deemed reliable only if $M^2_{PGB,(1))}$ and the converged PGB mass are not "too far" from each other, c.f. point 4 in Appendix B 1 c of [16].

3.2 The minimal SO(10) Higgs model analysis

The preliminary numerical analysis of the $\mathbf{45} \oplus \mathbf{126}$ SO(10) Higgs model is performed in the two symmetry breaking scenarios $\omega_{BL} \to 0$ and $\omega_R \to 0$ with $\mathrm{SU}(4)_C \times \mathrm{SU}(2)_L \times \mathrm{U}(1)_R$ and $\mathrm{SU}(3)_c \times \mathrm{SU}(2)_L \times \mathrm{SU}(2)_R \times \mathrm{U}(1)_{B-L}$ intermediate symmetry stages, respectively, which were identified in Sec. 3.1.3 as the only phenomenologically viable breaking chains leading to perturbative VEV combinations. Although the minimal SO(10) GUT requires adding a $\mathbf{10}_{\mathbb{C}}$ into the scalar sector of the theory to account for the observed SM fermion masses, c.f. Sec. 2.4.3, the aforementioned extra scalars do not influence spontaneous symmetry breaking of the SO(10) to the SM $\mathrm{SU}(3)_c \times \mathrm{SU}(2)_L \times \mathrm{U}(1)_Y$. Moreover, the one-loop mass corrections originating from $\mathbf{10}_{\mathbb{C}}$ are subdominant because of the small representation dimensionality. Hence the absence of $\mathbf{10}_{\mathbb{C}}$ has only a little qualitative effect on the high energy part of the spectrum and thus it allows us to analyse the shape of the *viable* parameter space enforced by non-tachyonicity, perturbativity and gauge coupling unification constraints in the simplified setting of the minimal SO(10) Higgs model.

First, we semi-analytically discuss the non-tachyonicity criterion in the $\sigma \to 0$, $a_2 \to 0$ limit in Sec. 3.2.1. The full numerical analysis of the parameter space and its results are presented in Sec. 3.2.2, where the preference for $\omega_{BL} \to 0$ regime is clearly demonstrated. The main results are summarized in Sec. 3.2.4.

3.2.1 Analytical aspects

It turns out that one can get a semi-analytical insight into the non-tachyonicity constraint in the limit $\sigma \to 0$, motivated by the seesaw-compatible hierarchy $|\sigma| \ll \max[|\omega_{BL}|, |\omega_R|]$, and $a_2 \to 0$, in which the tree-level potentially large tachyonic scalar mass contributions (2.46)–(2.47) are suppressed.

In such a $\sigma \to 0$, $a_2 \to 0$ regime of the minimal SO(10) Higgs model, the *intermediate-scale* masses vanish, the pseudo-Goldstone masses are fully determined by radiative corrections and the *heavy* scalar masses are well approximated by the tree-level expressions in Table E.1. Consequently, the whole tree-level scalar spectrum is dictated by three real scalar couplings a_0, β_4, β_4', one complex scalar coupling γ_2 and the unified gauge coupling, whose value can be fixed to $g = 0.5$ in consistency with the numerical results of Sec. 3.2.2. The coupling a_0 influences solely the mass of the heaviest SO(10)-breaking Higgs field (transforming as the SM singlet) whose non-tachyonicity can always be assured by a suitable choice of a_0 value.

Furthermore, the one-loop radiative corrections to PGBs do not depend on the phase of the γ_2 parameter. Such observation can be deduced from Figures 3.2–3.3 as the non-tachyonic regions of the PGB one-loop masses in the $\sigma \to 0$, $a_2 \to 0$ limit adhere to the $(\beta_4, \beta_4') \to (-\beta_4, -\beta_4')$ symmetry, which prohibits the presence of $\beta_4\gamma_2$, $\beta_4'\gamma_2$ mixed terms. Thus the relevant part of the scalar spectrum is fully controlled by the β_4, β_4', $|\gamma_2|$ parameters.

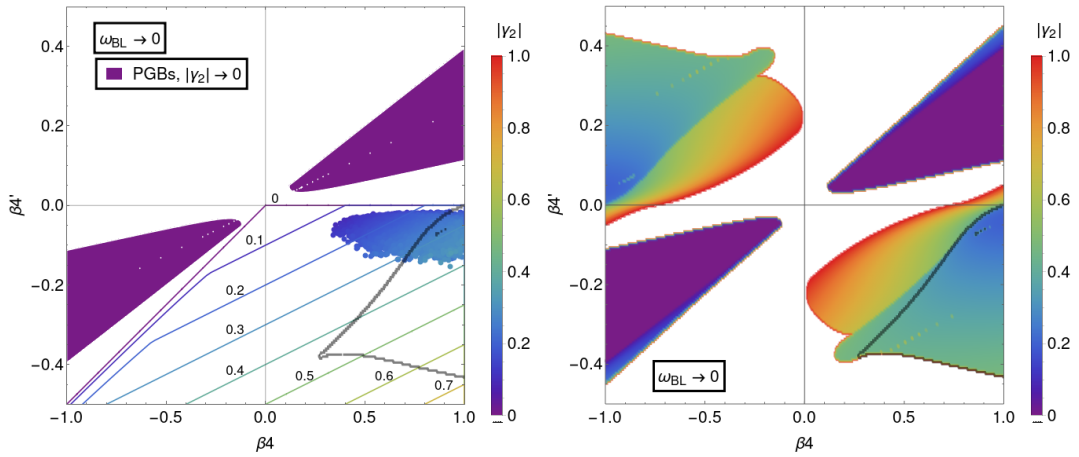

Figure 3.2: In the $\sigma \to 0$, $a_2 \to 0$ and $\omega_{BL} \to 0$ limit, we depict the β_4–β_4' regions where the tree-level *heavy* masses or one-loop PGB masses are non-tachyonic for different colour-coded $|\gamma_2|$ values. Left panel: Areas enclosed by coloured contours and labelled by $|\gamma_2|$ values represent regions in which *heavy* fields are non-tachyonic. Solid purple areas support non-tachyonic PGB masses for $|\gamma_2| = 0$ with dots along the $\beta_4' = \frac{1}{4}\beta_4$ line being numerical artifacts. The coloured points in the $\beta_4 > 0, \beta_4' < 0$ quadrant are data from the full numerical scan of Sec. 3.2.2. Right panel: Areas of non-tachyonic numerically evaluated one-loop PGB masses with the colour encoding the minimal $|\gamma_2|$ value for which all PGBs are non-tachyonic. The black contour in both panels enclosed an area where a fully non-tachyonic spectrum exists for a suitable choice of the $|\gamma_2|$ parameter.

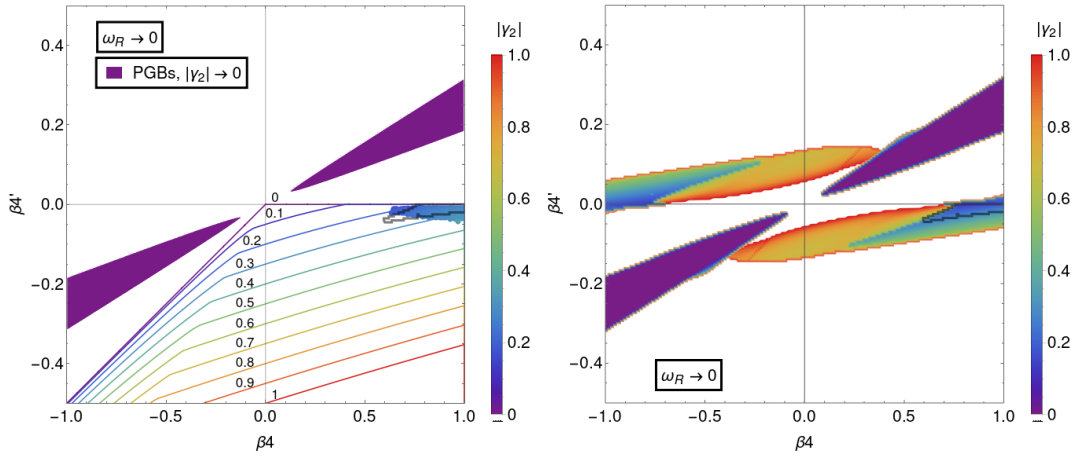

Figure 3.3: The same as in Fig. 3.2, only in the $\omega_R \to 0$ limit.

The $|\gamma_2| = 0$ regime

In the case of $|\gamma_2| = 0$, the scalar masses in question are determined by only two parameters: β_4, β_4'. In addition to that, all relevant mass formulae are available analytically, see Table E.1 for the tree-level expressions and Table X in [16] for the one-loop PGB masses. Non-tachyonicity of the tree-level *heavy* fields implies

$$\beta_4' < 0 \qquad\qquad \beta_4' < \frac{1}{2}\beta_4, \tag{3.18}$$

and the corresponding allowed region in the β_4-β_4' plane is depicted in left panels of Figures 3.2–3.3 by purple thin contour.

The PGB one-loop masses are non-tachyonic in the solid purple areas[2] in the $\beta_4 > 0$, $\beta_4' > 0$ and $\beta_4 < 0$, $\beta_4' < 0$ quadrants of the left panels of Figures 3.2–3.3. Observe that the regions of non-tachyonicity for the *heavy* fields and PGBs do not overlap, thus demonstrating that the one-loop scalar spectrum cannot be made non-tachyonic in the $|\gamma_2| = 0$ regime.

The $|\gamma_2| \neq 0$ regime

Non-tachyonicity of the tree-level *heavy* fields in the $|\gamma_2| \neq 0$ regime implies

$$\beta_4' < 0, \qquad \beta_4' < \frac{1}{4}\beta_4 - |\gamma_2|, \qquad \left(\beta_4' - \frac{1}{2}\beta_4\right)\left(\beta_4' - \frac{1}{18}\beta_4\right) > \frac{4}{9}|\gamma_2|^2 \tag{3.19}$$

for $\omega_{BL} \to 0$ and

$$\beta_4' < 0, \qquad \beta_4' < \frac{7}{18}\beta_4 - \frac{2}{9}|\gamma_2|, \qquad \left(\beta_4' - \tfrac{1}{2}\beta_4\right)\left(\beta_4' - \tfrac{1}{50}\beta_4\right) > \tfrac{4}{25}|\gamma_2|^2,$$

$$\left(\beta_4' - \tfrac{1}{4}\beta_4\right)\left(\beta_4' - \tfrac{1}{16}\beta_4\right) > \tfrac{1}{4}|\gamma_2|^2 \tag{3.20}$$

[2]Regions of non-tachyonic PGB masses do not extend to the point $\beta_4 = 0$, $\beta_4' = 0$ in the $a_2 \to 0$ limit as the gauge one-loop mass corrections cannot be made simultaneously non-negative for all PGBs, see Table X in [16], and these negative gauge mass contributions have to be overwhelmed by considering $\beta_4 \neq 0$, $\beta_4' \neq 0$.

for $\omega_R \to 0$, c.f. Table E.1, with corresponding allowed regions depicted by different $|\gamma_2|$-coloured contours for several values of $|\gamma_2| \in [0,1]$ in the left panels of Figures 3.2–3.3. Notice that these regions retreat with increasing $|\gamma_2|$ towards the bottom-right corner in the β_4-β_4' plane.

Numerically evaluated PGB one-loop masses are non-tachyonic in the areas displayed in the right panels of Figures 3.2–3.3, where for every relevant β_4 and β_4' point the assigned colour stands for the minimal $|\gamma_2|$ value needed to achieve non-tachyonic PGB scalar spectrum. Observe that for $|\gamma_2| \lesssim 0.15$ the PGB non-tachyonic regions are located in the $\beta_4 > 0, \beta_4' > 0$ or $\beta_4 < 0, \beta_4' < 0$ quadrants and bear no overlap with the areas where *heavy* fields are non-tachyonic. On the other hand, for $|\gamma_2| \gtrsim 0.15$ the non-tachyonic PGB one-loop spectrum can be found also in the $\beta_4 > 0, \beta_4' < 0$ quadrant into which the areas of non-tachyonic *heavy* masses recede.

Finally, the black contours showed in the panels of Figures 3.2–3.3 enclosed the β_4-β_4' regions where both tree-level *heavy* and one-loop PGB masses are non-tachyonic for a suitable choice $|\gamma_2| \neq 0$. In the limit $\omega_{BL} \to 0$, such region is obtained for $0.19 \lesssim |\gamma_2| \lesssim 0.47$, while in case $\omega_R \to 0$, it is attained for $0.14 \lesssim |\gamma_2| \lesssim 0.29$. Hence, a non-tachyonic scalar spectrum is expected to be found only for non-negligible $|\gamma_2|$ values. Note that the fully consistent region in the β_4-β_4' plane in the latter scenario is rather narrow, thus providing the first hint that the $\omega_R \to 0$ regime is much more restrictive.

The relevance of this simplified semi-analytic consideration is illustrated by adding the $|\gamma_2|$-coloured results of the numerical scans from Sec. 3.2.2 into the left panels of Figures 3.2–3.3. Observe that the *viable* points in the minimal SO(10) Higgs model are located in the $\beta_4 > 0$, $\beta_4' < 0$ quadrant as it is expected from the position of the black contours. The discrepancies between the scan data and the semi-analytic approach can be attributed to non-zero a_2 values allowed in the numerical scans.

3.2.2 Viable regions of the parameter space

We now discuss the full numerical analysis of the $\mathbf{45} \oplus \mathbf{126}$ SO(10) Higgs model at the one-loop level. The space of parameters covers 9 real dimensionless scalar couplings

$$a_2, a_0, \lambda_0, \lambda_2, \lambda_4, \lambda_4', \alpha, \beta_4, \beta_4', \tag{3.21}$$

2 complex dimensionless scalar couplings

$$\gamma_2, \eta_2, \tag{3.22}$$

the unified gauge coupling g and the VEVs

$$\omega_{BL}, \omega_R, \sigma; \tag{3.23}$$

in total spanning over 16 real dimensions.[3] Notice that all scalar couplings from Eqns. (2.21)–(2.24) associated with the Lagrangian terms containing $\mathbf{10}_{\mathbb{C}}$ effectively vanish in the minimal SO(10) Higgs model. The values of μ^2, ν^2 and τ

[3]We exploited the freedom in defining the overall phases of Σ and ϕ fields, so that $\sigma > 0$ is real and the larger of the ω's is positive.

are related by the stationarity conditions (2.31)–(2.33) to (3.21)–(3.23) and thus they do not belong to the set of independent parameters of the model. For every parameter point, the "optimal" renormalization scale μ_R^2 is calculated as an arithmetic average of all *heavy* tree-level scalar masses-squares. Dimensionless couplings are restricted to the $O(1)$ domain and VEVs have to satisfy the perturbativity constraint (3.10).

Viability of a point is determined by the criteria introduced in Sec. 3.1, in particular non-tachyonicity (see Sec. 3.1.1), gauge coupling unification (see Sec. 3.1.2) and perturbativity (see Sec. 3.1.3). It is worth repeating some of the shortcomings of *viability* constraints defined in the simplified setting of the minimal SO(10) Higgs model:

- We lack full information about mass matrices of the SM doublet $(1, 2, +\frac{1}{2})$ and triplet $(\bar{3}, 1, +\frac{1}{3})$ multiplets as the relevant states from **126** eventually mix with fields from $\mathbf{10}_{\mathbb{C}}$ in the $\mathbf{45} \oplus \mathbf{126} \oplus \mathbf{10}_{\mathbb{C}}$ SO(10) GUT. It is possible to formulate the necessary non-tachyonicity test by applying Sylvester's criterion, c.f. Sec. 3.1.1, whose influence upon parameter space scans was studied in Sec. IV C 4 of [16].

- The gauge coupling unification is implemented only at the one-loop level. Hence, for every parameter point the position of M_{GUT}, σ and g is analytically determined to fit experimental SM gauge coupling values exactly at M_Z scale, c.f. Sec. 3.1.2.

The *viability* constraints introduced in Sec. 3.1 are numerically implemented by introducing a penalization function which is always non-negative and monotonically raises with the quantitative amount of a violation of any *viability* criterion, c.f. Appendix B in [16] for its explicit form. Such penalization function is then applied on every point in the parameter space. *Viable* regions of the parameter space are located and examined by the stochastic version of the differential evolution algorithm, version "DE/rand/1" with $F \in (0.5, 2)$ randomly chosen for every point [154], which iteratively produces new improved generations of candidate parameter points from the preceding generation. The algorithm can be used in two modes:

1. *Minimization mode* in which the penalization function never reaches zero. The algorithm progressively explores parts of the parameter space with improved obedience to certain criteria. Scans obtained by adopting such a mode are referred to as *biased*.

2. *Search mode* in which only parameter points with zero penalization function are accepted. The algorithm thus almost uniformly explores regions of the parameter space with desired features.

All the datasets of parameter points with various constraints imposed and obtained by different algorithm modes are listed in Table 3.1. The main datasets containing *viable* parameter points are labeled $\mathcal{B}$ and $\mathcal{R}$ in the $\omega_{BL} \to 0$ and $\omega_R \to 0$ limits, respectively, and they satisfy, among other criteria, $t_+ > 0.5$ and $\overline{\Delta} < 1$. As the perturbativity criteria from Sec. 3.1.3 possess a certain level of arbitrariness, we produce several numerical parameter space scans with different

levels of RG perturbativity imposed on them. *Viable* points in the datasets $\mathcal{B}_x$ and $\mathcal{R}_x$ satisfy stricter $\bar{t} > x$ stability under the RG running in the $\omega_{BL} \to 0$ and $\omega_R \to 0$ cases, respectively. No points with $\bar{t} > 2$ were found in the $\omega_R \to 0$ limit, hence there are no $R_{2,3}$ datasets for this case. Finally, the *biased* datasets $\mathcal{B}_{RG}$ and $\mathcal{R}_{RG}$ were obtained by pushing the parameter space scans to highest possible $\bar{t}$ values in the $\omega_{BL} \to 0$ and $\omega_R \to 0$ regimes, respectively. Note that similar *biased* datasets were produced for quantity the $\overline{\Delta}$, c.f. Sec. IV in [16], however, we opt to omit them from the current discussion.

Table 3.1: The datasets of *viable* points in the parameter space obtained by imposing various constraints and using different modes of the differential evolution algorithm. Their detailed description is provided in the main text above the table.

Dataset	VEV regime	RG range	Bias	# of points	Mode
$\mathcal{B}$	$\omega_{BL} \to 0$	$t_+ > 0.5$		30000	Search
$\mathcal{B}_1$	$\omega_{BL} \to 0$	$\bar{t} > 1.0$		20000	Search
$\mathcal{B}_2$	$\omega_{BL} \to 0$	$\bar{t} > 2.0$		20000	Search
$\mathcal{B}_3$	$\omega_{BL} \to 0$	$\bar{t} > 3.0$		20000	Search
$\mathcal{B}_{RG}$	$\omega_{BL} \to 0$	$t_+ > 0.5$	$\bar{t}$	10000	Minimization
$\mathcal{R}$	$\omega_R \to 0$	$t_+ > 0.5$		30000	Search
$\mathcal{R}_1$	$\omega_R \to 0$	$\bar{t} > 1.0$		20000	Search
$\mathcal{R}_{RG}$	$\omega_R \to 0$	$t_+ > 0.5$	$\bar{t}$	10000	Minimization

Scatter plots of dimensionless scalar parameters

One way to represent the *viable* regions of the parameter space, with *viability* criteria introduced in Sec. 3.1, are 2D scatter plots correlating two dimensionless scalar couplings. We choose 6 such correlation pairs and the corresponding plots are shown in Figs. 3.4 and 3.5 for the $\omega_{BL} \to 0$ and $\omega_R \to 0$ regimes, respectively. Note that the values of the phases $\delta_{\gamma_2}, \delta_{\eta_2}$ are distributed almost uniformly over the $[0, 2\pi)$ interval and thus are excluded from the plots.[4]

In Figs. 3.4–3.5, the points in main *viable* datasets $\mathcal{B}$ and $\mathcal{R}$ are combined with the ones in the *biased* datasets $\mathcal{B}_{RG}$ and $\mathcal{R}_{RG}$. The colour scheme encodes various levels of $\bar{t}$ perturbativity measure fom Eq. (3.14). Points with better $\bar{t}$ are displayed in the front, thus allowing to identify the RG-stable *hot spots*.

There are several observations to be made:

- The highest value of the RG-perturbative measure $\bar{t}$ globally achieved was $\bar{t} \approx 3.1$ in the $\omega_{BL} \to 0$ case and $\bar{t} \approx 1.9$ for $\omega_R \to 0$, thus indicating that the former scenario is more perturbatively stable.

- The region in which all the scalar couplings vanish is not *viable* due to the need to balance out the gauge coupling contributions in the one-loop scalar beta functions for the RG-perturbative points, c.f. Appendix B.2.

[4] In the $\omega_R \to 0$ regime, one can observe a mild preference for phase values satisfying relation $2\delta_{\gamma_2} = \delta_{\eta_2}$ which ensures that the γ_2 and η_2 phases do not change during the one-loop RG running, c.f. Eqns. (B.28)–(B.29) with $\kappa_2, \kappa_2', \zeta, \zeta', \psi_0, \psi_1, \psi_2$ couplings zeroed out.

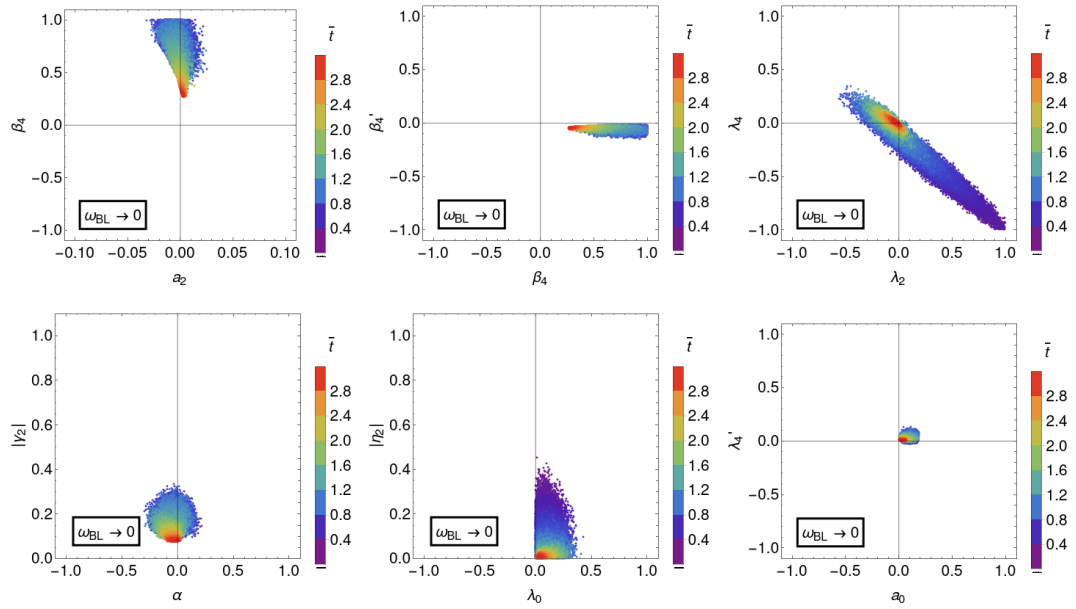

Figure 3.4: 2D scatter plots correlating pairs of dimensionless scalar parameters of the **45** $\oplus$ **126** SO(10) Higgs model in the $\omega_{BL} \to 0$ limit. The points were obtained by combining the $\mathcal{B}$ and $\mathcal{B}_{RG}$ datasets from Table 3.1 with the colour coding the value of the RG-perturbativity measure $\bar{t}$.

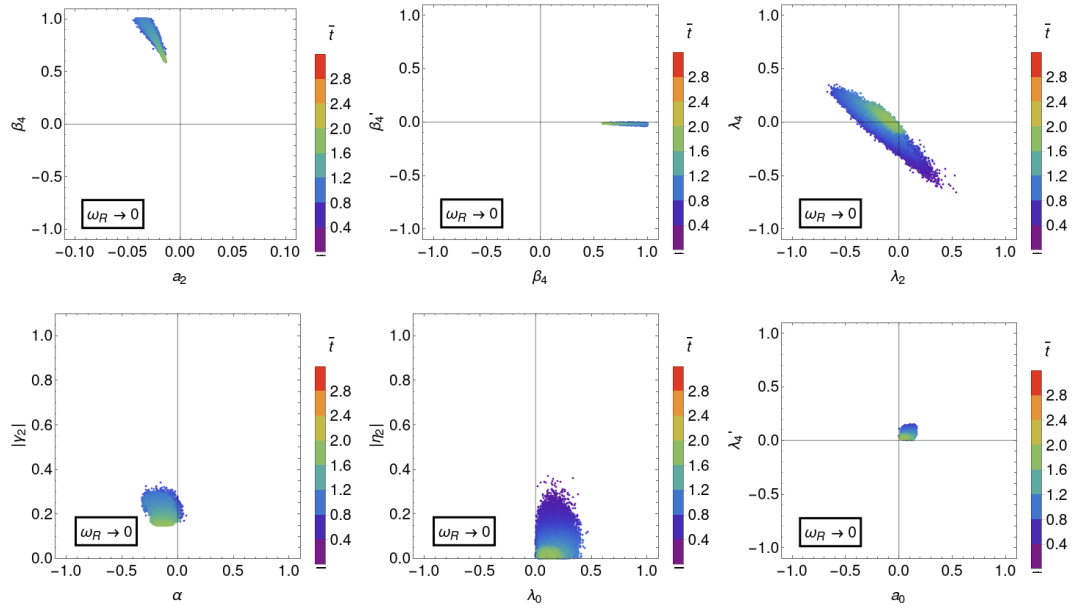

Figure 3.5: The same as in Fig. 3.4, only in the $\omega_R \to 0$ limit.

- $a_2 \ll 1$: Potentially tachyonic tree-level masses of the PGBs are suppressed for $a_2 \to 0$, thus allowing one-loop corrections to dominate. Having $a_2 < 0$ for all points in the $\omega_R \to 0$ regime implies that the PGB triplet always acquires non-tachyonic tree-level mass, see Table E.1.

- $\beta_4 > 0,\ \beta_4' \lesssim 0,\ 0.1 \lesssim |\gamma_2| \lesssim 0.4$: These ranges of β_4, β_4',$|\gamma_2|$ values are enforced by the required non-tachyonicity of the PGBs and the *heavy* fields, c.f. semi-analytical discussion in Sec. 3.2.1. Let us emphasise that no *viable* points were found in the $|\gamma_2| \to 0$ limit.

- $a_0 > 0,\ \lambda_0 \geq 0$: Positive a_0 is enforced by non-tachyonicity of the SO(10)-breaking Higgs field whose dominant tree-level mass contribution is calculated as $8a_0(3\omega_{BL}^2 + 2\omega_R^2)$ for $|a_2| \ll |a_0|$, c.f. Table E.1. Consequently, the σ-proportional tree-level mass of the $\mathrm{U}(1)_{B-L}$-breaking Higgs field is non-tachyonic only if $\lambda_0 \gtrsim \frac{(\alpha+\beta_4')^2}{4a_0} \geq 0$.
- $\lambda_4 \sim -\lambda_2$: The couplings λ_2 and λ_4 exhibit the linear correlation that can be attributed to the shape of the one-loop scalar β-functions for which the $\lambda_4 \sim -\lambda_2$ with the condition $\lambda_4' \ll 1$ leads to a partial cancellations of the terms with large numerical factors, c.f. Eqns. B.21,(B.22) and (B.25), thus contributing to the overall stability under the RG running.

Parameter ranges

The datasets $\mathcal{B}$, $\mathcal{B}_{1,2,3}$, $\mathcal{R}$ and $\mathcal{R}_1$ obtained by the *search mode* of the differential evolution algorithm, c.f. point 2 discussed on page 46, approximately correspond to the uniformly sampled *viable* points satisfying desired level of stability under the RG running, see Table 3.1. Projections of such datasets onto one parameter subspaces are therefore interpreted as the parameter's marginal probability distributions in the context of Bayesian statistics and the ranges of individual scalar parameters can be represented by their *highest density intervals* (HDI).

In Figs. 3.6 and 3.7 the clustered vertical bars with the same horizontal position show the 1-, 2- and 3-σ HDIs (distinguished by decreasing opacity) of the individual dimensionless parameters, χ and the VEVs σ, $\max[|\omega_{BL}|, |\omega_R|]$, respectively, for the $\omega_{BL} \to 0$ (upper/left panels) or $\omega_R \to 0$ (bottom/right panels) limit. We compare the main *viable* datasets $\mathcal{B}, \mathcal{R}$ (coloured in **blue**) with those in which stricter stability under the RG running is imposed via demanding $\bar{t} > 1$, $\bar{t} > 2$ and $\bar{t} > 3$ (coloured in **light blue**, **green** and **orange**, respectively).

By increasing the required stability under the RG running the *viable* ranges for the parameters shrink as indicated by the position of the *hot spots* in the correlation plots in Figs. 3.4–3.5. Moreover, the parameters' HDIs of the datasets with stricter $\bar{t}$ threshold are located in the unlikely regions of the *viable* parts of the parameter space. This is best demonstrated in the case of the β_4 parameter in the $\omega_{BL} \to 0$ regime, where the 3-σ HDI of the $\mathcal{B}_3$ dataset is outside the 3-σ HDI of the main dataset $\mathcal{B}$. In the $\omega_R \to 0$ limit, no parameter points were found which could be run in renormalization scale on average for more than two orders of magnitude up and down without encountering a Landau pole, therefore there are no $\mathcal{R}_{2,3}$ datasets. It clearly illustrates that the $\omega_R \to 0$ symmetry breaking limit is "less perturbative" of the two.

The absolute positions of the $\max[|\omega_{BL}|, |\omega_R|]$, σ VEVs (and unified coupling g) are fixed by the gauge coupling unification since perturbativity and non-tachyonicity constraints are practically independent of a rescaling of the dimensionful parameters by a common factor. Resulting scales as displayed in Fig. 3.7 are very different for the two symmetry breaking patterns, i.e.

$$\omega_{BL} \sim 10^{18}\,\mathrm{GeV}, \qquad \sigma \sim 10^{8}\,\mathrm{GeV} \tag{3.24}$$

in the $\omega_R \to 0$ limit with the $\mathrm{SU}(3)_c \times \mathrm{SU}(2)_L \times \mathrm{SU}(2)_R \times \mathrm{U}(1)_{B-L}$ intermediate-symmetry stage and

$$\omega_R \sim 10^{15}\,\mathrm{GeV}, \qquad \sigma \sim 10^{10.5-12}\,\mathrm{GeV} \tag{3.25}$$

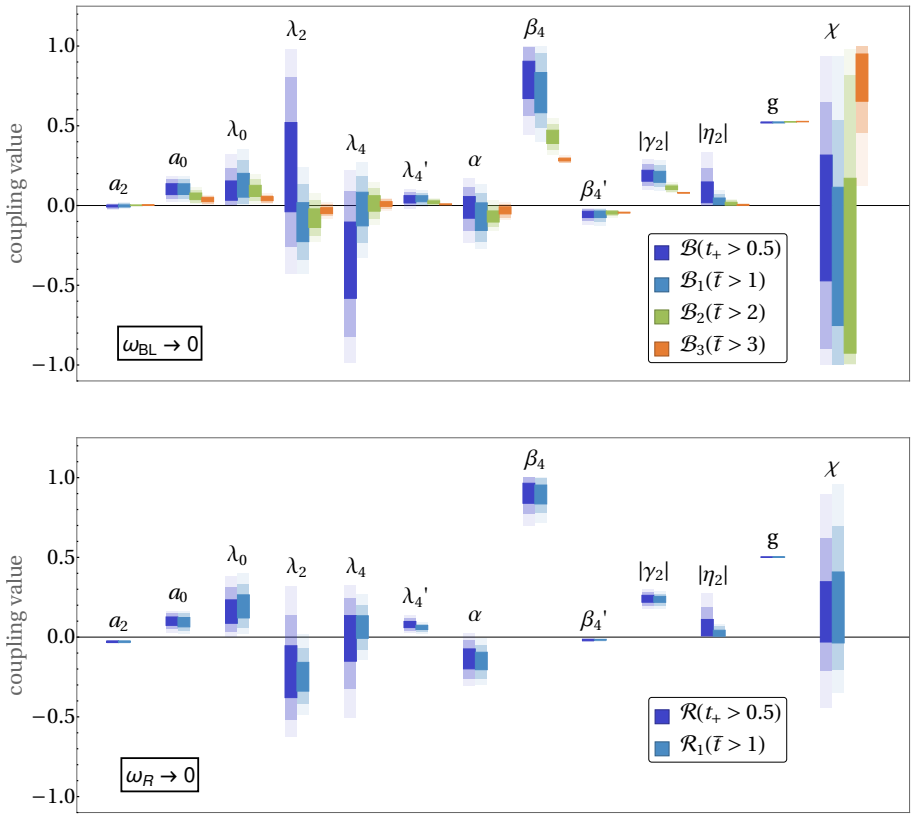

Figure 3.6: The 1-, 2- and 3-σ HDIs (depicted by decreasing opacity) of the scalar dimensionless parameters (3.21)–(3.22), g and χ from the datasets obtained in the *search mode* in the $\omega_{BL} \to 0$ (upper panel, $\mathcal{B}, \mathcal{B}_{1,2,3}$ datasets) and $\omega_R \to 0$ (bottom panel, $\mathcal{R}, \mathcal{R}_1$ datasets) limit, c.f. Table 3.1. The colours encode different stability under the RG running.

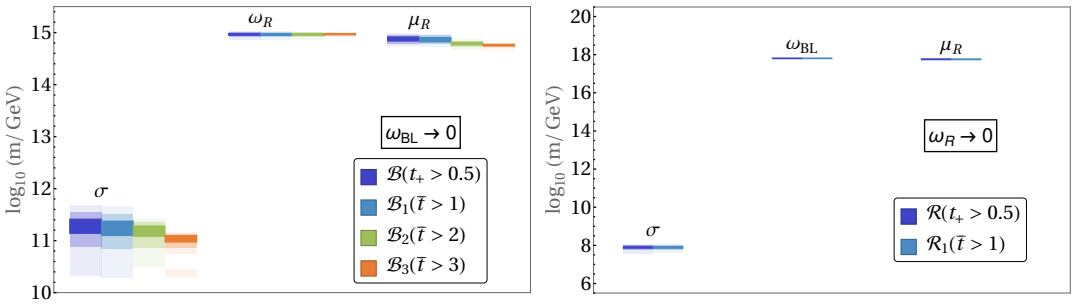

Figure 3.7: The 1-, 2- and 3-σ HDIs (depicted by decreasing opacity) of the VEVs σ, $\max[|\omega_{BL}|, |\omega_R|]$ and the renormalization scale μ_R from datasets obtained in the *search mode* in the $\omega_{BL} \to 0$ (left panel, $\mathcal{B}, \mathcal{B}_{1,2,3}$ datasets) and $\omega_R \to 0$ (right panel, $\mathcal{R}, \mathcal{R}_1$ datasets) limit. The colours encode different stability under the RG running.

in the $\omega_{BL} \to 0$ regime with the $\mathrm{SU}(4)_C \times \mathrm{SU}(2)_L \times \mathrm{U}(1)_R$ intermediate-symmetry stage. The VEV values in Eqns. (3.24)–(3.25) are to similar to those of [104, 123, 155] based on the minimal survival hypothesis [156, 157]. In the former case of

$\omega_R \to 0$, there is almost a ten orders of magnitude hierarchy between ω_{BL} and σ with the GUT scale being rather close to the Planck scale and the seesaw scale σ located near the Davidson-Ibarra leptogenesis bound $\sim 10^9$ GeV restricting the mass of the lightest heavy neutrino from below [158]. On the other hand, in the latter case of $\omega_{BL} \to 0$, the position of the GUT scale is somewhat close to the lower bound indicated by the proton decay searches [134–139]. Nevertheless, the VEVs (3.24)–(3.25) were obtained from a one-loop gauge coupling unification and should be modified by two-loop corrections in any robust theoretical proton lifetime analysis, c.f. Sec. 2.5. Lastly, the effect of the induced VEV $\min[|\omega_{BL}|, |\omega_R|]$ cannot be neglected as it enters non-tachyonicity considerations through the universal VEV ratio χ defined in Eq. (2.37). The distribution of its values shown in Fig. 3.6 suggests that both ω's tend to have the same sign in the $\omega_R \to 0$ case and in the $\mathcal{B}_3$ dataset of the $\omega_{BL} \to 0$ limit, whilst there seems to be a slight tendency towards opposite-sign ω's in the remaining datasets of the $\omega_{BL} \to 0$ regime.

For every point in the parameter space, the renormalization scale μ_R is calculated as the square root of the average *heavy* tree-level scalar mass-squares so that the logarithmic one-loop mass contributions are tamed. Although the *viable* points should be correctly compared only after running all parameters to the same renormalization scale, we see from Fig. 3.7 that the spread of all point-specific μ_R values is rather small in both regimes, thus justifying the comparison of the *viable* points right away as they are computed at their specific μ_R's. Besides that, the imposed stability under the RG running condition guarantees that all *viable* points can be, in principle, safely run to one common renormalization scale.

Finally, let us mention that we have deliberately omitted from this thesis the results for the mass spectrum as they conform to the shape anticipated by the symmetry breaking pattern and the parameter ranges in Figs. 3.6–3.7 in both limiting cases; i.e. the *intermediate-scale* masses cluster near the σ scale, *heavy* masses reside near the GUT scale and the PGB fields have masses around $\frac{1}{16\pi^2} M_{GUT}$. The interested reader is deferred to Sec. IV D of article [16].

Gauge coupling unification

For completeness, we present the gauge coupling unification patterns in Fig. 3.8 for two sample points, one from each of the two $\omega_{BL} \to 0$ and $\omega_R \to 0$ limiting cases. The corresponding input coupling values are listed in Table 3.2.

3.2.3 Calculation of the partial proton decay widths

Let us employ the $\mathcal{B}$ and $\mathcal{R}$ main datasets to perform a partial proton width calculation for the decay channels with antineutrinos in the final state

$$p \to \pi^+ \overline{\nu}, \qquad\qquad p \to K^+ \overline{\nu}, \tag{3.26}$$

with incoherent summation over all neutrino flavours implicitly assumed. As we discussed in Sec. 2.5, the corresponding partial decay widths from Eqns. (2.77)–(2.78) do not depend on the details of the flavour fit and instead, they are fixed by the observable CKM mixing parameters. Moreover, the numerical study [7] showed that proton width prediction of decay channels (3.26) are relatively robust with respect to the Planck-scale induced theoretical uncertainties in the Yukawa as well as gauge-kinetic parts of the Lagrangian.

Table 3.2: The input parameters corresponding to sample points for which the gauge unification patterns are shown in Fig. 3.8. The signs of the VEVs are positive and $\lg(x) := \log_{10}(x/\mathrm{GeV})$.

	$\omega_{BL} \to 0$	$\omega_R \to 0$
a_2	0.002	−0.027
a_0	0.048	0.060
λ_0	0.065	0.138
λ_2	−0.070	−0.158
λ_4	0.037	0.025
λ_4'	0.001	0.046
α	−0.062	−0.063
β_4	0.341	0.856
β_4'	−0.043	−0.018
$\lvert\gamma_2\rvert$	0.092	0.228
$\arg\gamma_2$	3.38	4.78
$\lvert\eta_2\rvert$	0.007	0.025
$\arg\eta_2$	6.22	3.10
g	0.526	0.502
$\lg\lvert\omega_{BL}\rvert$	7.06	17.80
$\lg\lvert\omega_R\rvert$	14.96	−2.20
$\lg\lvert\sigma\rvert$	11.01	7.94
$\lg\mu_R$	14.75	17.76

We first list the numerical values of the quantities entering the proton decay width formulae (2.77)–(2.78) with estimated theoretical uncertainties. The proton decay constant

$$\tilde{\alpha} = -0.01106 \pm 0.00039 \ \mathrm{GeV}^3 \tag{3.27}$$

is extracted from the lattice calculations carried out in [144] for the fixed values of the chiral Lagrangian coefficients

$$D = 0.8, \tag{3.28}$$
$$F = 0.47, \tag{3.29}$$
$$f_\pi = 0.13055\,\mathrm{GeV}, \tag{3.30}$$
$$m_N = 0.94\,\mathrm{GeV}, \tag{3.31}$$
$$m_B = 1.15\,\mathrm{GeV} \tag{3.32}$$

and $\mu_{had} = 2\,\mathrm{GeV}$, where we adopted the finer "32ID sample" results. Factors governing the one-loop running effects of the effective four-fermion BNV operators are obtained from Eqns. (2.85)–(2.86):

$$A_L = 1.303 \pm 0.028, \tag{3.33}$$
$$A^{(1)}_{S,\,\omega_{BL}\to 0} = 3.749 \pm 0.408 \pm 0.035, \tag{3.34}$$
$$A^{(1)}_{S,\,\omega_R\to 0} = 4.328 \pm 0.525 \pm 0.017, \tag{3.35}$$

with factor $A_S^{(1)}$ being specific to dataset $\mathcal{B}$ ($\omega_{BL} \to 0$) or $\mathcal{R}$ ($\omega_R \to 0$). The first contributions to the uncertainties in expressions (3.33)–(3.35) were estimated by

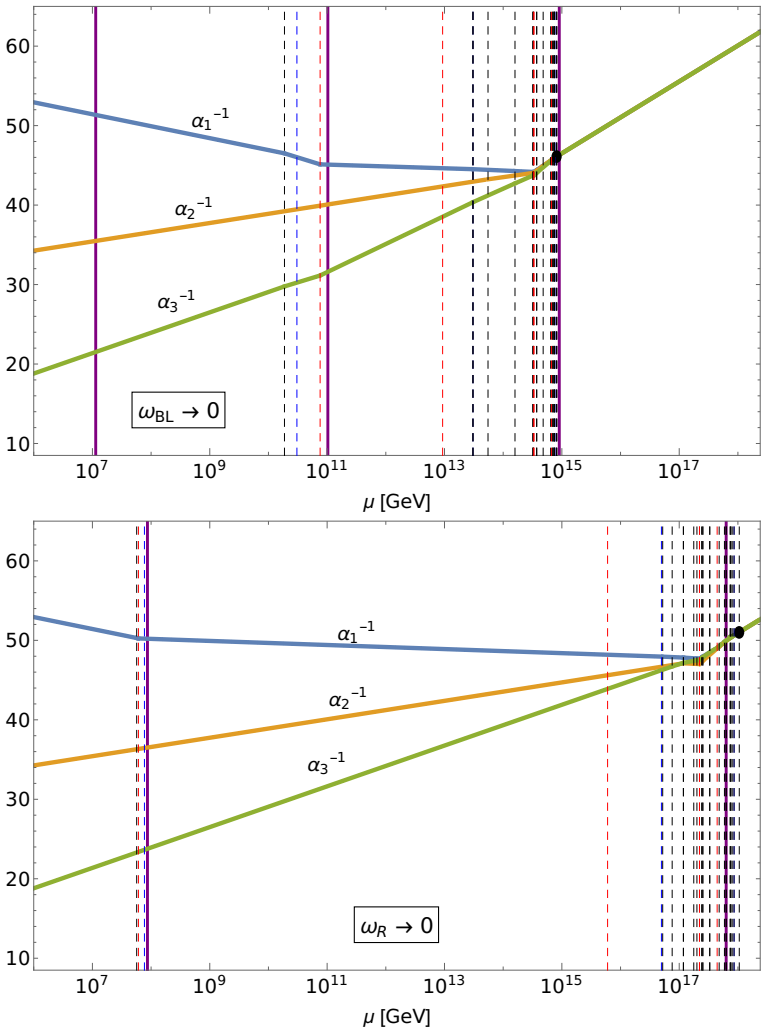

Figure 3.8: Gauge-coupling-unification patterns are shown for two *viable* sample points in the $\omega_{BL} \to 0$ (upper panel) and $\omega_R \to$ (bottom panel) limits with the corresponding input parameter values listed in Table 3.2. The **black**, blue and red dashed vertical lines mark the location of the SM non-singlet scalar, SM-singlet scalar and gauge masses, respectively; whilst purple solid lines indicate the position of the VEVs. The **black dots** indicate the point of the one-loop SM gauge coupling unification and simultaneously the position of the heaviest non-singlet mass threshold.

approximating the two-loop running effects via perturbing exponents in formulae (2.85)–(2.86) by $\mathcal{O}(1)/4\pi$ relative change. The second contributions to the uncertainties in Eqns. (3.34)–(3.35) are determined from the spread of $A_S^{(1)}$ values calculated for all *viable* parameter points. The VEVs in the *viable* region of the parameter space are

$$\lg \omega_R = 14.92 \pm 0.20 \pm 0.12, \tag{3.36}$$
$$\lg |\sigma| = 11.09 \pm 0.10 \pm 0.78 \tag{3.37}$$

in the $\omega_{BL} \to 0$ regime and

$$\lg \omega_{BL} = 17.796 \pm 0.500 \pm 0.078, \tag{3.38}$$

$$\lg|\sigma| = 7.86 \pm 0.50 \pm 0.37 \tag{3.39}$$

in the $\omega_R \to 0$ regime. The lg function is defined in Table 3.2. The first contributions to the uncertainties in expressions (3.36)–(3.39) arise from the higher-loop corrections to the one-loop gauge coupling unification. We estimate them by assessing the shift in the breaking scales resulting from one-loop and two-loop gauge coupling unification analysis performed in [104]. Notice that such uncertainties are rather large and any robust proton lifetime calculation thus requires at least two-loop gauge coupling RGE analysis, see discussion in Sec. 2.5.3. The second contributions to the uncertainties of Eqns. (3.36)–(3.39) come from the spread of the VEV values of all *viable* parameter points in $\mathcal{B}$ or $\mathcal{R}$. The $\min[|\omega_{BL}|, |\omega_R|]$-dependent contributions in denominators of k_1, k_2 from Eqns. (2.79)–(2.80) are neglected since $\min[|\omega_{BL}|, |\omega_R|] \ll |\sigma| \ll \max[|\omega_{BL}|, |\omega_R|]$. Finally, the values of the experimental inputs are [127]

$$m_p = 938.27208816 \pm 0.00000029\,\text{MeV}, \tag{3.40}$$
$$m_{\pi^\pm} = 139.57039 \pm 0.00018\,\text{MeV}, \tag{3.41}$$
$$m_{K^\pm} = 493.677 \pm 0.016\,\text{MeV}, \tag{3.42}$$
$$|(V_{CKM})_{11}| = 0.97373 \pm 0.00031, \tag{3.43}$$
$$|(V_{CKM})_{12}| = 0.2243 \pm 0.0008. \tag{3.44}$$

Taking the numerical values in Eqns. (3.27)–(3.44) and inserting them into the partial proton decay widths (2.77)–(2.78) for decay channels (3.26) with antineutrinos in the final state, one gets

$$\tau_{p\to\pi^+\overline{\nu}} \equiv \frac{\hbar}{\Gamma_{p\to\pi^+\overline{\nu}}} = 10^{28.90^{+1.43}_{-1.42}}\,\text{yr}, \tag{3.45}$$
$$\tau_{p\to K^+\overline{\nu}} \equiv \frac{\hbar}{\Gamma_{p\to K^+\overline{\nu}}} = 10^{30.97^{+1.43}_{-1.42}}\,\text{yr} \tag{3.46}$$

in the $\omega_{BL} \to 0$ limit and

$$\tau_{p\to\pi^+\overline{\nu}} \equiv \frac{\hbar}{\Gamma_{p\to\pi^+\overline{\nu}}} = 10^{40.30^{+2.48}_{-2.46}}\,\text{yr}, \tag{3.47}$$
$$\tau_{p\to K^+\overline{\nu}} \equiv \frac{\hbar}{\Gamma_{p\to K^+\overline{\nu}}} = 10^{42.37^{+2.48}_{-2.46}}\,\text{yr} \tag{3.48}$$

in the $\omega_R \to 0$ limit.

Asymmetrical theoretical uncertainties of $\tau_{p\to\pi^+\overline{\nu}}$ and $\tau_{p\to K^+\overline{\nu}}$ indicated in Eqns. (3.45)–(3.48) were obtained by taking the minimum and maximum values of the partial decay widths calculated by inserting the quantities (3.27)–(3.44) into formulae (2.77)–(2.78) over the entire range given by their respective uncertainties. Let us emphasise that by far the biggest proton lifetime theoretical uncertainty comes from the accuracy of the $\max[|\omega_{BL}|, |\omega_R|]$ VEV determination, whose error can be reduced by improving the gauge running analysis to two loops.

In Fig. 3.9, we show the theoretically predicted ranges of $\tau_{p\to\pi^+\overline{\nu}}$ and $\tau_{p\to K^+\overline{\nu}}$ (**black** horizontal bar) in both VEV regimes with the "expected" value denoted by the **red** dashed vertical line. It is compared to the corresponding experimental 90% confidence level exclusion bounds (**black** dashed vertical line) from

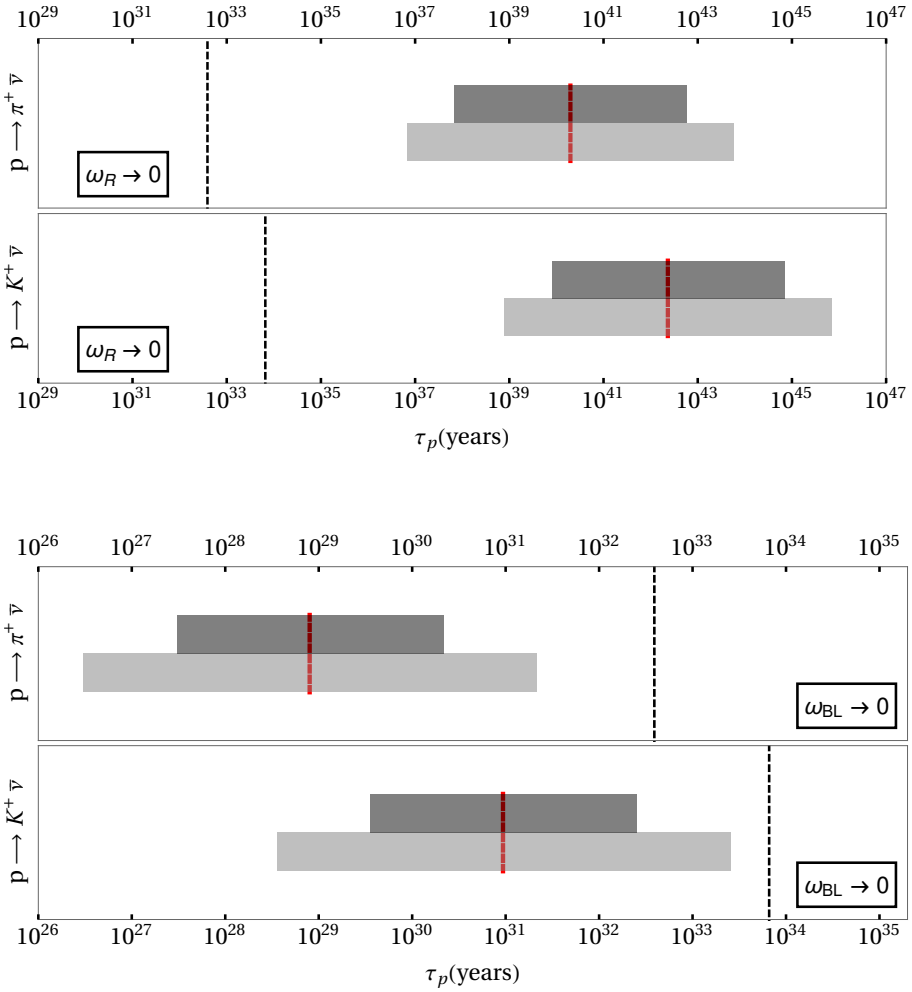

Figure 3.9: Theoretical ranges of $\tau_{p\to\pi^+\overline{\nu}}$ and $\tau_{p\to K^+\overline{\nu}}$ from Eqns. (3.45)–(3.48) in the $\mathbf{45}\oplus\mathbf{126}$ SO(10) Higgs model in the $\omega_R \to 0$ (upper panel) or $\omega_{BL} \to 0$ (lower panel) regime without (**black** bar) and with (**gray** bar) Planck-scale-induced flavour fit uncertainties [7] taken into account. The **red** dashed vertical lines denote the "expected" values. Experimental 90% confidence level exclusion bounds from Table 2.4 are marked by **black** dashed lines.

Table 2.4. The plot also contains the theoretical ranges of $\tau_{p\to\pi^+\overline{\nu}}$ and $\tau_{p\to K^+\overline{\nu}}$ expanded by one order of magnitude (**gray** horizontal bar) due to superimposing hypothetical Planck-scale-induced flavour fit uncertainties studied in [7]. The theoretical ranges of inverse partial decay widths (3.47)–(3.48) in the $\omega_R \to 0$ limit are well above the 90% confidence level exclusion bounds. On the other hand, the theoretically predicted proton decay rates in the $\omega_{BL} \to 0$ limit are too fast for both decay channels (3.26). Note that one cannot proclaim the $\omega_{BL} \to 0$ regime non-viable based on such a result as there are still several ways to improve the proton decay width analysis, i.e. upgrade the gauge unification analysis at least to two loops or bring a suitable scalar multiplet down to the desert to sufficiently raise the GUT scale [12–14].

3.2.4 Main conclusions of the $\mathbf{45}\oplus\mathbf{126}$ SO(10) Higgs model analysis

Viable points in the parameter space passing non-tachyonicity, gauge coupling unification and perturbativity constraints defined in Sec. 3.1 were found in both $\omega_{BL} \to 0$ ($\mathrm{SU}(4)_C \times \mathrm{SU}(2)_L \times \mathrm{U}(1)_R$ intermediate symmetry) and $\omega_R \to 0$ ($\mathrm{SU}(3)_c \times \mathrm{SU}(2)_L \times \mathrm{SU}(2)_R \times \mathrm{U}(1)_{B-L}$ intermediate symmetry) regimes of the $\mathbf{45}\oplus\mathbf{126}$ SO(10) Higgs model. The *viable* part of the parameter space does not include the region in which all scalar couplings vanish, namely $|\gamma_2| \gtrsim 0.1$ is enforced by non-tachyonicity of the one-loop scalar spectrum. This is in contradiction to the assumptions made in the preceding simplified studies [13–15].

The results of the numerical SO(10) Higgs model analysis clearly demonstrate a preference for the $\omega_{BL} \to 0$ limit as the $\omega_R \to 0$ regime is disfavoured for the following reasons:

1. *Viable* parameter points are less stable under the RG running in the $\omega_R \to 0$ case, admitting only $\bar{t} < 2$. Hence no point can be RG-run on average up and down in renormalization scale by more than two orders of magnitude without encountering a Landau-type singularity in a scalar coupling. Compare it to the limit $\omega_{BL} \to 0$ in which the $\bar{t}$ may be bigger than 3.

2. The SO(10) breaking VEV $\omega_{BL} \sim 10^{18}\,\mathrm{GeV}$ in the $\omega_R \to 0$ case is located rather close to the Planck scale, which raises concern with theoretical uncertainties induced by the Planck-scale suppressed $d > 4$ operators. Moreover, the seesaw scale $\sigma \sim 10^{8}\,\mathrm{GeV}$ is somewhat low and potentially leads to violation of the Davidson-Ibarra leptogenesis bound. The GUT scale and the seesaw scale in the $\omega_{BL} \to 0$ regime have more phenomenologically attractive values around $10^{15}\,\mathrm{GeV}$ and $10^{11}\,\mathrm{GeV}$, respectively.

Although the latter concern might be alleviated by fine-tuning a suitable scalar mass into the desert [12–14], it is rather unlikely to have enough freedom to perform such a fine-tuning in the scalar spectrum considering the very narrow *viable* domain of the parameter space in the $\omega_R \to 0$ regime.

From now on, we will focus solely on the $\omega_{BL} \to 0$ limiting case. The $\mathbf{45}\oplus\mathbf{126}$ SO(10) Higgs model study discussed in this section is upgraded to the analysis of the $\mathbf{45} \oplus \mathbf{126} \oplus \mathbf{10}_{\mathbb{C}}$ SO(10) GUT with realistically implemented Yukawa sector and the gauge coupling unification considered at two-loop level to fully account for its phenomenological viability.

3.3 The minimal SO(10) GUT in the $\omega_{BL} \to 0$ regime

In the following section, we examine the phenomenological viability of the minimal $\mathbf{45} \oplus \mathbf{126} \oplus \mathbf{10}_{\mathbb{C}}$ SO(10) Grand Unified Theory. In the $\mathbf{45} \oplus \mathbf{126}$ SO(10) Higgs model, there were identified two potentially realistic symmetry breaking patterns with the $\mathrm{SU}(3)_c \times \mathrm{SU}(2)_L \times \mathrm{SU}(2)_R \times \mathrm{U}(1)_{B-L}$ ($\omega_R \to 0$ limit) or the $\mathrm{SU}(4)_C \times \mathrm{SU}(2)_L \times \mathrm{U}(1)_R$ ($\omega_{BL} \to 0$ regime) intermediate symmetry. The simplified SO(10) Higgs model analysis showed that only the latter case is sensibly perturbative, albeit in the rather restricted part of the parameter space. Adding an extra $\mathbf{10}_{\mathbb{C}}$

into the scalar sector has very little quantitative effect on the high energy part of the spectrum, and so the aforementioned observation is expected to hold for the minimal SO(10) GUT. Therefore we perform the analysis of the minimal SO(10) GUT solely in the $\omega_{BL} \to 0$ limit.

The $\omega_{BL} \to 0$ regime, despite being favoured, is not without concerns as the predicted GUT scale $\sim 10^{15}\,\mathrm{GeV}$ is somewhat small and the corresponding theoretical proton lifetime predictions do not exceed experimental exclusion bounds, c.f. Fig. 3.9. However, the minimal SO(10) GUT provides several means to improve upon the Higgs model analysis before declaring the $\omega_{BL} \to 0$ limit nonviable:

1. An additional $\mathbf{10}_{\mathbb{C}}$ scalar representation brings new quantum corrections into the one-loop calculations. Moreover, the scalar mass matrices of the $(1, 2, +\frac{1}{2})$ and $(\overline{3}, 1, +\frac{1}{3})$ SM multiplets are expanded to dimension 4×4 and 5×5, respectively.

2. The gauge coupling unification analysis has to be upgraded from one-loop to two-loops, which is the lowest order of the perturbative expansion needed for robust proton lifetime prediction, c.f. Sec. 2.5.3. Such an improvement in the precision is, however, unlikely to significantly raise the GUT scale as was demonstrated in the minimally fine-tuned model realizations and it is probably necessary to resort to bringing a certain number of scalar multiplets down to the desert [12–14].

One should also not forget that having **126** and $\mathbf{10}_{\mathbb{C}}$ representations in the minimal SO(10) GUT allows us to address the Yukawa sector of the theory. We have shown in Sec. 2.4.3 that the question of a potentially realistic fit of fermion masses and mixing is closely related to the problem of a successful fine-tuning in the SM doublet $(1, 2, +\frac{1}{2})$ scalar mass matrix to attain a light SM-like Higgs doublet. In particular, phenomenologically viable flavour fits require the SM Higgs to be an admixture of fields from both $\mathbf{10}_{\mathbb{C}}$ and **126**.

We shall demonstrate that there is a significant tension between the perturbativity constraints and the possibility of obtaining the light SM Higgs doublet in the scalar spectrum. Hence the physical viability of the minimal SO(10) GUT is questioned even without embarking on the tedious task of testing all possible light scalar thresholds to properly raise the GUT scale as discussed in point 2.

The section is organized in the following way: in Sec. 3.3.1 we compare the shapes of the *viable* parameter space domains in the minimal SO(10) GUT and in the minimal SO(10) Higgs model. Next, the fine-tuning in the mass matrix of the SM $(1, 2, +\frac{1}{2})$ multiplets for the purpose of attaining a SM-like Higgs doublet is discussed in Sec. 3.3.2 at the tree and one-loop level. Finally, we summarize the main conclusions in Sec. 3.3.3.

3.3.1 The minimal SO(10) GUT vs the minimal SO(10) Higgs model

In the $\omega_{BL} \to 0$ regime of the $\mathbf{45} \oplus \mathbf{126} \oplus \mathbf{10}_{\mathbb{C}}$ SO(10) theory, the parameter space spans over the following set of couplings

$$\{\lambda_{\mathbb{R}}, \lambda_{\mathbb{C}}, g, \tau', \xi^2, \xi'^2, \omega_R, \sigma, \chi\} \tag{3.49}$$

with $\lambda_{\mathbb{R}}$ and $\lambda_{\mathbb{C}}$ denoting the real and the complex dimensionless scalar parameters listed already in Eqns. (2.21)–(2.22), respectively. The unified gauge coupling is labelled g as usual; τ', ξ^2, ξ'^2 are new dimensionful scalar parameters and ω_R, σ, χ comprise the full VEV information via Eq. (2.37). The "optimal" renormalization scale μ_R^2 is again calculated for every parameter point as an average of all the *heavy* tree-level scalar masses-squares. In total, the parameters span the 51-dimensional space with the imposed perturbativity constraints

$$|\lambda_{\mathbb{R}}|, |\lambda_{\mathbb{C}}|, |\chi| < 1 \quad 1\,\mathrm{GeV} < |\tau'|, |\xi|, |\xi'| < 10\omega_R \quad M_Z < |\sigma| < \omega_R < M_{Pl}, \quad (3.50)$$

where M_Z and M_{Pl} are the Z-boson mass and the Planck scale, respectively. The *viable* regions of the parameter space are identified by employing again the differential evolution algorithm in the *search mode*, in the same manner as described in Sec. 3.2.2, with the penalisation function vanishing only if all *viability* criteria (tachyonicity, gauge coupling unification, perturbativity) introduced in Sec. 3.1 are fulfilled. The resulting dataset of the *viable* points is labelled $\mathcal{D}$. Let us note that gauge coupling unification is studied at two loops and all one-loop corrections originating from $\mathbf{10}_{\mathbb{C}}$ are taken into account.

The *viable* dataset $\mathcal{D}$ can be readily compared with the dataset $\mathcal{B}$ of the *viable* parameter points in the $\mathbf{45} \oplus \mathbf{126}$ SO(10) Higgs model case, c.f. Sec. 3.2.2. Their main differences are compiled in Table 3.3.

Table 3.3: Characteristic features of the *viable* datasets $\mathcal{D}$ and $\mathcal{B}$ from the minimal SO(10) GUT and the minimal SO(10) Higgs model, both in the $\omega_{BL} \to 0$ regime, respectively.

Dataset	# of points	Scalar content	Gauge RGEs
$\mathcal{B}$	30000	$\mathbf{45} \oplus \mathbf{126}$	One-loop
$\mathcal{D}$	20000	$\mathbf{45} \oplus \mathbf{126} \oplus \mathbf{10}_{\mathbb{C}}$	Two-loop

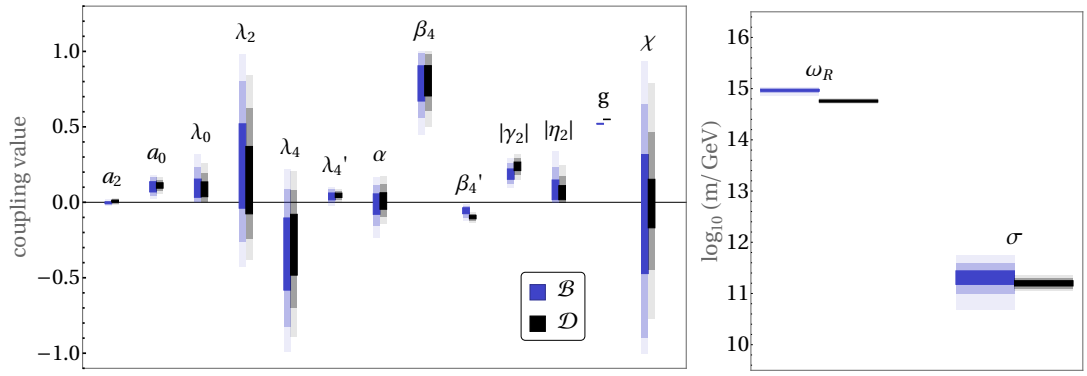

Figure 3.10: The 1-, 2- and 3-σ HDIs, differentiated by decreasing opacity, of the common dimensionless scalar parameters (left panel) and VEVs (right panel) for datasets $\mathcal{B}$ and $\mathcal{D}$.

In analogy with Sec. 3.2.2, we display in Fig. 3.10 and 3.11 all ranges of the common parameters (i.e. the ones which are present in the full theory as well as in the pure Higgs model) by showing the 1-, 2- and 3-σ HDIs of individual couplings

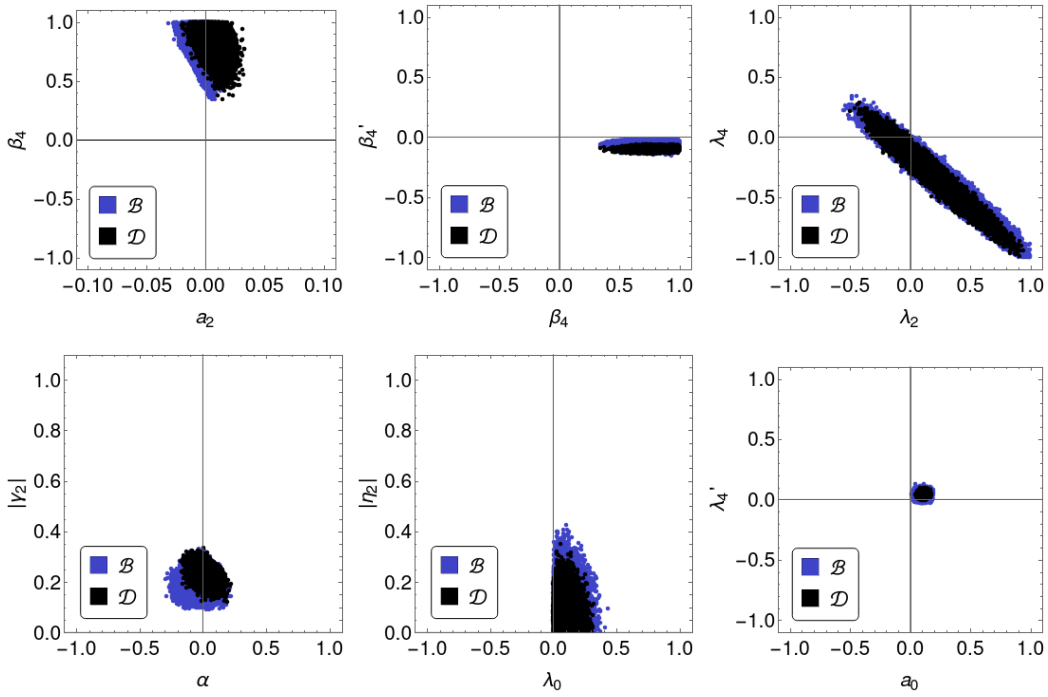

Figure 3.11: 2D scatter plots correlating pairs of dimensionless scalar parameters common to the minimal SO(10) GUT ($\mathcal{D}$ dataset) and the minimal SO(10) Higgs model ($\mathcal{B}$ dataset) in the $\omega_{BL} \to 0$ limit.

and the 2D correlation scatter plots, respectively. The two *viable* datasets assume almost identical shapes, thus salient features of the minimal SO(10) Higgs model apply also to the minimal SO(10) GUT under the study. However, there are some minor differences that are worth mentioning:

- The ω_R, σ VEVs and the gauge coupling g: There is a small shift in the ω_R and g values between the $\mathcal{B}$ and $\mathcal{D}$ datasets due to the gauge unification upgrade from one-loop to two-loop. The same effect was observed in [104]. The central value of the $|\sigma|$ VEV decreases from $\mathcal{B}$ to $\mathcal{D}$, contrary to the expectations based on the minimal fine-tuning unification analysis [104], because one SM doublet $(1, 2, +\frac{1}{2})$ has mass fixed to the σ scale in the two-loop gauge unification procedure, which is expected in case of the successful SM Higgs fine-tuning, c.f. Sec. 3.3.2 and Appendix B 3 in [16].

- Parameter ranges: The 3-σ HDIs of most of the common dimensionless parameters and the VEVs tend to be reduced in $\mathcal{D}$ as compared to $\mathcal{B}$. Intuitively, one would expect to see the opposite effect as a plethora of new couplings is introduced thanks to adding $\mathbf{10}_{\mathbb{C}}$ into the minimal SO(10) GUT. However, the two-loop gauge unification in combination with non-tachyonicity and perturbativity constraints induces even more serious parameter space restrictions. Finally, let us mention that the central values of a_2, β_4' and $|\gamma_2|$ are subject to small shifts betweem $\mathcal{B}$ and $\mathcal{D}$ datasets, c.f. Figs. 3.10–3.11.

3.3.2 The doublet mass fine-tuning

Contrary to the minimal SO(10) Higgs model, the fermion masses can be accommodated in the $\mathbf{45} \oplus \mathbf{126} \oplus \mathbf{10}_{\mathbb{C}}$ SO(10) GUT, which contains the **126** as well as $\mathbf{10}_{\mathbb{C}}$ in the scalar sector. Phenomenologically viable flavour fits require the SM VEV v_{SM} to be an admixture of the VEVs from both of the aforementioned SO(10) representations, c.f. Sec. 2.4.3, thus implying that the SM Higgs doublet $(1, 2, +\frac{1}{2})$ must be a significant admixure of the components from the $\mathbf{10}_{\mathbb{C}}$ and **126**.

Such observation has implications on the structure of the 4×4 doublet mass-squared matrix, which has the schematic form

$$M_S^2(1, 2, +\tfrac{1}{2}) = \begin{pmatrix} M_{126}^2 & M_{mix}^2 \\ M_{mix}^{2\dagger} & M_{10}^2 \end{pmatrix} \tag{3.51}$$

if written in the basis of the row states

$$\{(15, 2, +\tfrac{1}{2})_{\Sigma}, (15, 2, -\tfrac{1}{2})_{\Sigma^*}^*, (1, 2, +\tfrac{1}{2})_H, (1, 2, -\tfrac{1}{2})_{H^*}\} \tag{3.52}$$

with the basis fields specified by their $\mathrm{SU}(4)_C \times \mathrm{SU}(2)_L \times \mathrm{U}(1)_R$ transformation properties. The 2×2 sub-blocks M_{126}^2 and M_{10}^2 comprise contributions mixing solely doublets from the **126** and $\mathbf{10}_{\mathbb{C}}$, respectively, whilst M_{mix}^2 is the 2×2 sub-block governing the mixing of the doublets originating from the two different SO(10) representations. The expected sizes of the diagonal blocks are around the GUT scale, i.e.

$$M_{126}^2, M_{10}^2 \sim \mathcal{O}(\omega_R^2), \tag{3.53}$$

while the off-diagonal mixing falls around the $|\sigma|$ scale, that is

$$M_{mix}^2 \sim |\sigma|^2, \tag{3.54}$$

since no mixing between doublets from the **126** and $\mathbf{10}_{\mathbb{C}}$ representations can be invoked until the intermediate symmetry $\mathrm{SU}(4)_C \times \mathrm{SU}(2)_L \times \mathrm{U}(1)_R$ is spontaneously broken. In the phenomenologically viable GUT, one of the eigenvalues of the doublet mass matrix $M_S^2(1, 2, +\frac{1}{2})$ from Eq. (3.51) sets the scale of the SM Higgs doublet mass term at about 125 GeV. Moreover, the SM Higgs doublet eigenvector has to be a significant admixture of the components from the **126** as well as $\mathbf{10}_{\mathbb{C}}$. The latter requirement can be satisfied only if at least one of the eigenvalues of both diagonal blocks M_{126}^2, M_{10}^2 is *pre-tuned* from the GUT scale down to $M_{mix}^2 \sim |\sigma|^2$. Such a *pre-tuning* constraint is a necessary but not sufficient condition for the successful SM Higgs doublet fine-tuning.

Let us denote $m_{126,\pm}^2$ and $m_{10,\pm}^2$ the eigenvalues of the diagonal blocks M_{126}^2 and M_{10}^2, respectively, where the $+$ sign labels the larger and the $-$ sign refers to the smaller eigenvalue. In Sec. 2.4.3, we used the flavour fit [113] to estimate the approximate "amount" of the v_{SM} residing in **126**:

$$\sqrt{\frac{|v_{126}^u|^2 + |v_{126}^d|^2}{v_{SM}^2}} \gtrsim 3 \times 10^{-2} \equiv \epsilon, \tag{3.55}$$

which at the same time estimates the weights of the **126** and $\mathbf{10}_{\mathbb{C}}$ components in the SM Higgs doublet. Thus the *pre-tuning* constraint reads

$$m^2_{10,-} \sim |\sigma|^2 \qquad\qquad m^2_{126,-} \sim \frac{|\sigma|^2}{\epsilon}, \tag{3.56}$$

bringing an extra set of constraints to be applied to the scalar potential parameters. By plugging in the numerical values for the VEVs from the *viable* dataset $\mathcal{D}$ of Sec. 3.3.1, we obtain approximately

$$m^2_{10,-} \lesssim 10^{-7}\omega_R^2 \qquad\qquad m^2_{126,-} \lesssim 3.3\cdot 10^{-6}\omega_R^2. \tag{3.57}$$

Pre-tuning at the tree-level — analytically

We first study the doublet *pre-tuning* at the tree-level as the quantum loop corrections play a sub-dominant role in the non-PGB scalar sector. The tree-level doublet mass matrix in the basis (3.52) has the form

$$M^2(1,2,+\tfrac{1}{2})_{\text{tree}} = \begin{pmatrix} \left(\frac{\beta_4}{2}-9\beta_4'-3a_2\chi\right)\omega_R^2 & -2\gamma_2\omega_R^2 & -\sqrt{6}\zeta'\chi|\sigma|^2 & -\sqrt{6}\zeta\chi|\sigma|^2 \\ -2\gamma_2^*\omega_R^2 & \left(\frac{\beta_4}{2}-\beta_4'-a_2\chi\right)\omega_R^2 & \sqrt{6}(16\phi^*+\zeta^*\chi)|\sigma|^2 & \sqrt{6}(16\phi'^*+\zeta'^*\chi)|\sigma|^2 \\ -\sqrt{6}\zeta'^*\chi|\sigma|^2 & \sqrt{6}(16\phi+\zeta\chi)|\sigma|^2 & -\xi^2-\frac{\tau'\omega_R}{24}+(2\kappa_0+\kappa_2)\omega_R^2 & -2\xi'^2+2\left(2\kappa_0'+\kappa_2'\right)\omega_R^2 \\ -\sqrt{6}\zeta^*\chi|\sigma|^2 & \sqrt{6}(16\phi'+\zeta'\chi)|\sigma|^2 & -2\xi'^{2*}+2\left(2\kappa_0'^*+\kappa_2'^*\right)\omega_R^2 & -\xi^2+\frac{\tau'\omega_R}{24}+(2\kappa_0+\kappa_2)\omega_R^2 \end{pmatrix}, \tag{3.58}$$

where only dominant contributions in the $\omega_{BL}\to 0$ limit were retained.

- M^2_{126} sub-block tree-level eigenvalues: The tree-level M^2_{126} eigenvalues are

$$m^2_{126,\pm,(0)} = \left(\frac{\beta_4}{2} - 5\beta_4' - 2a_2\chi \pm \sqrt{(4\beta_4'+a_2\chi)^2+4|\gamma_2|^2}\right)\omega_R^2 + O\left(|\sigma|^2\right). \tag{3.59}$$

  The *pre-tuning* requires the ω_R^2-proportional contribution to the $m^2_{126,-,(0)}$ in Eq. (3.59) to be zeroed out in order to bring it down to the $|\sigma|^2$ scale, i.e. we demand

$$\frac{m^2_{126,-,(0)}}{\omega_R^2} \equiv \frac{\beta_4}{2} - 5\beta_4' - 2a_2\chi - \sqrt{(4\beta_4'+a_2\chi)^2+4|\gamma_2|^2} = 0. \tag{3.60}$$

  Eq. (3.60) can be viewed as q constraint imposed upon $|\gamma_2|$ since it only enters tree-level mass expressions of the $(15,2,+\frac{1}{2})$ and $(6,1,0)$ multiplets of $\mathrm{SU}(4)_C\times\mathrm{SU}(2)_L\times\mathrm{U}(1)_R$ to which the SM doublets $(1,2,+\frac{1}{2})$ and triplets $(\bar{3},1,+\frac{1}{3})$ belong, respectively. The tree-level *pre-tuning* (3.60) of $m^2_{126,-}$ thus directly influences non-tachyonicity of eigenvalues of the $|\gamma_2|$-dependent scalar mass matrices $M^2(1,2,+\frac{1}{2})_{\text{tree}}$ from Eq. (3.58) and $M^2(\overline{3},1,+\frac{1}{3})_{\text{tree}}$ that is computed as

$$M^2(\overline{3},1+\tfrac{1}{3})_{\text{tree}} = \begin{pmatrix} \left(\beta_4-4\beta_4'-2a_2\chi\right)\omega_R^2 & 4\gamma_2\omega_R^2 & 2\sqrt{2}(\beta_4\chi-8\lambda_4')\,|\sigma|^2 & -\sqrt{2}\zeta\omega_R^2 & -\sqrt{2}\zeta'\omega_R^2 \\ 4\gamma_2^*\omega_R^2 & \left(\beta_4-4\beta_4'-2a_2\chi\right)\omega_R^2 & 0 & -\sqrt{2}\zeta'^*\omega_R^2 & -\sqrt{2}\zeta^*\omega_R^2 \\ 2\sqrt{2}(\beta_4\chi-8\lambda_4')|\sigma|^2 & 0 & \left(2\beta_4-4\beta_4'-2a_2\chi\right)\omega_R^2 & -4(8\varphi+\zeta\chi)|\sigma|^2 & -4(8\varphi'+\zeta'\chi)|\sigma|^2 \\ -\sqrt{2}\zeta^*\omega_R^2 & -\sqrt{2}\zeta'\omega_R^2 & -4(8\varphi^*+\zeta^*\chi)|\sigma|^2 & -\xi^2+2\kappa_0\omega_R^2 & -2\xi'^{*2}+4\kappa_0'^*\omega_R^2 \\ -\sqrt{2}\zeta'^*\omega_R^2 & -\sqrt{2}\zeta\omega_R^2 & -4(8\varphi'^*+\zeta'^*\chi)|\sigma|^2 & -2\xi'^2+4\kappa_0'\omega_R^2 & -\xi^2+2\kappa_0\omega_R^2 \end{pmatrix} \tag{3.61}$$

with the basis of the row states defined as

$$\{(6,1,0)_\Sigma, (6,1,0)^*_{\Sigma^*}, (\overline{10},1,0)_\Sigma, (6,1,0)_H, (6,1,0)^*_{H^*}\} \tag{3.62}$$

under $\mathrm{SU}(4)_C \times \mathrm{SU}(2)_L \times \mathrm{U}(1)_R$. Again, only the dominant contributions in the $\omega_{BL} \to 0$ limit were kept in Eq. (3.61).

The necessary condition for non-tachyonicity of the triplet states can be quantified via Sylvester's criterion which states that $M^2(\overline{3},1,+\frac{1}{3})_{\text{tree}}$ has positive eigenvalues if and only if all its leading principal minors are positive, namely if the determinants of all upper-left $1\times 1, 2\times 2, 3\times 3, \ldots$ blocks are positive. For simplicity, let us focus only on the 3×3 upper-left sub-block of $M^2(\overline{3},1,+\frac{1}{3})_{\text{tree}}$ in Eq. (3.61) that mixes triplets purely from the **126**. Sylvester's criterion requires its leading principal minors

$$\mathcal{M}^2_{1\times 1} = (\beta_4 - 4\beta_4' - 2a_2\chi)\,\omega_R^2, \tag{3.63}$$
$$\mathcal{M}^2_{2\times 2} = \theta\;\omega_R^4, \tag{3.64}$$
$$\mathcal{M}^2_{3\times 3} = \theta\,(\beta_4 - 4\beta_4' - 2a_2\chi)\,\omega_R^6 + \mathcal{O}(|\sigma|^2\omega_R^2) \tag{3.65}$$

to be positive. For later convenience, we hid the entire $|\gamma_2|$-dependence in a single parameter

$$\theta := (\beta_4 - 4\beta_4' - 2a_2\chi)^2 - 16|\gamma_2|^2. \tag{3.66}$$

The triplet non-tachyonicity conditions can then be streamlined to

$$\theta > 0, \qquad\qquad \beta_4 - 4\beta_4' - 2a_2\chi > 0, \tag{3.67}$$

and they have to be accompanied by the tree-level non-tachyonicity requirements originating from all remaining *heavy* fields:

$$4\beta_4' + a_2\chi < 0, \qquad\qquad 2\beta_4' + a_2\chi < 0, \tag{3.68}$$
$$\beta_4 - 2\beta_4' - a_2\chi > 0, \qquad\qquad \beta_4 - 10\beta_4' - 4a_2\chi > 0, \tag{3.69}$$

cf. Table E.1. Thus Eqns. (3.67)–(3.69) constrain the allowed values of the parameters $\beta_4, \beta_4', |\gamma_2|, a_2, \chi$ and, as we shall see later, they are incompatible with the condition (3.60).

The $|\gamma_2|$-dependence of the M^2_{126} tree-level eigenvalues can be replaced by the θ-dependence, hence

$$m^2_{126,-,(0)}(\theta) = \left(\frac{\beta_4}{2} - 5\beta_4' - 2a_2\chi - \frac{1}{2}\sqrt{4\,(4\beta_4' + a_2\chi)^2 + (\beta_4 - 4\beta_4' - 2a_2\chi)^2 - \theta}\right)\omega_R^2. \tag{3.70}$$

The eigenvalue $m^2_{126,-,(0)}(\theta)$ is an increasing function of θ since

$$\frac{\partial m^2_{126,-,(0)}}{\partial\theta} = \frac{1}{4}\frac{\omega_R^2}{\sqrt{4\,(4\beta_4' + a_2\chi)^2 + (\beta_4 - 4\beta_4' - 2a_2\chi)^2 - \theta}} > 0. \tag{3.71}$$

Thus, the triplet non-tachyonicity constraint $\theta > 0$ implies that

$$m^2_{126,-,(0)}(\theta) \geq m^2_{126,-,(0)}(0) \tag{3.72}$$

with

$$m^2_{126,-,(0)}(0) = \left(\frac{\beta_4}{2} - 5\beta_4' - 2a_2\chi - \frac{1}{2}\sqrt{4\left(4\beta_4' + a_2\chi\right)^2 + \left(\beta_4 - 4\beta_4' - 2a_2\chi\right)^2}\right)\omega_R^2 \tag{3.73}$$

for any fixed choice of β_4, β_4', a_2 and χ parameters satisfying (3.67)–(3.69).

Numerically, we invoke the results of the *viable* dataset $\mathcal{D}$ from Sec. 3.3.1, which suggests that *viable* regions of the parameter space obey

$$\beta_4 \in [0.3, 1]\,, \qquad \beta_4' \in [-0.2, -0.02]\,, \tag{3.74}$$

$$a_2 \in [-0.03, 0.05]\,, \qquad \chi \in [-1, 1]\,. \tag{3.75}$$

Therefore, the lowest possible numerical value of the $m^2_{126,-,(0)}$ mass-square eigenvalue conforming to (3.67)–(3.69) is

$$\min_{\beta_4, \beta_4', a_2\chi} m^2_{126,-,(0)}(0) \approx 0.007\omega_R^2 \tag{3.76}$$

for $\beta_4 = 0.3$, $\beta_4' = -0.02$ and $a_2\chi = 0.05$. Thus $m^2_{126,-,(0)}$ can never be zeroed out and the *pre-tuning* constraint (3.56) is not satisfied at the tree-level.

- M^2_{10} sub-block tree-level eigenvalues: The tree-level M^2_{10} sub-block is the only part of the overall tree-level scalar mass-squared spectrum that depends on the scalar couplings κ_0', κ_2' and τ'. Therefore, we can always choose these parameters appropriately so that one of the M^2_{10} tree-level eigenvalues is fine-tuned to be of the order of $|\sigma|^2$.

Hence, we demonstrated that the tree-level *pre-tuning* in the M^2_{126} sub-block is problematic due to non-tachyonicity constraints required for other fields. Nevertheless, the $m^2_{126,-,(0)}$ tree-level eigenvalue can still be sufficiently suppressed so that one can hope that loop corrections, which in some cases reach up to $\sim 10\%\ \omega_R^2$, can be properly aligned and help to achieve the desired *pre-tuning* of Eq. (3.57) at the loop level.

Pre-tuning in the perturbation theory

As we saw in the previous section, successful *pre-tuning* in the **126**-sector has to rely on the appropriate alignment of quantum corrections with respect to the tree-level contribution. Ideally, the *pre-tuning* constraint (3.56) concerns quantities calculated to all orders of perturbation theory. However, one usually has access only to the lowest orders of the perturbative expansion; nevertheless, the effect of the higher-order corrections, although typically sub-dominant, should not be neglected.

We denote eigenvalues of the M^2_{126} and M^2_{10} sub-blocks of the doublet mass-squared matrix (3.51) calculated at the n-th loop level as $m^2_{126,\pm,(n)}$ and $m^2_{10,\pm,(n)}$,

respectively, with $n = 0$ representing the tree level; n-th loop eigenvalue corrections are labeled $\delta m^2_{126,\pm,(n)}$ and $\delta m^2_{10,\pm,(n)}$, so that

$$m^2_{126,\pm,(n+1)} = m^2_{126,\pm,(n)} + \delta m^2_{126,\pm,(n+1)}, \tag{3.77}$$

$$m^2_{10,\pm,(n+1)} = m^2_{10,\pm,(n)} + \delta m^2_{10,\pm,(n+1)}. \tag{3.78}$$

For any loop order n for which loop corrections $\delta m^2_{126,-,(n+1)}$ and $\delta m^2_{10,-,(n+1)}$ are larger than $\sim |\sigma|^2$ and $\sim |\sigma|^2/\epsilon$, respectively, the *pre-tuning* has to be achieved at least down to the level of the next-order loop corrections, i.e.

$$\left|m^2_{126,-,(n)}\right| \lesssim \left|\delta m^2_{126,-,(n+1)}\right|, \tag{3.79}$$

$$\left|m^2_{10,-,(n)}\right| \lesssim \left|\delta m^2_{10,-,(n+1)}\right|, \tag{3.80}$$

while one anticipates proper alignment of the higher loop corrections to satisfy the *pre-tuning* constraint (3.56). Conditions (3.79)–(3.80) at the n-th perturbative level are referred to as n-PL *pre-tuning* and they form necessary but not sufficient doublet fine-tuning constraints. If n-PL *pre-tuning* fails, the proper *pre-tuning* cannot be attained.

In practice, the n-th loop level is the highest perturbative order one has access to and the $(n+1)$-th loop level mass corrections may only be estimated via e.g. *loop expansion parameter* η_x that can be defined as

$$\eta^n_x \approx \left|\frac{\delta m^2_{x,(n)}}{m^2_{x,(0)}}\right| \tag{3.81}$$

for a scalar field generally labeled x. Values of η_x are specific to the selected parameter point and the quantity of comparison in the denominator ($m^2_{x,(0)}$) is assumed not to be spuriously suppressed. Consequently, the $(n+1)$-th loop level mass corrections of the lighter eigenvalues are estimated using the loop expansion factor calculated for their heavier eigenvalue counterparts (the ones not suppressed by fine-tuning):

$$\delta m^2_{126,-,(n+1)} \approx (\eta_{126+})^{n+1} \left|m^2_{126,+,(0)}\right|, \tag{3.82}$$

$$\delta m^2_{10,-,(n+1)} \approx (\eta_{10+})^{n+1} \left|m^2_{10,+,(0)}\right|. \tag{3.83}$$

In the present study of the minimal SO(10) GUT, we have access only to the numerical one-loop scalar mass corrections. Hence we set $n = 1$ and test for 1-PL *pre-tuning* which demands suppression of one-loop doublet eigenvalues $m^2_{126,-,(1)}$, $m^2_{10,-,(1)}$ to the level of the two-loop corrections. We estimate the loop expansion parameters of the heavier eigenvalues $m^2_{126,+}$, $m^2_{10,+}$ as

$$\eta_{126} := \left|\frac{\delta m^2_{126,+,(1)}}{m^2_{126,+,(0)}}\right| = \left|\frac{m^2_{126,+,(1)} - m^2_{126,+,(0)}}{m^2_{126,+,(0)}}\right|, \tag{3.84}$$

$$\eta_{10} := \left|\frac{\delta m^2_{10,+,(1)}}{m^2_{126,+,(0)}}\right| = \left|\frac{m^2_{10,+,(1)} - m^2_{10,+,(0)}}{m^2_{126,+,(0)}}\right|, \tag{3.85}$$

where the $m^2_{10,+,(0)}$ quantity in the denominator of η_{10} in Eq. (3.85) has been replaced by $m^2_{126,+,(0)}$ to account for instances where the numerical 1-PL *pre-tuning*

in the M_{10}^2 diagonal block spuriously suppresses both of its tree-level eigenvalues due to the large number of relatively unconstrained scalar parameters available there. Two-loop doublet mass corrections are thus estimated as

$$\delta m^2_{126,-,(2)} \approx (\eta_{126})^2 \ \left| m^2_{126,+,(0)} \right|, \tag{3.86}$$

$$\delta m^2_{10,-,(2)} \approx (\eta_{10})^2 \ \left| m^2_{126,+,(0)} \right|, \tag{3.87}$$

and the 1-PL *pre-tuning* requires

$$\left| m^2_{126,-,(1)} \right| \lesssim (\eta_{126})^2 \ \left| m^2_{126,+,(0)} \right|, \tag{3.88}$$

$$\left| m^2_{10,-,(1)} \right| \lesssim (\eta_{10})^2 \ \left| m^2_{126,+,(0)} \right|, \tag{3.89}$$

in accordance to Eqns. (3.79)–(3.80).

For later convenience, we introduce a pair of *suppression ratios*

$$R_{126} := \left| \frac{m^2_{126,-,(1)}}{m^2_{126,+,(0)}} \right|, \tag{3.90}$$

$$R_{10} := \left| \frac{m^2_{10,-,(1)}}{m^2_{126,+,(0)}} \right| \tag{3.91}$$

of the smaller one-loop eigenvalues $m^2_{126,-,(1)}, m^2_{10,-,(1)}$ with respect to the generic unsuppressed tree-level mass $m^2_{126,+,(0)}$. The level of the 1-PL *pre-tuning* (3.88)–(3.89) can then be measured for every point in the parameter space by evaluating

$$S_{126} := \frac{R_{126}}{\eta^2_{126}}, \tag{3.92}$$

$$S_{10} := \frac{R_{10}}{\eta^2_{10} \cdot 10^{-2}} \tag{3.93}$$

with factor 10^{-2} being inserted in the definition of S_{10} to increase the strictness of the 1-PL *pre-tuning* criterion (3.89) in order to compensate for the usage of $m^2_{126,+,(0)}$ instead of $m^2_{126,-,(0)}$ in η_{10} and R_{10}. Note that such a stricter constraint imposed upon the $\mathbf{10}_{\mathbb{C}}$-sector faces no obstructions as the sufficient *pre-tuning* in the M_{10}^2 block can be achieved already at the tree-level. We then claim that a point in the parameter space satisfies the 1-PL *pre-tuning* conditions if

$$S_{126} \leq 1, \tag{3.94}$$

$$S_{10} \leq 1. \tag{3.95}$$

Whenever such a point is also *viable*, i.e. meets the *viability* criteria introduced in Sec. 3.1, it is referred to as *SM-compatible*.

Pre-tuning at the one-loop level — numerically

In analogy to the SO(10) Higgs model numerical study in Sec. 3.2, the suitability criteria (*viability* constraints introduced in Sec. 3.1 and 1-PL *pre-tuning* (3.95)–(3.94)) are implemented via penalization function and suitable regions of the parameter space are examined by the stochastic version of the differential evolution algorithm. We generate various datasets, labeled $\mathcal{S}^{(x)}$ with $x = 2.0, 1.5, 1.0,$

of *viable* parameter points which satisfy the 1-PL *pre-tuning* constraint $S_{10} \leq 1$ of Eq. (3.95) in the M_{10}^2 doublet mass block and an increasingly more stringent criterion $S_{126} \leq x$ in the M_{126}^2 sector. Note that only dataset $\mathcal{S}^{(1.0)}$ contains the fully *SM-compatible* parameter points. For every dataset, we first use the differential evolution algorithm in the *minimization mode* to locate the appropriate part of the parameter space and only after that, the *search mode* is engaged to explore such region. As already indicated in the tree-level discussions, the 1-PL *pre-tuning* in the **126**-sector is difficult to attain as opposed to the *viability* and $S_{10} \leq 1$ criteria which were easily met. Moreover, it was noticed that the location of the 1-PL *fine-tuned* parts of the parameter space tend to strongly correlate with perturbatively problematic regions. Thus the $\mathcal{S}^{(x)}$ datasets are compared to the dataset $\mathcal{D}$ of the generally non-finetuned *viable* points discussed in Sec. 3.3.1 as well as to the dataset $\mathcal{T}$ of *viable* parameter points with increased stability under the RG running imposed by demanding $\bar{t} \geq 1$. The main attributes of all aforementioned datasets are conveniently listed in Table 3.4.

Table 3.4: *Viable* datasets with several extra constraints imposed on them. The penultimate and the last column specify $\bar{t}$ and S_{126} ranges for points in datasets, respectively.

Dataset	# of points	constraints	$\bar{t}$ range	S_{126} range
$\mathcal{D}$	20000	unconstrained	$0.36 - 1.06$	$2.88 - 267$
$\mathcal{S}^{(2.0)}$	2000	$S_{10} \leq 1,\ S_{126} \leq 2$	$0.34 - 0.49$	$1.57 - 2.00$
$\mathcal{S}^{(1.5)}$	2000	$S_{10} \leq 1,\ S_{126} \leq 1.5$	$0.34 - 0.52$	$1.19 - 1.50$
$\mathcal{S}^{(1.0)}$	2000	$S_{10} \leq 1,\ S_{126} \leq 1$	$0.34 - 0.41$	$0.92 - 1.00$
$\mathcal{T}$	20000	$\bar{t} \geq 1$	$1.00 - 1.20$	$5.67 - 30.3$

There are several observations one can make already from Table 3.4. Although we were able to confirm the existence of the *SM-compatible* parameter points, collected in $\mathcal{S}^{(1.0)}$, they tend to acquire relatively high S_{126} measure, close to the 1-PL *fine-tuning* threshold. Such finding corresponds to the trend noticed during searches for suitably fine-tuned points via the *minimization mode* of the differential evolution algorithm when it was more and more difficult to obtain better 1-PL *fine-tuned* points. Furthermore, comparison of the $\bar{t}$ ranges of $\mathcal{S}^{(x)}$ datasets with $\mathcal{D}$ and $\mathcal{T}$ hints that *pre-tuning* favours regions with low RG-stability ($\bar{t} \lesssim 0.5$), implying a scalar coupling value blows up when run half-an-order of magnitude in the renormalization scale up or down for points in the $\mathcal{S}$-type datasets. Such points, although *viable*, cannot be considered perturbatively stable.

The same issue can be observed in Fig. 3.12, where we show the suppression ratios R_{126} and the loop expansion parameters η_{126} for all points in the datasets $\mathcal{D}$, $\mathcal{S}^{(2.0)}$, $\mathcal{S}^{(1.5)}$, $\mathcal{S}^{(1.0)}$ and $\mathcal{T}$ colour-coded by **black**, **purple**, **magenta**, **red** and **cyan**, respectively. Larger values of the expansion parameter η_{126} indicate an increased relative size of the radiative corrections, and smaller suppression ratio R_{126} implies a bigger hierarchy between the M_{126}^2 eigenvalues. The straight solid grey line labeled η depicts points for which the one-loop lighter-doublet eigenvalue $m^2_{126,-,(1)}$ (the one subject to the 1-PL *pre-tuning*) has the size of one-loop mass corrections estimated from the heavier $m^2_{126,+,(1)}$. The orange curves marked $x \cdot \eta^2$ indicate boundaries of regions where the lighter-doublet eigenvalue of the **126**-

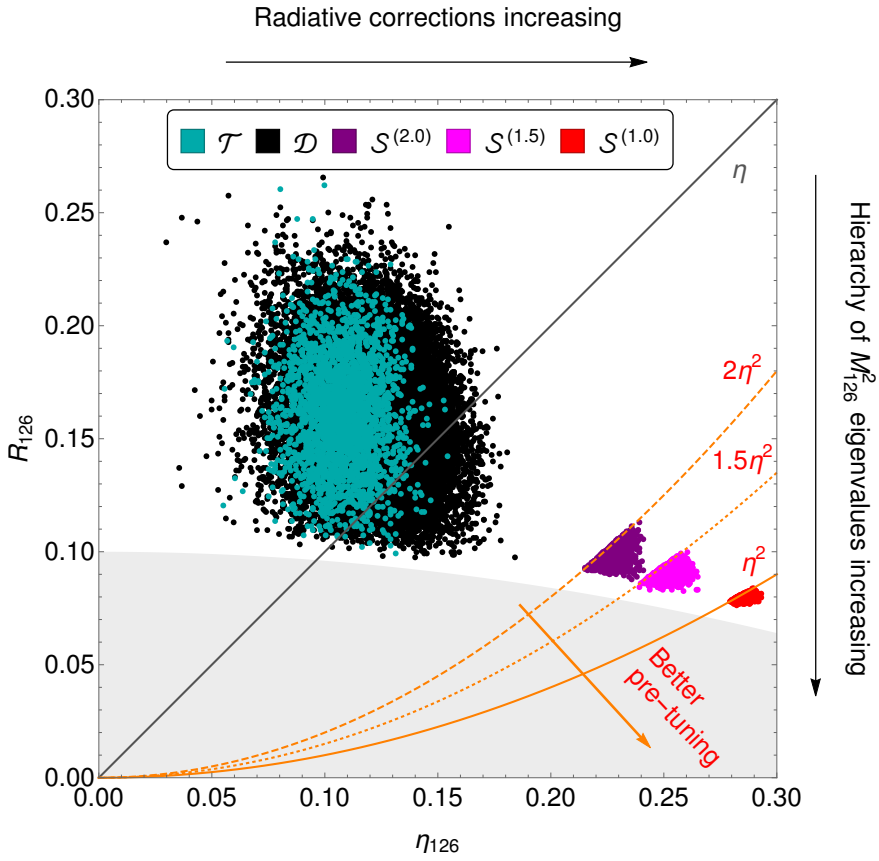

Figure 3.12: The figure shows the suppression ratio R_{126} with respect to the loop expansion parameter η_{126} values for all points in the datasets listed in Table 3.4. The non-finetuned *viable* points from the $\mathcal{D}$ and $\mathcal{T}$ datasets reside around the grey solid line $R_{126} = \eta_{126}$, while the points complying with 1-PL *fine-tuning* of various strictness $S_{126} \leq x$, $x = 2.0, 1.5, 1.0$, are below the orange-colored $R_{126} = x \cdot \eta^2_{126}$ curves. It is clear that the *SM-compatible* parameter points of $\mathcal{S}^{(1.0)}$ are found only in regions where large radiative corrections with $\eta_{126} \gtrsim 0.28$ have to be invoked.

sector is 1-PL *pre-tuned* to the level $S_{126} \leq x$. The smaller the x, the more the corresponding $\mathcal{S}^{(x)}$ domains shrink and recede towards regions with larger expected loop corrections. For all *SM-compatible* parameter points, the loop suppression factor is even $\eta_{126} \gtrsim 0.28$. Rather than enlarging hierarchy between the two M^2_{126} eigenvalues, i.e. entering grey region with $R_{126} \lesssim 0.08$, the successful 1-PL *pre-tuning* is carried out by enlarging quantum corrections at the expense of stability under the RG running that prefers smaller η_{126}, c.f. dataset $\mathcal{T}$ clustering around $\eta_{126} < 0.15$, leading to the clear dichotomy between requiring *pre-tuning* and perturbative stability. The same inconsistency between the $\mathcal{S}$-type datasets and the dataset $\mathcal{T}$ with increased RG-stability can be observed in Figs. 3.13–3.15, which show 1-,2- and 3-σ HDIs for all relevant couplings. This is most evident in the case of λ_2, λ_4, η_2, ζ, ζ', φ' and χ dimensionless parameters whose magnitudes in the $\mathcal{S}^{(x)}$ datasets are pushed towards larger values due to fine-tuning in the SM doublet sector, whereas absolute values of the same couplings in the $\mathcal{T}$ datasets are rather suppressed to maintain perturbative stability.

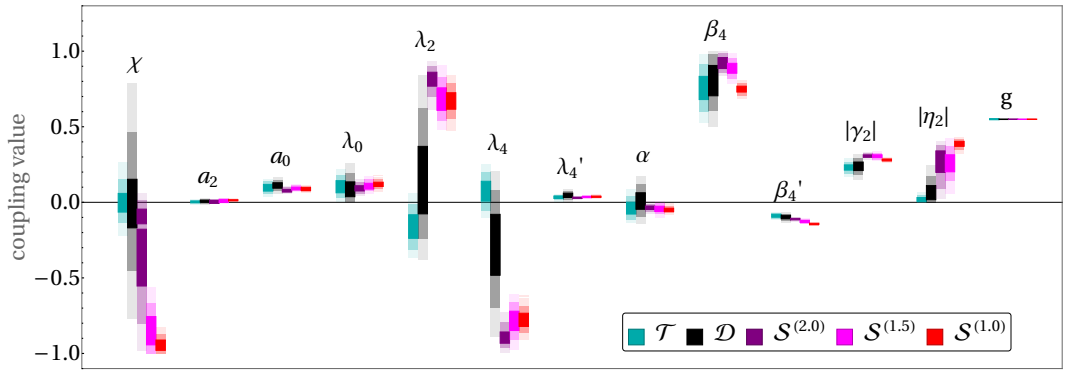

Figure 3.13: 1-, 2- and 3-σ HDIs (decreasing opacity) of VEV ratio χ, unified gauge coupling g and dimensionless scalar parameters common to the minimal SO(10) Higgs model and the minimal SO(10) GUT under study for all datasets listed in Table 3.4.

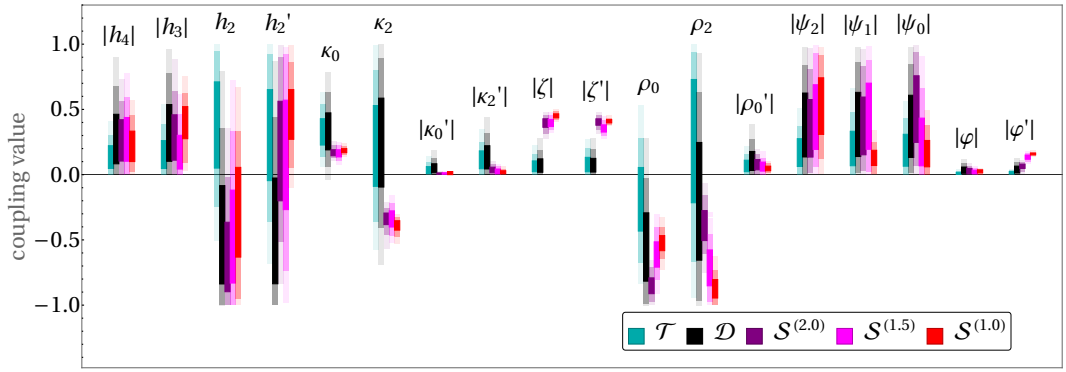

Figure 3.14: 1-, 2- and 3-σ HDIs (decreasing opacity) of dimensionless scalar parameters present in the minimal SO(10) GUT solely due to adding scalar $\mathbf{10}_{\mathbb{C}}$ for all datasets listed in Table 3.4.

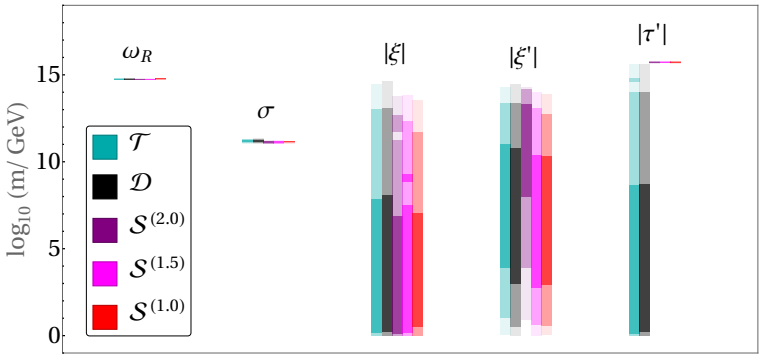

Figure 3.15: 1-, 2- and 3-σ HDIs (decreasing opacity) of VEVs and dimensionful scalar parameters for all datasets listed in Table 3.4.

Finally, notice that the τ' dimensionful parameter in the fine-tuned datasets $\mathcal{S}^{(x)}$ acquires very specific values $|\tau'| \sim \omega_R$, c.f. Fig. 3.15. This is due to the

1-PL *fine-tuning* criterion $S_{10} \leq 1$ imposed upon $\mathbf{10}_{\mathbb{C}}$-sector of the doublet mass matrix from Eq. (3.58) as the M_{10}^2 sub-block is the only part of tree-level scalar spectrum dependent on τ'. Furthermore, it turns out that the *pre-tuning* criterion applied in the $\mathcal{S}$-type datasets inflicts constraints also on the complex phases of dimensionless parameters, see Fig. 3.16, as opposed to the datasets $\mathcal{D}$ and $\mathcal{T}$ where all phases are uniformly distributed over the $[0, 2\pi)$ interval.

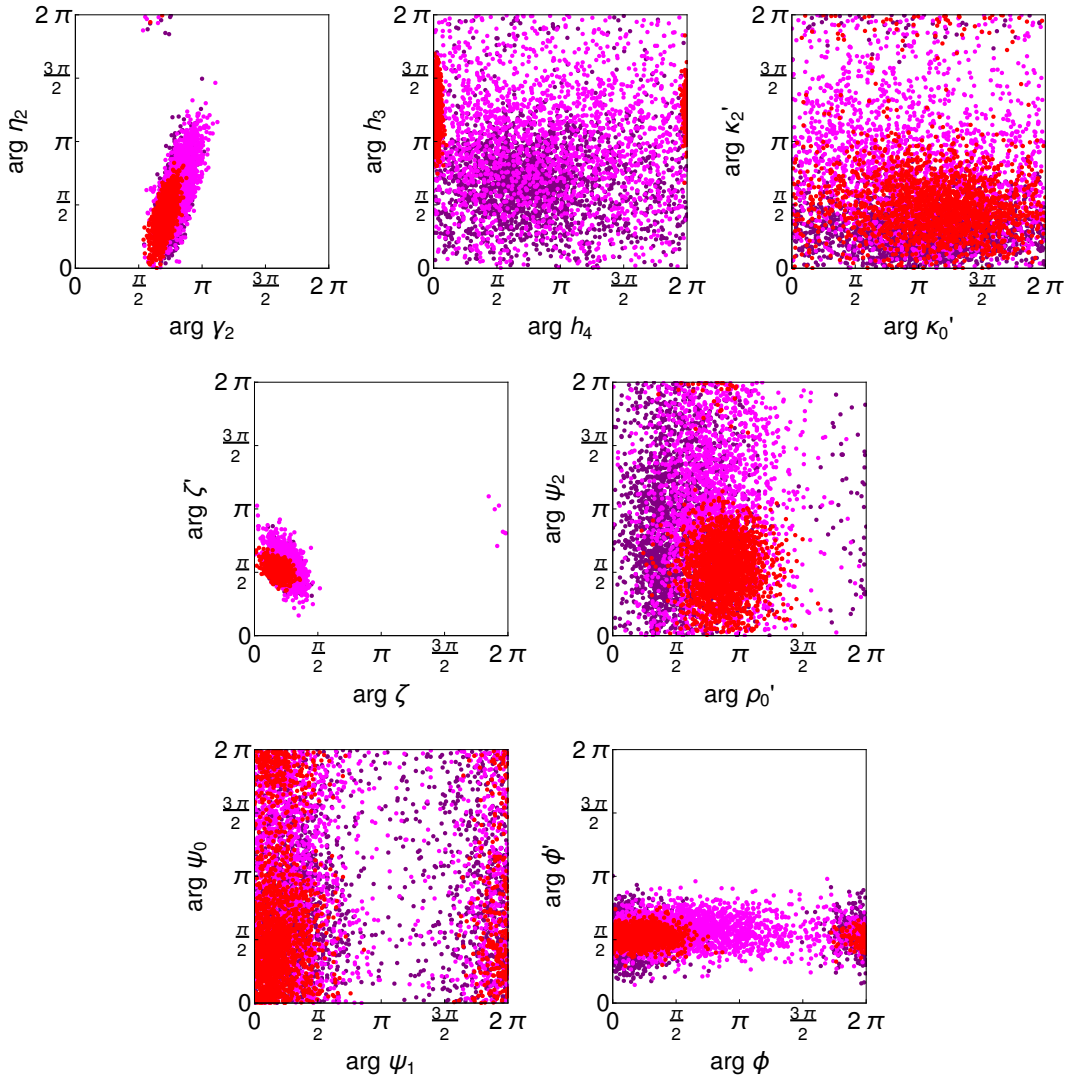

Figure 3.16: 2D scatter plots correlating pairs of phases of dimensionless scalar parameters of points from $\mathcal{S}^{(2.0)}$, $\mathcal{S}^{(1.5)}$ and $\mathcal{S}^{(1.0)}$ datasets colour-coded by **purple**, **magenta** and **red**.

3.3.3 Main conclusions of the $\mathbf{45} \oplus \mathbf{126} \oplus \mathbf{10}_{\mathbb{C}}$ SO(10) GUT analysis

The scalar sector of the $\mathbf{45} \oplus \mathbf{126} \oplus \mathbf{10}_{\mathbb{C}}$ SO(10) GUT, particularly the structure of the mass matrix of the SM doublet $(1, 2, +\frac{1}{2})$ multiplets, were thoroughly studied in the $\omega_{BL} \to 0$ regime. We argued that the SM Higgs doublet can be properly realized along with the phenomenologically viable flavour fits only if the doublet

mass matrix $M_S^2(1,2,+\frac{1}{2})$ satisfies *pre-tuning* criteria, i.e. both diagonal sub-blocks M_{126}^2, M_{10}^2 contain at least one eigenvalue as low as $|\sigma|^2$.

The *pre-tuning* at tree-level turned out to be impossible in the **126**-sector due to tachyonicity of other scalar fields, hence we had to rely on the loop corrections to be properly aligned. By carrying out numerical parameter space analysis at the one-loop level, we indeed identified patches of the parameter space which are *SM-compatible* (comply with the *viability* and 1-PL *pre-tuning* requirements) and can, in principle, support *pre-tuned* doublet masses. However, these regions of the parameter space are rather unstable with respect to the RG-running with $\bar{t} \lesssim 0.5$. Every *SM-compatible* point thus hits a Landau-pole singularity in at least one of the scalar couplings within half an order of magnitude around the GUT scale and the perturbative stability of these parameter points is strongly questionable. Hence, the realistic fermion mass fit cannot be realized at the perturbative level in the $\omega_{BL} \to 0$ regime of the $\mathbf{45} \oplus \mathbf{126} \oplus \mathbf{10}_{\mathbb{C}}$ SO(10) GUT.

4. Conclusions

The minimal renormalizable non-supersymmetric SO(10) Grand Unified Theory with the scalar sector $\mathbf{45}\oplus\mathbf{126}\oplus\mathbf{10}_{\mathbb{C}}$, where the former two representations trigger spontaneous symmetry breaking of SO(10) to $\mathrm{SU}(3)_c \times \mathrm{SU}(2)_L \times \mathrm{U}(1)_Y$ and the latter two representations support a realistic Yukawa sector, raises attention as a potentially viable candidate for a beyond the Standard Model theory which is also capable to provide proton decay predictions with theoretical uncertainties severely restrained. Such favourable features are however compensated by the need to study the model at the quantum level [11] as its tree-level scalar spectrum suffers from tachyonic instabilities [8–10].

For that reason we developed a numerical procedure to calculate the full one-loop mass corrections to all scalar masses for the general configuration of VEVs of $\mathbf{45}\oplus\mathbf{126}$, i.e. for a general symmetry breaking pattern. We thus improved the previous state-of-the-art analytical results for one-loop mass corrections [15, 159] devised only for potentially tachyonic scalars (dubbed PGBs), which were carried out in the $a_2 \to 0$, $|\gamma_2| \to 0$, $\sigma \to 0$ limit of the $\mathbf{45} \oplus \mathbf{126}$ SO(10) Higgs model. Furthermore, the full set of one-loop beta functions of all dimensionless scalar parameters in the scalar potential was analytically derived.

With these new computational tools at hand, we formulated a set of *viability* criteria that have to be satisfied by any realistic setting of the minimal SO(10) model, namely the non-tachyonicity of the mass spectrum, gauge coupling unification at a suitable GUT scale and perturbativity. The last criterion ensures all calculations are under perturbative control by restricting the magnitude of the one-loop mass corrections and by controlling the stability of the scalar couplings under the RG running. Consequently, it was shown that only two potentially viable symmetry breaking patterns with well-pronounced $\mathrm{SU}(4)_C \times \mathrm{SU}(2)_L \times \mathrm{U}(1)_R$ (referred to as $\omega_{BL} \to 0$ regime) or $\mathrm{SU}(3)_c \times \mathrm{SU}(2)_L \times \mathrm{SU}(2)_R \times \mathrm{U}(1)_{B-L}$ (referred to as $\omega_R \to 0$ regime) intermediate symmetries lead to a perturbative VEV configurations that keep the VEV structure (3.7) under control.

Initially, we carried out numerical analysis of the $\mathbf{45} \oplus \mathbf{126}$ SO(10) Higgs model in both the $\omega_{BL} \to 0$ and $\omega_R \to 0$ limiting cases with gauge coupling unification considered at one loop. Such study allowed us to examine the basic *viability* aspects (non-tachyonicity, gauge coupling unification, perturbativity) in the simplified setting as the influence of the scalar $\mathbf{10}_{\mathbb{C}}$ is subdominant outside the flavour sector. We found *viable* points of the parameter space in both symmetry breaking regimes. Contrary to previous simplified studies [13–15], the *viable* regions of the parameter space did not admit vanishing $|\gamma_2|$, namely $|\gamma_2| \gtrsim 0.1$, since full one-loop mass corrections to the PGBs were taken into account. Such observation is further supported by the semi-analytical non-tachyonicity analysis performed in the $a_2 \to 0$, $\sigma \to 0$ limit.

The results of the minimal SO(10) Higgs model study revealed preference for the $\omega_{BL} \to 0$ regime with the $\mathrm{SU}(4)_C \times \mathrm{SU}(2)_L \times \mathrm{U}(1)_R$ intermediate symmetry stage because the $\omega_R \to 0$ case is disfavoured by decreased perturbative stability, where only parameter points with $\bar{t} < 2$ are admitted, as well as by the position of the GUT scale at $\sim 10^{18}$ GeV and the seesaw scale at $\sim 10^8$ GeV, which are rather close to the Planck scale and the Davidson-Ibarra bound [158], respectively.

Finally, we provided proton lifetime predictions in the framework of the minimal SO(10) Higgs model and rough estimates of the corresponding theoretical uncertainties for two decay channels $p \to \pi^+ \overline{\nu}$ and $p \to K^+ \overline{\nu}$ with antineutrinos in the final states. We showed that the predicted partial proton decay rates are above the experimental upper bounds in the $\omega_{BL} \to 0$ case. However, such a result can be alleviated by upgrading the gauge unification analysis to two-loops or by fine-tuning mass of a suitable scalar sector down to the desert [12–14].

The full minimal $\mathbf{45} \oplus \mathbf{126} \oplus \mathbf{10}_{\mathbb{C}}$ SO(10) GUT was subsequently analyzed in the $\omega_{BL} \to 0$ limit with gauge unification examined at two loops. We demonstrated that the overall shape of the *viable* parameter space in the minimal SO(10) GUT and in the minimal SO(10) Higgs model do not differ, thus retrospectively supporting the assumption that the additional $\mathbf{10}_{\mathbb{C}}$ has only insignificant influence on the salient features of the *viable* parameter space. The GUT scale is found to be $\sim 10^{15}\,\mathrm{GeV}$, which raises concerns about proton decay that were already demonstrated in the SO(10) Higgs model analysis, suggesting that one should resort to bringing mass of a suitable scalar multiplet down to the desert. Nevertheless, we managed to reveal a feature of the $\mathbf{45} \oplus \mathbf{126} \oplus \mathbf{10}_{\mathbb{C}}$ SO(10) GUT that makes the aforementioned potential matter stability concerns obsolete. Namely, we argued that the Standard-Model-like Higgs doublet has to be a sufficient admixture of the components from the $\mathbf{126}$ and the $\mathbf{10}_{\mathbb{C}}$ in all realistic flavour fits; however such admixture cannot be achieved in the perturbative regime as the parameter points satisfying doublet mixing hit a Landau-pole singularity when run for less than half-an-order of magnitude up or down in the renormalization scale. Hence parts of the *viable* parameter space accommodating the Standard Model fermion masses and mixings correlate with regions of severely reduced perturbative stability in the minimal $\mathbf{45} \oplus \mathbf{126} \oplus \mathbf{10}_{\mathbb{C}}$ SO(10) GUT. Such an issue was hinted at semi-analytically at the tree level and fully confirmed numerically at the one-loop level.

The $\mathbf{45} \oplus \mathbf{126}$ SO(10) Higgs model and the $\mathbf{45} \oplus \mathbf{126} \oplus \mathbf{10}_{\mathbb{C}}$ SO(10) GUT analyses illustrated the importance of perturbativity considerations as powerful tools for model discrimination in the theories with a large number of field degrees of freedom. Implementing perturbativity constraints can therefore help to severely restrain potentially viable regions of the parameter space without adopting any further phenomenological requirements.

A. M_Z-scale gauge couplings

We discuss the initial condition of the gauge running factors $\{\alpha_c^{-1}, \alpha_L^{-1}, \alpha_1^{-1}\}$ at the M_Z scale.

Strong coupling

The strong coupling at M_Z scale in the $\overline{\text{MS}}$ renormalization scheme without top threshold contribution and averaged over the values obtained by experiment and lattice calculations is [160]

$$\alpha_{\overline{\text{MS}},c}^{(5)}(M_Z) = 0.1179 \pm 0.0009. \tag{A.1}$$

The two-loop level top quark threshold corrections follow from [161–163]

$$\left(\alpha_{\overline{\text{MS}},c}^{(6)}\right)^{-1}(M_Z) = \left(\alpha_{\overline{\text{MS}},c}^{(5)}\right)^{-1}(M_Z) + 4\pi\lambda_{top}(M_Z), \tag{A.2}$$

where λ_{top} is the one-loop threshold factor computed as

$$\lambda_{top}(M_Z) = \frac{1}{12\pi^2}\log\frac{M_t}{M_Z} \tag{A.3}$$

with the Z mass [160]

$$M_Z = 91.1876 \pm 0.0021\,\text{GeV} \tag{A.4}$$

and the top quark mass [160]

$$M_t = 172.89 \pm 0.28_{exp} \pm 0.52_{MC}\,\text{GeV}. \tag{A.5}$$

Subscripts "exp" and "MC" differentiate between uncertainties given by the experimental measurements and mass parameter implementation in Monte Carlo generators, respectively. Hence

$$\left(\alpha_{\overline{\text{MS}},c}^{(6)}\right)^{-1}(M_Z) = 8.550 \pm 0.065. \tag{A.6}$$

Electromagnetic coupling

The QED coupling in the $\overline{\text{MS}}$ renormalization scheme and at the M_Z scale without top quark threshold contribution is given by [151]

$$\alpha_{\overline{\text{MS}}}^{(5)}(M_Z) = \frac{\alpha}{1 - \Delta\alpha_{lep}^{(5)}(M_Z) - \Delta\alpha_{had}^{(5)}(M_Z) - \Delta\alpha_{top}^{(5)}(M_Z) - \tilde{\Delta}(M_Z)}, \tag{A.7}$$

where [160]

$$\alpha^{-1} = 137.035999084 \pm 0.000000021. \tag{A.8}$$

Four-loop contributions from leptons are calculated as [152]

$$\Delta\alpha_{lep}^{(5)}(M_Z) = \left(\frac{\alpha}{\pi}\right)13.52631(8) + \left(\frac{\alpha}{\pi}\right)^2 14.38553(6) + \left(\frac{\alpha}{\pi}\right)^3 84.8285(7) +$$

$$+\left(\frac{\alpha}{\pi}\right)^4 [810.65(1) - 39.8893(5)] + O\left(\alpha^5\right), \tag{A.9}$$

thus employing Eq. A.8 one has

$$\Delta\alpha^{(5)}_{lep}(M_Z) = 0.0314979 \pm 0.0000002. \tag{A.10}$$

The corresponding hadronic contribution is [160]

$$\Delta\alpha^{(5)}_{had}(M_Z) = 0.02766 \pm 0.00007 \tag{A.11}$$

and the three-loop QCD effects originating from the top quark are included by [150]

$$\begin{aligned}\Delta\alpha^{(5)}_{top}(M_Z) = &-\frac{4}{45}\frac{\alpha}{\pi}\frac{M_Z^2}{M_t^2}\left\{1 + 5.062\frac{\alpha_s^{\overline{\rm MS},(5)}(M_Z)}{\pi} + \left(28.220 + 9.702\ln\frac{M_Z^2}{M_t^2}\right)\cdot\right.\\ &\cdot\left(\frac{\alpha_s^{\overline{\rm MS},(5)}(M_Z)}{\pi}\right)^2 + \frac{M_Z^2}{M_t^2}\left[0.1071 + 0.8315\frac{\alpha_s^{\overline{\rm MS},(5)}(M_Z)}{\pi} + \right.\\ &\left.\left.+\left(6.924 + 1.594\ln\frac{M_Z^2}{M_t^2}\right)\left(\frac{\alpha_s^{\overline{\rm MS},(5)}(M_Z)}{\pi}\right)^2\right]\right\},\end{aligned} \tag{A.12}$$

which leads to

$$\Delta\alpha^{(5)}_{top}(M_Z) = -0.0000719 \pm 0.0000007 \tag{A.13}$$

after inserting (A.4)–(A.5). The difference between $\overline{\rm MS}$ and on-shell schemes is given by [160]

$$\tilde{\Delta} = 0.007127 \pm 0.000002. \tag{A.14}$$

After putting all numerical values from Eqns. (A.10)–(A.11) and (A.13)–(A.14) into Eq. (A.7), one obtains

$$\left(\alpha^{(5)}_{\overline{\rm MS}}\right)^{-1}(M_Z) = 127.96244387 \pm 0.00000002. \tag{A.15}$$

Finally, the QED coupling with the top quark threshold contributions is calculated by [151]

$$\begin{aligned}\alpha^{(6)}_{\overline{\rm MS}}(M_Z) = &\alpha^{(5)}_{\overline{\rm MS}}(M_Z)\left\{1 + \frac{4}{9}\frac{\alpha^{(5)}_{\overline{\rm MS}}(M_Z)}{\pi}\left[\frac{15}{4}\left(\frac{\alpha^{(5)}_{\overline{\rm MS},c}(M_Z)}{5} + \frac{\alpha^{(5)}_{\overline{\rm MS}}(M_Z)}{3\pi}\right) + \right.\right.\\ &\left.\left. + \log\frac{M_Z^2}{M_t^2}\left(1 + \frac{\alpha^{(5)}_{\overline{\rm MS},c}(M_Z)}{5} + \frac{\alpha^{(5)}_{\overline{\rm MS}}(M_Z)}{3\pi}\right)\right]\right\},\end{aligned} \tag{A.16}$$

hence

$$\left(\alpha^{(6)}_{\overline{\rm MS}}\right)^{-1}(M_Z) = 128.13515390 \pm 0.00000002. \tag{A.17}$$

Weak mixing angle

The value of the weak mixing angle at the M_Z scale in the $\overline{\rm MS}$ renormalization scheme including top quark threshold corrections is[149, 160]

$$\sin^2\theta_W^{\overline{\rm MS}}(M_Z) = 0.23121 \pm 0.00004. \tag{A.18}$$

Gauge factors at the M_Z scale

Values of the gauge factors $\{\alpha_c^{-1}(M_Z), \alpha_L^{-1}(M_Z), \alpha_1^{-1}(M_Z)\}$, at the M_Z scale are related to the parameters

$$\{\alpha_{\overline{\rm MS}}^{(6)}(M_Z), \sin^2\theta_W^{\overline{\rm MS}}(M_Z), \alpha_{\overline{\rm MS},c}^{(6)}(M_Z)\} \tag{A.19}$$

in the following way:

$$\alpha_1^{-1}(M_Z) = \frac{3}{5}(1-\sin^2\theta_W^{\overline{\rm MS}}(M_Z))\cdot\left(\alpha_{\overline{\rm MS}}^{(5)}\right)^{-1}(M_Z), \tag{A.20}$$

$$\alpha_L^{-1}(M_Z) = \sin^2\theta_W^{\overline{\rm MS}}(M_Z)\cdot\left(\alpha_{\overline{\rm MS}}^{(5)}\right)^{-1}(M_Z), \tag{A.21}$$

$$\alpha_c^{-1}(M_Z) = \left(\alpha_{\overline{\rm MS},c}^{(6)}\right)^{-1}(M_Z), \tag{A.22}$$

thus

$$\alpha_1^{-1}(M_Z) = 59.1054 \pm 0.0031, \tag{A.23}$$

$$\alpha_L^{-1}(M_Z) = 29.6261 \pm 0.0051, \tag{A.24}$$

$$\alpha_c^{-1}(M_Z) = 8.550 \pm 0.065. \tag{A.25}$$

B. Beta functions of scalar couplings

Beta functions of scalar couplings can be derived with the help of the effective potential approach, in which the tree-level scalar potential V_0 is replaced by the effective potential V_{eff}. At one loop,

$$V_{eff} = V_0 + V_1 \tag{B.1}$$

with V_1 involving contributions from the one-loop Feynman diagrams. In the Landau gauge and $\overline{\text{MS}}$ renormalization scheme it reads [148]

$$V_1 = \frac{1}{64\pi^2}\text{Tr}\left[M_S^4(\Phi)\left(\log\frac{M_S^2(\Phi)}{\mu^2} - \frac{3}{2}\right)\right] + \frac{3}{64\pi^2}\text{Tr}\left[M_G^4(\Phi)\left(\log\frac{M_G^2(\Phi)}{\mu^2} - \frac{5}{6}\right)\right], \tag{B.2}$$

where

$$M_S^2(\Phi)_{ij} = \frac{\partial^2 V_0}{\partial\Phi_j \partial\Phi_j^*}, \tag{B.3}$$

$$M_G^2(\Phi)_{ab} = g^2 \left(T^a\Phi\right)^\dagger \left(T^b\Phi\right) \tag{B.4}$$

are elements of the tree-level 317×317 scalar and 45×45 gauge field-dependent mass matrices, $a, b = 1, \ldots, 45$ and $i, j = 1, \ldots, 317$. T^a denotes the SO(10) generators in the reducible representation corresponding to the scalar field Φ encompassing all 317 scalar degrees of freedom

$$\Phi = \begin{pmatrix}\phi & \Sigma & \Sigma^* & H & H^*\end{pmatrix}^T. \tag{B.5}$$

The effective potential satisfies the Callan-Symanzik renormalization group equation

$$\left(\frac{\partial}{\partial\log\mu_R} + \beta_\lambda\frac{\partial}{\partial\lambda} + \beta_g\frac{\partial}{\partial g} + \beta_{m^2}\frac{\partial}{\partial m^2} + \sum_{i=1}^{317}\gamma_{\Phi_i}\Phi_i\frac{\partial}{\partial\Phi_i}\right)V_{eff}(\Phi) = 0 \tag{B.6}$$

with i running over all scalar fields (B.5), μ_R and γ_{Φ_i} being the running renormalization scale and Φ-field anomalous dimensions, respectively. The RGE (B.6) at one loop yields

$$\frac{\partial V_1}{\partial\log\mu_R} + \beta_\lambda\frac{\partial V_0}{\partial\lambda} + \beta_g\frac{\partial V_0}{\partial g} + \beta_{m^2}\frac{\partial V_0}{\partial m^2} + \sum_{i=1}^{317}\gamma_{\Phi_i}\Phi_i\frac{\partial V_0}{\partial\Phi_i} = 0. \tag{B.7}$$

Simultaneously, every tree-level scalar coupling λ can be expressed as a derivative of the tree-level scalar potential with respect to a suitable choice of a set of scalar fields $\{\Phi_{i_i}, \Phi_{i_2}, \Phi_{i_3}, \Phi_{i_4}\}$:

$$\lambda = \frac{\partial^4 V_0(\Phi)}{\partial\Phi_{i_1}\partial\Phi_{i_2}\partial\Phi_{i_3}\partial\Phi_{i_4}}. \tag{B.8}$$

The examples of a possible choice of the quadruples of fields $\{\Phi_{i_i}, \Phi_{i_2}, \Phi_{i_3}, \Phi_{i_4}\}$ for all dimensionless scalar couplings in the $\mathbf{45} \oplus \mathbf{126} \oplus \mathbf{10}_{\mathbb{C}}$ SO(10) GUT is listed in Table B.1.

Applying the derivative (B.8) on the renormalization group equation (B.7) gives

$$\frac{\partial^4}{\prod_{j=1}^4 \partial \Phi_{i_j}} \frac{\partial V_1}{\partial \log \mu_R} + \beta_\lambda + \lambda \sum_{j=1}^4 \gamma_{\Phi_{i_j}} = 0, \tag{B.9}$$

and consequently, the one-loop scalar beta function is calculated as

$$\beta_\lambda = \beta_{\lambda,EFF} + \beta_{\lambda,FS}, \tag{B.10}$$

where

$$\beta_{\lambda,EFF} = -\frac{\partial^4}{\prod_{j=1}^4 \partial \Phi_{i_j}} \frac{\partial V_1}{\partial \log \mu_R} = \frac{1}{32\pi^2} \frac{\partial^4}{\prod_{j=1}^4 \partial \Phi_{i_j}} \left(\mathrm{Tr}\left[M_S^4(\Phi)\right] + 3\mathrm{Tr}\left[M_G^4(\Phi)\right] \right) \tag{B.11}$$

and

$$\beta_{\lambda,FS} = -\lambda \sum_{j=1}^4 \gamma_{\Phi_{i_j}} \tag{B.12}$$

are scalar-potential-dependent and field-strength-dependent parts of the beta function, respectively.

B.1 Field-strength-dependent part

Calculating the field-strength-dependent parts of the scalar beta functions requires the computation of the Φ_i-field anomalous dimension, which is defined as [164]

$$\gamma_{\Phi_i} = \frac{1}{2} \frac{1}{Z_{\Phi_i}} \frac{\partial Z_{\Phi_i}}{\partial \log \mu_R}, \tag{B.13}$$

where Z_{Φ_i} is the Φ_i-field-strength renormalization factor in the $\overline{\mathrm{MS}}$ renormalization scheme. It depends on the Φ_i-field self-energy $\Sigma_{\Phi_i}^{\overline{\mathrm{MS}}}$

$$Z_{\Phi_i} = 1 + \left. \frac{\partial \Sigma_{\Phi_i}^{\overline{\mathrm{MS}}}(p^2)}{\partial p^2} \right|_{p^2 = m_{\Phi_i}^2}, \tag{B.14}$$

whose p^2-dependent part arises from the diagram depicted in Fig. B.1. The direct Feynman diagram calculation yields

$$\Sigma_{\Phi_i}^{\overline{\mathrm{MS}}}(p^2) = C_2(R_{\Phi_i}) \cdot p^2 \cdot \frac{3g^2}{16\pi^2} \log \mu_R^2 + p^2 \text{ and/or } \mu_R \text{ independent part}, \tag{B.15}$$

where $C_2(R_{\Phi_i})$ denotes the quadratic Casimir operator of the SO(10) representation R to which the Φ_i field belongs. Inserting relations (B.14)-(B.15) into Eq. (B.13) one obtains

$$\gamma_{\Phi_i} = C_2(R_{\Phi_i}) \frac{3g^2}{16\pi^2}, \tag{B.16}$$

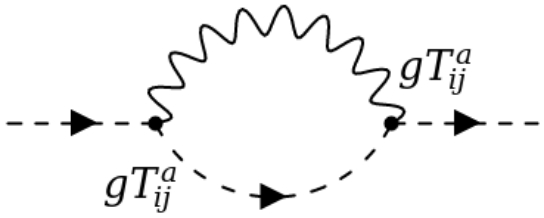

Figure B.1: The Feynman diagram contributing to the p^2-dependent part of the scalar field self-energy which is relevant for the calculation of the field-strength-dependent part of the scalar beta function.

and consequently, the field-dependent part of the scalar beta function (B.12) is

$$\beta_{\lambda,FS} = -\lambda \frac{3g^2}{16\pi^2} \sum_{j=1}^{4} C_2(R_{\Phi_{i_j}}). \tag{B.17}$$

As all the scalar fields Φ_i reside in one of the three SO(10) representations **45**, **126** and **10**, by inserting appropriate Casimir operators we can write

$$\beta_{\lambda,FS} = -\lambda \frac{3g^2}{16\pi^2} \left(8n_\phi + \frac{25}{2} n_\Sigma + \frac{9}{2} n_H \right), \tag{B.18}$$

where n_ϕ, n_Σ and n_H count the number of ϕ, Σ and H fields in the quadruple of the scalar fields $\{\Phi_{i_1}, \Phi_{i_2}, \Phi_{i_3}, \Phi_{i_4}\}$, respectively, and their values for all dimensionless scalar couplings are given in Table B.1.

B.2 Resulting expressions

$$\begin{aligned} 16\pi^2\, \beta_{a_0} = \quad & 126\alpha^2 + 56\alpha\beta_4 + 112\alpha\beta_4' + 424a_0^2 + 152a_0a_2 + 12a_2^2 + \\ & + \tfrac{33}{2}\beta_4^2 + 26\beta_4\beta_4' + 106\beta_4'^2 - 56|\gamma_2|^2 + 12|\zeta|^2 + 12|\zeta'|^2 + \\ & + 10\kappa_0^2 + 4\kappa_0\kappa_2 + 40|\kappa_0'|^2 + 8\kappa_0'\kappa_2'^* + 8\kappa_0'^*\kappa_2' + \frac{9}{2}g^4 - 96a_0g^2, \end{aligned} \tag{B.19}$$

$$\begin{aligned} 16\pi^2\beta_{a_2} = \quad & 96a_0a_2 + 76a_2^2 - 5\beta_4^2 + 60\beta_4\beta_4' - 100\beta_4'^2 + 560|\gamma_2|^2 - \\ & - 24|\zeta|^2 - 24|\zeta'|^2 + 4\kappa_2^2 + 16|\kappa_2'|^2 + 3g^4 - 96a_2g^2, \end{aligned} \tag{B.20}$$

$$\begin{aligned} 16\pi^2\beta_{\lambda_0} = \quad & 90\alpha^2 + 40\alpha\beta_4 + 80\alpha\beta_4' + 10\beta_4^2 + 80\beta_4'^2 + 520\lambda_0^2 + \\ & + 2440\lambda_0\lambda_2 + 2680\lambda_0\lambda_4 + 4960\lambda_0\lambda_4' + 3460\lambda_2^2 + 7880\lambda_2\lambda_4 + \\ & + 12320\lambda_2\lambda_4' + 4660\lambda_4^2 + 13280\lambda_4\lambda_4' + 16960\lambda_4'^2 + \\ & + 10\rho_0^2 + 10\rho_0\rho_2 + 40|\rho_0'|^2 + 5\rho_2^2 + 3840|\varphi|^2 + 3840|\varphi'|^2 + \\ & + \frac{135}{2}g^4 - 150\lambda_0g^2, \end{aligned} \tag{B.21}$$

Table B.1: Example of a choice of the quadruple $\{\Phi_{i_1}, \Phi_{i_2}, \Phi_{i_3}, \Phi_{i_4}\}$ that can be used to derive one-loop beta functions of a scalar coupling combination and the corresponding field counts n_ϕ, n_Σ, n_H.

scalar coupling combination	a choice of $\{\Phi_{i_1}, \Phi_{i_2}, \Phi_{i_3}, \Phi_{i_4}\}$	n_ϕ	n_Σ	n_H
a_0	$\phi_{12},\ \phi_{12},\ \phi_{78},\ \phi_{78}$	4	0	0
$a_2 + 2a_2$	$\phi_{12},\ \phi_{12},\ \phi_{12},\ \phi_{12}$	4	0	0
α	$\phi_{78},\ \phi_{78},\ \Sigma_{123810},\ \Sigma^*_{123810}$	2	2	0
β_4	$\phi_{810}, \phi_{46}, \Sigma_{12346}, \Sigma^*_{123810}$	2	2	0
$2\beta'_4 + 2\alpha + \beta_4$	$\phi_{12}, \phi_{12}, \Sigma_{123810}, \Sigma^*_{123810}$	2	2	0
γ_2	$\phi_{12}, \phi_{12}, \Sigma_{123810}, \Sigma_{123810}$	2	2	0
$\lambda_0 + 2\lambda_2 + 3\lambda_4 + 8\lambda'_4$	$\Sigma_{12345}, \Sigma^*_{12345}, \Sigma_{12346}, \Sigma^*_{12346}$	0	4	0
$\lambda_2 + 4\lambda_4 + 4\lambda'_4$	$\Sigma_{12345}, \Sigma_{12345}, \Sigma^*_{12346}, \Sigma^*_{12346}$	0	4	0
$2\lambda_0 + 5\lambda_2 + 5\lambda_4 + 8\lambda'_4$	$\Sigma_{12345}, \Sigma^*_{12345}, \Sigma_{123810}, \Sigma^*_{123810}$	0	4	0
λ_4	$\Sigma_{12345}, \Sigma_{12345}, \Sigma^*_{123810}, \Sigma^*_{123810}$	0	4	0
η_2	$\Sigma_{12345}, \Sigma_{12345}, \Sigma_{12345}, \Sigma_{12345}$	0	4	0
h_2	H_1, H_1^*, H_2, H_2^*	0	0	4
h'_2	H_1, H_1, H_2^*, H_2^*	0	0	4
h_3	H_1, H_1, H_1, H_1^*	0	0	4
h_4	H_1, H_1, H_1, H_1	0	0	4
κ_0	$\phi_{78}, \phi_{78}, H_1, H_1^*$	2	0	2
$\kappa_0 + \kappa_2$	$\phi_{12}, \phi_{12}, H_1, H_1^*$	2	0	2
κ'_0	$\phi_{78}, \phi_{78}, H_1, H_1$	2	0	2
$\kappa'_0 + \kappa'_2$	$\phi_{12}, \phi_{12}, H_1, H_1$	2	0	2
ζ	$\phi_{13}, \phi_{810}, \Sigma_{123810}, H_2$	2	1	1
ζ'	$\phi_{13}, \phi_{810}, \Sigma_{123810}, H_2^*$	2	1	1
ρ_2	$\Sigma_{12345}, \Sigma^*_{12346}, H_5, H_6^*$	0	2	2
$2\rho_0 + \rho_2$	$\Sigma_{12345}, \Sigma^*_{12345}, H_5, H_5^*$	0	2	2
ρ'_0	$\Sigma_{12345}, \Sigma^*_{12345}, H_5, H_5$	0	2	2
ψ_2	$\Sigma_{12345}, \Sigma_{12345}, H_5, H_5$	0	2	2
ψ_1	$\Sigma_{12345}, \Sigma_{12345}, H_5, H_5^*$	0	2	2
ψ_0	$\Sigma_{12345}, \Sigma_{12345}, H_5^*, H_5^*$	0	2	2
φ	$\Sigma_{12345}, \Sigma_{123810}, \Sigma^*_{145810}, H_1$	0	3	1
φ'	$\Sigma_{12345}, \Sigma_{123810}, \Sigma^*_{145810}, H_1^*$	0	3	1

$$
\begin{aligned}
16\pi^2\beta_{\lambda_2} = &-4\beta_4^2 - 32\beta_4'^2 - 32|\gamma_2|^2 - 1264|\eta_2|^2 + 24\lambda_0\lambda_2 - 180\lambda_2^2 - \\
&- 584\lambda_2\lambda_4 - 160\lambda_2\lambda'_4 - 656\lambda_4^2 - 800\lambda_4\lambda'_4 - 2560\lambda_4'^2 - \rho_2^2 - \\
&- 4|\psi_0|^2 - 2|\psi_1|^2 - 4|\psi_2|^2 - 1408|\varphi|^2 - 1408|\varphi'|^2 - 24g^4 - \\
&- 150\lambda_2 g^2,
\end{aligned}
\tag{B.22}
$$

$$
\begin{aligned}
16\pi^2\beta_{\lambda_4} = \quad & 2\beta_4^2 + 16\beta_4'^2 + 32|\gamma_2|^2 + 1328|\eta_2|^2 + 24\lambda_0\lambda_4 + 16\lambda_2^2 + \\
& + 112\lambda_2\lambda_4 + 128\lambda_2\lambda_4' + 268\lambda_4^2 + 640\lambda_4\lambda_4' + 1408\lambda_4'^2 + \\
& + 4|\psi_0|^2 + 2|\psi_1|^2 + 4|\psi_2|^2 + 768|\varphi|^2 + 768|\varphi'|^2 + 12g^4 - \\
& - 150\lambda_4 g^2,
\end{aligned} \tag{B.23}
$$

$$
\begin{aligned}
16\pi^2\beta_{\lambda_4'} = \quad & 4\beta_4\beta_4' - 4\beta_4'^2 + 32|\eta_2|^2 + 24\lambda_0\lambda_4' - 4\lambda_2^2 - 8\lambda_2\lambda_4 - 16\lambda_2\lambda_4' + \\
& + 4\lambda_4^2 + 112\lambda_4\lambda_4' - 240\lambda_4'^2 - 416|\varphi|^2 - 416|\varphi'|^2 - 3g^4 - \\
& - 150\lambda_4' g^2,
\end{aligned} \tag{B.24}
$$

$$
\begin{aligned}
16\pi^2\beta_{\alpha} = \quad & 8\alpha^2 + 508\alpha\lambda_0 + 1220\alpha\lambda_2 + 1340\alpha\lambda_4 + 2480\alpha\lambda_4' + 376\alpha a_0 + \\
& + 80a_0\beta_4 + 160a_0\beta_4' + 76\alpha a_2 + 16a_2\beta_4 + 32a_2\beta_4' + 4\beta_4^2 + \\
& + 16\beta_4\beta_4' + 112\beta_4\lambda_0 + 272\beta_4\lambda_2 + 288\beta_4\lambda_4 + 512\beta_4\lambda_4' + \\
& + 144\beta_4'^2 + 224\beta_4'\lambda_0 + 544\beta_4'\lambda_2 + 576\beta_4'\lambda_4 + 1024\beta_4'\lambda_4' + \\
& + 64|\gamma_2|^2 + 20\kappa_0\rho_0 + 10\kappa_0\rho_2 + 40\kappa_0'\rho_0'^* + 40\kappa_0'^*\rho_0' + 4\kappa_2\rho_0 + \\
& + 2\kappa_2\rho_2 + 8\kappa_2'\rho_0'^* + 8\kappa_2'^*\rho_0' + 12g^4 - 123\alpha g^2,
\end{aligned} \tag{B.25}
$$

$$
\begin{aligned}
16\pi^2\beta_{\beta_4} = \quad & 16\alpha\beta_4 + 16a_0\beta_4 + 16a_2\beta_4' + 48\beta_4^2 + 80\beta_4\beta_4' + 4\beta_4\lambda_0 - \\
& - 8\beta_4\lambda_2 + 32\beta_4\lambda_4 + 16\beta_4\lambda_4' + 16\beta_4'^2 + 16\beta_4'\lambda_2 + 48\beta_4'\lambda_4 + \\
& + 640\beta_4'\lambda_4' + 64|\gamma_2|^2 + 24|\zeta|^2 + 96\zeta\varphi^* + 96\zeta^*\varphi + 24|\zeta'|^2 + \\
& + 96\zeta'\varphi'^* + 96\zeta'^*\varphi' + 12g^4 - 123\beta_4 g^2,
\end{aligned} \tag{B.26}
$$

$$
\begin{aligned}
16\pi^2\beta_{\beta_4'} = \quad & 16\alpha\beta_4' + 16a_0\beta_4' + 2a_2\beta_4 - 4a_2\beta_4' - \beta_4^2 - 28\beta_4\beta_4' + 2\beta_4\lambda_2 + \\
& + 6\beta_4\lambda_4 + 80\beta_4\lambda_4' - 124\beta_4'^2 + 4\beta_4'\lambda_0 - 12\beta_4'\lambda_2 + 20\beta_4'\lambda_4 - \\
& - 144\beta_4'\lambda_4' + 16|\gamma_2|^2 - 48\zeta\varphi^* - 48\zeta^*\varphi - 48\zeta'\varphi'^* - 48\zeta'^*\varphi' - \\
& - 3g^4 - 123\beta_4' g^2,
\end{aligned} \tag{B.27}
$$

$$
\begin{aligned}
16\pi^2\beta_{\gamma_2} = \quad & 16\alpha\gamma_2 + 16a_0\gamma_2 + 36a_2\gamma_2 + 28\beta_4\gamma_2 + 56\beta_4'\gamma_2 + 4\gamma_2\lambda_0 + \\
& + 40\gamma_2\lambda_2 + 180\gamma_2\lambda_4 + 160\gamma_2\lambda_4' + 440\gamma_2^*\eta_2 + 12\zeta\zeta' + 2\kappa_2\psi_1 + \\
& + 4\kappa_2'\psi_0 + 4\kappa_2'^*\psi_2 - 123\gamma_2 g^2,
\end{aligned} \tag{B.28}
$$

$$
\begin{aligned}
16\pi^2\beta_{\eta_2} = \quad & 16\gamma_2^2 + 24\eta_2\lambda_0 + 160\eta_2\lambda_2 + 600\eta_2\lambda_4 + 640\eta_2\lambda_4' + 4\psi_0\psi_2 + \\
& + \psi_1^2 - 150\eta_2 g^2.
\end{aligned} \tag{B.29}
$$

$$
\begin{aligned}
16\pi^2\beta_{h_2} = \quad & 56h_2^2 + 16h_2h_2' + 16h_2'^2 + 72|h_3|^2 + 64|h_4|^2 + 90\kappa_0^2 + \\
& + 36\kappa_0\kappa_2 + 10\kappa_2^2 + 32|\kappa_2'|^2 + 126\rho_0^2 + 126\rho_0\rho_2 + 49\rho_2^2 + \\
& + 140|\psi_0|^2 + 56|\psi_1|^2 + 140|\psi_2|^2 + \frac{15}{8}g^4 - 54h_2 g^2,
\end{aligned} \tag{B.30}
$$

$$
\begin{aligned}
16\pi^2\beta_{h_2'} = \quad & 24h_2h_2' + 40h_2'^2 + 36|h_3|^2 + 224|h_4|^2 + 180|\kappa_0'|^2 + \\
& + 36\kappa_0'\kappa_2'^* + 36\kappa_0'^*\kappa_2' + 8\kappa_2^2 + 4|\kappa_2'|^2 + 252|\rho_0'|^2 - \tfrac{35}{2}\rho_2^2 - \\
& - 14|\psi_0|^2 + 70|\psi_1|^2 - 14|\psi_2|^2 + \frac{3}{2}g^4 - 54h_2' g^2,
\end{aligned} \tag{B.31}
$$

$$
\begin{aligned}
16\pi^2\beta_{\kappa_0} = \quad & 252\alpha\rho_0 + 126\alpha\rho_2 + 376a_0\kappa_0 + 72a_0\kappa_2 + 76a_2\kappa_0 + \\
& + 8a_2\kappa_2 + 56\beta_4\rho_0 + 28\beta_4\rho_2 + 112\beta_4'\rho_0 + 56\beta_4'\rho_2 - 28\gamma_2\psi_1^* - \\
& - 28\gamma_2^*\psi_1 + 84|\zeta|^2 + 84|\zeta'|^2 + 44h_2\kappa_0 + 8h_2\kappa_2 + 8h_2'\kappa_0 + \\
& + 48h_3\kappa_0'^* + 8h_3\kappa_2'^* + 48h_3^*\kappa_0' + 8h_3^*\kappa_2' + 8\kappa_0^2 + 32|\kappa_0'|^2 + 4\kappa_2^2 + \\
& + 16|\kappa_2'|^2 + \frac{3}{2}g^4 - 75g^2\kappa_0,
\end{aligned}
\tag{B.32}
$$

$$
\begin{aligned}
16\pi^2\beta_{\kappa_2} = \quad & 16a_0\kappa_2 + 36a_2\kappa_2 + 140\gamma_2\psi_1^* + 140\gamma_2^*\psi_1 - 84|\zeta|^2 - 84|\zeta'|^2 + \\
& + 4h_2\kappa_2 + 8h_2'\kappa_2 + 8h_3\kappa_2'^* + 8h_3^*\kappa_2' + 16\kappa_0\kappa_2 + 32\kappa_0'\kappa_2'^* + \\
& + 32\kappa_0'^*\kappa_2' + 20\kappa_2^2 + 80|\kappa_2'|^2 + \frac{9}{2}g^4 - 75\kappa_2 g^2,
\end{aligned}
\tag{B.33}
$$

$$
\begin{aligned}
16\pi^2\beta_{\rho_0} = \quad & 180\alpha\kappa_0 + 36\alpha\kappa_2 + 40\beta_4\kappa_0 + 8\beta_4\kappa_2 + 80\beta_4'\kappa_0 + 16\beta_4'\kappa_2 + \\
& + 24|\zeta|^2 + 44h_2\rho_0 + 20h_2\rho_2 + 8h_2'\rho_0 + 8h_2'\rho_2 + 48h_3\rho_0'^* + \\
& + 48h_3^*\rho_0' + 508\lambda_0\rho_0 + 252\lambda_0\rho_2 + 1220\lambda_2\rho_0 + 692\lambda_2\rho_2 + \\
& + 1340\lambda_4\rho_0 + 788\lambda_4\rho_2 + 2480\lambda_4'\rho_0 + 1232\lambda_4'\rho_2 + 4\rho_0^2 + \\
& + 16|\rho_0'|^2 + 4\rho_2^2 + 24|\psi_1|^2 + 96|\psi_2|^2 + 9984|\varphi|^2 + 1536|\varphi'|^2 + \\
& + \frac{15}{2}g^4 - 102\rho_0 g^2,
\end{aligned}
\tag{B.34}
$$

$$
\begin{aligned}
16\pi^2\beta_{\rho_2} = \quad & -24|\zeta|^2 + 24|\zeta'|^2 + 4h_2\rho_2 - 8h_2'\rho_2 + 4\lambda_0\rho_2 - 164\lambda_2\rho_2 - \\
& - 236\lambda_4\rho_2 + 16\lambda_4'\rho_2 + 8\rho_0\rho_2 + 4\rho_2^2 + 96|\psi_0|^2 - 96|\psi_2|^2 - \\
& - 8448|\varphi|^2 + 8448|\varphi'|^2 - 102\rho_2 g^2,
\end{aligned}
\tag{B.35}
$$

$$
\begin{aligned}
16\pi^2\beta_{h_4} = \quad & 24h_2h_4 + 96h_2'h_4 + 18h_3^2 + 90\kappa_0'^2 + 36\kappa_0'\kappa_2' + 18\kappa_2'^2 + \\
& + 126\rho_0'^2 + 126\psi_0^*\psi_2 - 54h_4 g^2,
\end{aligned}
\tag{B.36}
$$

$$
\begin{aligned}
16\pi^2\beta_{h_3} = \quad & 72h_2h_3 + 72h_2'h_3 + 144h_3^*h_4 + 180\kappa_0\kappa_0' + 36\kappa_0\kappa_2' + \\
& + 36\kappa_0'\kappa_2 + 36\kappa_2\kappa_2' + 252\rho_0\rho_0' + 126\rho_0'\rho_2 + 126\psi_0^*\psi_1 + \\
& + 126\psi_1^*\psi_2 - 54h_3 g^2,
\end{aligned}
\tag{B.37}
$$

$$
\begin{aligned}
16\pi^2\beta_{\kappa_0'} = \quad & 252\alpha\rho_0' + 376a_0\kappa_0' + 72a_0\kappa_2' + 76a_2\kappa_0' + 8a_2\kappa_2' + 56\beta_4\rho_0' + \\
& + 112\beta_4'\rho_0' - 28\gamma_2\psi_0^* - 28\gamma_2^*\psi_2 + 84\zeta\zeta'^* + 4h_2\kappa_0' + 40h_2'\kappa_0' + \\
& + 8h_2'\kappa_2' + 24h_3\kappa_0 + 4h_3\kappa_2 + 96h_4\kappa_0'^* + 16h_4\kappa_2'^* + 16\kappa_0\kappa_0' + \\
& + 8\kappa_2\kappa_2' - 75\kappa_0' g^2,
\end{aligned}
\tag{B.38}
$$

$$
\begin{aligned}
16\pi^2\beta_{\kappa_2'} = \quad & 16a_0\kappa_2' + 36a_2\kappa_2' + 140\gamma_2\psi_0^* + 140\gamma_2^*\psi_2 - 84\zeta\zeta'^* + 4h_2\kappa_2' + \\
& + 4h_3\kappa_2 + 16h_4\kappa_2'^* + 16\kappa_0\kappa_2' + 16\kappa_0'\kappa_2 + 40\kappa_2\kappa_2' - 75\kappa_2' g^2,
\end{aligned}
\tag{B.39}
$$

$$
\begin{aligned}
16\pi^2\beta_{\zeta} = \quad & 8\alpha\zeta + 16a_0\zeta - 8a_2\zeta + 64\beta_4\zeta + 160\beta_4\varphi + 48\beta_4'\zeta - 640\beta_4'\varphi + \\
& + 96\gamma_2\zeta'^* + 8\zeta\kappa_0 - 8\zeta\kappa_2 + 2\zeta\rho_0 - 4\zeta\rho_2 + 24\zeta^*\psi_2 + 16\zeta'\kappa_0' - \\
& - 16\zeta'\kappa_2' + 4\zeta'\rho_0' + 12\zeta'^*\psi_1 - 99\zeta g^2,
\end{aligned}
\tag{B.40}
$$

$$
\begin{aligned}
16\pi^2\beta_{\zeta'} = \quad & 8\alpha\zeta' + 16a_0\zeta' - 8a_2\zeta' + 64\beta_4\zeta' + 160\beta_4\varphi' + 48\beta_4'\zeta' - \\
& - 640\beta_4'\varphi' + 96\gamma_2\zeta^* + 16\zeta\kappa_0'^* - 16\zeta\kappa_2'^* + 4\zeta\rho_0'^* + 12\zeta^*\psi_1 + \\
& + 8\zeta'\kappa_0 - 8\zeta'\kappa_2 + 2\zeta'\rho_0 + 6\zeta'\rho_2 + 24\zeta'^*\psi_0 - 99\zeta' g^2,
\end{aligned}
\tag{B.41}
$$

$$
\begin{aligned}
16\pi^2\beta_{\rho_0'} = \quad & 180\alpha\kappa_0' + 36\alpha\kappa_2' + 40\beta_4\kappa_0' + 8\beta_4\kappa_2' + 80\beta_4'\kappa_0' + 16\beta_4'\kappa_2' + \\
& + 12\zeta\zeta'^* + 4h_2\rho_0' + 40h_2'\rho_0' + 24h_3\rho_0 + 12h_3\rho_2 + 96h_4\rho_0'^* + \\
& + 508\lambda_0\rho_0' + 1220\lambda_2\rho_0' + 1340\lambda_4\rho_0' + 2480\lambda_4'\rho_0' + 8\rho_0\rho_0' + \\
& + 4\rho_0'\rho_2 + 24\psi_0^*\psi_1 + 24\psi_1^*\psi_2 + 5760\varphi\varphi'^* - 102\rho_0' g^2,
\end{aligned} \tag{B.42}
$$

$$
\begin{aligned}
16\pi^2\beta_{\psi_2} = \quad & 32\gamma_2\kappa_2' + 12\zeta^2 + 440\eta_2\psi_0^* + 4h_2\psi_2 + 4h_3\psi_1 + 16h_4\psi_0 + \\
& + 4\lambda_0\psi_2 + 40\lambda_2\psi_2 + 180\lambda_4\psi_2 + 160\lambda_4'\psi_2 + 8\rho_0\psi_2 + 8\rho_0'\psi_1 - \\
& - 16\rho_2\psi_2 + 3840\varphi^2 - 102\psi_2 g^2,
\end{aligned} \tag{B.43}
$$

$$
\begin{aligned}
16\pi^2\beta_{\psi_1} = \quad & 32\gamma_2\kappa_2 + 24\zeta\zeta' + 440\eta_2\psi_1^* + 4h_2\psi_1 + 8h_2'\psi_1 + 8h_3\psi_0 + \\
& + 8h_3^*\psi_2 + 4\lambda_0\psi_1 + 40\lambda_2\psi_1 + 180\lambda_4\psi_1 + 160\lambda_4'\psi_1 + 8\rho_0\psi_1 + \\
& + 16\rho_0'\psi_0 + 16\rho_0'^*\psi_2 + 4\rho_2\psi_1 + 7680\varphi\varphi' - 102\psi_1 g^2,
\end{aligned} \tag{B.44}
$$

$$
\begin{aligned}
16\pi^2\beta_{\psi_0} = \quad & 32\gamma_2\kappa_2'^* + 12\zeta'^2 + 440\eta_2\psi_2^* + 4h_2\psi_0 + 4h_3^*\psi_1 + 16h_4^*\psi_2 + \\
& + 4\lambda_0\psi_0 + 40\lambda_2\psi_0 + 180\lambda_4\psi_0 + 160\lambda_4'\psi_0 + 8\rho_0\psi_0 + 8\rho_0'^*\psi_1 + \\
& + 24\rho_2\psi_0 + 3840\varphi'^2 - 102\psi_0 g^2,
\end{aligned} \tag{B.45}
$$

$$
\begin{aligned}
16\pi^2\beta_{\varphi} = \quad & \beta_4\zeta - 4\beta_4'\zeta + 12\lambda_0\varphi - 8\lambda_2\varphi + 40\lambda_4\varphi - 656\lambda_4'\varphi + 6\rho_0\varphi + \\
& + 12\rho_0'\varphi' - 8\rho_2\varphi + 48\psi_2\varphi^* + 24\psi_1\varphi'^* - 126\varphi g^2,
\end{aligned} \tag{B.46}
$$

$$
\begin{aligned}
16\pi^2\beta_{\varphi'} = \quad & \beta_4\zeta' - 4\beta_4'\zeta' + 12\lambda_0\varphi' - 8\lambda_2\varphi' + 40\lambda_4\varphi' - 656\lambda_4'\varphi' + \\
& + 6\rho_0\varphi' + 12\rho_0'^*\varphi + 14\rho_2\varphi' + 24\psi_1\varphi^* + 48\psi_0\varphi'^* - 126\varphi' g^2.
\end{aligned} \tag{B.47}
$$

C. RGEs for $d = 6$ proton decay operators

In this Appendix, we derive the form of the coefficients which take care of the one-loop running effects for the effective four-fermion BNV operators $O^{(1)}$ and $O^{(2)}$, c.f (2.86). Note that these two operators are of our main interest as they give rise to the dominant gauge-boson-mediated proton decay contributions.

Suppose $C^{(i)}(\mu)$ is a renormalization-scale-dependent coefficient associated with the operator $O^{(i)}$. Typically,

$$C^{(i)}(M_{GUT}) \sim \frac{g^2}{M_G^2} \tag{C.1}$$

with g and M_G being the unified gauge coupling and the gauge boson mass, respectively. It was shown that these coefficients satisfy one-loop RGEs [165]

$$\mu \frac{dC^{(i)}}{d\mu} = -\frac{1}{2\pi} \sum_{j=1}^{3} \gamma_j^{(i)} \alpha_j C^{(i)}, \tag{C.2}$$

where only the leading order contributions from the one-loop Feynman diagrams depicted in Fig C.1 were included, $\alpha_j = g_j^2/4\pi$ are the SM gauge coupling factors and

$$\gamma^{(i)} = \begin{cases} \{\frac{11}{2}, \frac{9}{4}, 2\} & \text{for } i = 1, \\ \{\frac{23}{12}, \frac{9}{4}, 2\} & \text{for } i = 2. \end{cases} \tag{C.3}$$

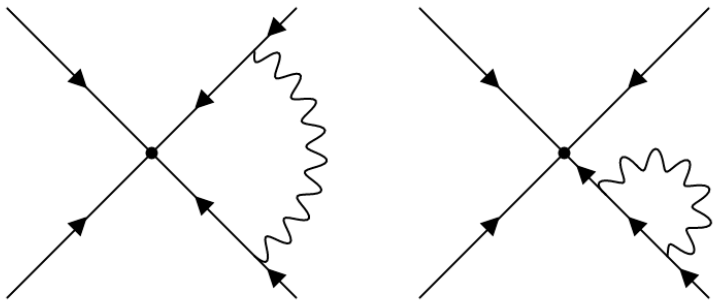

Figure C.1: One-loop diagrams dominating the one-loop proton decay operators' RGEs (C.2).

We reshuffle (C.2) to obtain

$$\frac{dC^{(i)}}{C^{(i)}} = -\frac{1}{2\pi} \sum_{j=1}^{3} \gamma_j^{(i)} \alpha_j \frac{d\mu}{\mu} = -\sum_{j=1}^{3} \frac{\gamma_j^{(i)}}{b_j} \frac{d\alpha_j}{\alpha_j}, \tag{C.4}$$

where the one-loop gauge coupling RGEs

$$\mu \frac{d\alpha_j}{d\mu} = \frac{1}{2\pi} b_j \alpha_j^2 \tag{C.5}$$

were employed in the second step and b_j are the one-loop beta coefficient of gauge couplings α_j whose specific values depend on the effective theory under consideration.

Once the differential equation (C.4) is integrated between two renormalization scales μ_1 and μ_2, $\mu_1 > \mu_2$, we obtain the relation

$$\log\left[\frac{C^{(i)}(\mu_2)}{C^{(i)}(\mu_1)}\right] = -\sum_{j=1}^{3}\frac{\gamma_j^{(i)}}{b_j}\log\left[\frac{\alpha_j(\mu_2)}{\alpha_j(\mu_1)}\right], \tag{C.6}$$

and consequently

$$C^{(i)}(\mu_2) = C^{(i)}(\mu_1)\prod_{j=1}^{3}\left(\frac{\alpha_j(\mu_2)}{\alpha_j(\mu_1)}\right)^{\frac{\gamma_j^{(i)}}{b_j}}. \tag{C.7}$$

In a realistic case, we typically have to work through all intermediate effective field theories between the renormalization scales μ_2 and μ_1, i.e.

$$C^{(i)}(\mu_2) = C^{(i)}(\mu_1)\prod_{j=1}^{3}\prod_{I}^{\mu_2<\mu_I<\mu_1}\left(\frac{\alpha_j(\mu_{I+1})}{\alpha_j(\mu_I)}\right)^{\frac{\gamma_j^{(i)}}{b_{Ij}}}, \tag{C.8}$$

where the b_I coefficients include contributions from all fields in the effective field theory between the μ_I and μ_{I+1} scales. Note that the exponent in Eq. (C.8) differs from the ones listed in [87, 166], where its denominator involved only contributions of fields with masses in the range from μ_2 to μ_1.

D. Abelian Higgs model as a case study

It is instructive to demonstrate the peculiarities of the one-loop calculations on the example of a simple Abelian U(1) gauge model containing a Higgs boson Φ and a gauge field A_μ (see also [167]). The general Lagrangian in the unbroken phase is

$$\mathcal{L} = \mathcal{L}_{kin} - V_0, \tag{D.1}$$

where

$$\mathcal{L}_{kin} = -\frac{1}{4}F_{\mu\nu}F^{\mu\nu} + (D_\mu\Phi)^\dagger(D^\mu\Phi), \tag{D.2}$$

$$V_0 = -m^2\Phi^\dagger\Phi + \lambda\left(\Phi^\dagger\Phi\right)^2. \tag{D.3}$$

The covariant derivative is defined as $D_\mu\Phi = (\partial_\mu - igA_\mu)\Phi$, the gauge field tensor is $F_{\mu\nu} = \partial_\mu A_\nu - \partial_\nu A_\mu$ and the complex scalar field Φ can be written using real components

$$\Phi(x) = \frac{1}{\sqrt{2}}\left(H(x) + iG(x)\right). \tag{D.4}$$

Let us further assume that the U(1) symmetry is spontaneously broken by the non-zero VEV $\langle\Phi\rangle = \langle H\rangle = v$ acquired by the Higgs field. Thus one obtains a nontrivial stationarity condition

$$\left.\frac{\partial V_0}{\partial H}\right|_{\substack{\langle H\rangle = v \\ \langle G\rangle = 0}} = 0. \tag{D.5}$$

It relates the mass parameter m^2 with the VEV v by the tree-level relation

$$m^2 = \lambda v^2. \tag{D.6}$$

The scalar tree-level masses are obtained by employing Eq. (D.6):

$$m_H^2 = 3\lambda v^2 - m^2 = 2\lambda v^2, \tag{D.7}$$

$$m_G^2 = \lambda v^2 - m^2 = 0. \tag{D.8}$$

The mass m_G^2 vanishes due to the would-be Goldstone nature of the G field.

One-loop scalar spectrum calculations are most conveniently performed in the framework of the effective potential $V_{eff} = V_0 + V_1$ with the one-loop part V_1 defined in Eq. (B.2). The tree-level field-dependent scalar and gauge mass matrices (B.3)–(B.4) in the current mode take the following form:

$$M_G^2(\phi) = g^2(H^2 + G^2), \tag{D.9}$$

$$M_S^2(\phi) = \begin{pmatrix} -m^2 + \lambda(3H^2 + G^2) & 2\lambda HG \\ 2\lambda HG & -m^2 + \lambda(H^2 + 3G^2) \end{pmatrix}, \tag{D.10}$$

where $\phi = \{H, G\}$. The only non-trivial one-loop stationarity condition is computed from

$$\left.\frac{\partial V_{eff}}{\partial H}\right|_{\substack{\langle H\rangle = v \\ \langle G\rangle = 0}} = 0 \tag{D.11}$$

and the one-loop effective scalar masses are calculated as

$$\left.\frac{\partial^2 V_{eff}}{\partial \phi^2}\right|_{\phi=\langle\phi\rangle}, \tag{D.12}$$

where expression (D.12) is assumed to be evaluated in the one-loop vacuum by means of the stationarity condition(D.11).

D.1 Beta function for λ

Let us calculate the scalar coupling one-loop beta function. It can be always written as a sum $\beta = \beta_{EFF} + \beta_{FS}$ of the scalar-potential-dependent part (B.11) and the field-strength-dependent part (B.12); we follow the methods introduced in Appendix B.

The scalar coupling λ can be extracted from the field-dependent tree-level scalar potential V_0 from Eq. (D.3) via

$$\lambda = \frac{1}{6}\frac{\partial^4 V_0}{\partial H^4}. \tag{D.13}$$

Thus, applying (B.11) one has

$$\beta_{\lambda,EFF} = \frac{1}{6}\frac{1}{32\pi^2}\frac{\partial^4}{\partial H^4}\left(\mathrm{Tr}\left[M_S^4(\phi)\right] + 3\mathrm{Tr}\left[M_G^4(\phi)\right]\right) = \frac{1}{8\pi^2}(10\lambda^2 + 3g^4), \tag{D.14}$$

provided

$$\begin{aligned}\mathrm{Tr}\left[M_S^4(\phi)\right] + 3\mathrm{Tr}\left[M_G^4(\phi)\right] = \; & (-m^2 + 3\lambda H^2 + \lambda G^2)^2 + 8\lambda^2 H^2 G^2 + \\ & + (-m^2 + 3\lambda G^2 + \lambda H^2)^2 + 3g^4(H^2 + G^2)^2\end{aligned} \tag{D.15}$$

which was acquired by inserting the field-dependent matrices (D.9)-(D.10) into Eq. (D.15).

The field-strength-dependent part of the beta function for λ is connected to the $\phi-$field anomalous dimension. Generators of the underlying U(1) gauge symmetry in all representations are normalized in such a way that the quadratic Casimir is $C_2(\phi) = 1$, thus Eqns. (B.16)-(B.17) yield

$$\gamma_\phi = \frac{3g^2}{16\pi^2} \tag{D.16}$$

and, thus

$$\beta_{\lambda,FS} = -\lambda\frac{3g^2}{4\pi^2}. \tag{D.17}$$

Finally, with relation (D.14) and (D.17) at hand we obtain the full one-loop scalar beta function:

$$\beta_\lambda = \frac{1}{8\pi^2}(10\lambda^2 + 3g^4 - 6\lambda g^2). \tag{D.18}$$

D.2 The VEV beta function

In general, all the couplings in the Lagrangian (D.1) run with the renormalization scale, particularly the m parameter with the dimension of mass. As the stationarity condition (D.6) relates m to v, the VEV will also acquire the non-trivial renormalization-scale dependence.

Let us derive the one-loop VEV beta function β_v from the renormalization scale dependence of m^2. At the tree-level, the mass parameter m^2 can be expressed as

$$\left.\frac{\partial^2 V_0}{\partial H^2}\right|_{\langle H\rangle,\langle G\rangle=0} = -m^2. \tag{D.19}$$

Applying derivative (D.19) on the one-loop RGE from Eq. (B.7), and evaluating it at $\langle H\rangle = 0$, $\langle G\rangle = 0$ leads to the one-loop β_{m^2} in the form

$$\beta_{m^2} = \left.\left(\frac{\partial^2}{\partial H^2}\frac{\partial V_1}{\partial \log\mu}\right)\right|_{\langle H\rangle,\langle G\rangle=0} - 2\gamma_H m^2 \tag{D.20}$$

with V_1 being the one-loop effective potential calculated as (B.2). At the same time, the effective potential is subject to the stationarity condition

$$0 = \left.\frac{\partial V_{eff}}{\partial H}\right|_{\substack{\langle H\rangle=v\\ \langle G\rangle=0}} = -m^2 v + \lambda v^3 + \left.\frac{\partial V_1}{\partial H}\right|_{\substack{\langle H\rangle=v\\ \langle G\rangle=0}}, \tag{D.21}$$

which allows us to relate the beta functions of m^2 and that of the VEV v in the following way:

$$\frac{\beta_v}{v} = -\frac{\beta_\lambda}{2\lambda} + \frac{\beta_{m^2}}{2\lambda v^2} - \frac{1}{2\lambda v^3}\frac{\partial}{\partial\log\mu}\left.\frac{\partial V_1}{\partial H}\right|_{\substack{\langle H\rangle=v\\ \langle G\rangle=0}} \tag{D.22}$$

for non-zero λ an v. Inserting β_{m^2} from Eq. (D.20) and the tree-level relation (D.6) into Eq. (D.22) gives

$$\frac{\beta_v}{v} = -\frac{\beta_\lambda}{2\lambda} - \gamma_H + \frac{1}{2\lambda v^2}\left.\left(\frac{\partial^2}{\partial H^2}\frac{\partial V_1}{\partial\log\mu}\right)\right|_{\langle H\rangle,\langle G\rangle=0} - \frac{1}{2\lambda v^3}\left.\left(\frac{\partial}{\partial H}\frac{\partial V_1}{\partial\log\mu}\right)\right|_{\substack{\langle H\rangle=v\\ \langle G\rangle=0}}, \tag{D.23}$$

and consequently

$$\frac{\beta_v}{v} = -\frac{1}{2\lambda}\beta_\lambda - \gamma_H + \frac{1}{2\lambda}\frac{1}{v^2}\frac{1}{32\pi^2}\frac{\partial^2}{\partial H^2}\left(\mathrm{Tr}\left[M_S^4(\Phi)\right] + 3\mathrm{Tr}\left[M_G^4(\Phi)\right]\right)\Big|_{\langle H\rangle,\langle G\rangle=0} - \\ - \frac{1}{2\lambda}\frac{1}{v^3}\frac{1}{32\pi^2}\frac{\partial}{\partial H}\left(\mathrm{Tr}\left[M_S^4(\Phi)\right] + 3\mathrm{Tr}\left[M_G^4(\Phi)\right]\right)\Big|_{\substack{\langle H\rangle=v\\ \langle G\rangle=0}}, \tag{D.24}$$

c.f. Eq. (B.11). At one loop,

$$\frac{1}{v^2}\frac{1}{32\pi^2}\frac{\partial^2}{\partial H^2}\left(\mathrm{Tr}\left[M_S^4(\Phi)\right] + 3\mathrm{Tr}\left[M_G^4(\Phi)\right]\right)\Big|_{\langle H\rangle,\langle G\rangle=0} = -\frac{1}{16\lambda\pi^2}4\lambda^2, \tag{D.25}$$

$$-\frac{1}{v^3}\frac{1}{32\pi^2}\,\frac{\partial}{\partial H}\left(\mathrm{Tr}\left[M_S^4(\Phi)\right]+3\mathrm{Tr}\left[M_G^4(\Phi)\right]\right)\Big|_{\substack{\langle H\rangle=v\\ \langle G\rangle=0}}=-\frac{1}{16\lambda\pi^2}\left(6\lambda^2+3g^4\right) \tag{D.26}$$

and

$$\frac{1}{2\lambda}\beta_\lambda=\frac{1}{16\lambda\pi^2}\left(10\lambda^2+3g^4\right)-2\gamma_H, \tag{D.27}$$

where Eqns. (D.14)–(D.15) and (D.17) were employed. In total,

$$\frac{\beta_v}{v}=\gamma_H=\frac{3g^2}{16\pi^2} \tag{D.28}$$

with the anomalous dimension taken from Eq. (D.16).

D.3 The Higgs boson one-loop effective mass

As the Higgs field possesses the non-vanishing VEV, i.e. $\langle H\rangle = v$, its one-loop effective mass contribution can be derived from the one-loop effective potential (B.1) evaluated in the vacuum

$$\begin{aligned}\langle V_1\rangle=\frac{1}{64\pi^2}\Bigg[&(3\lambda v^2-m^2)^2\left(\log\frac{3\lambda v^2-m^2}{\mu^2}-\frac{3}{2}\right)+\\&(\lambda v^2-m^2)^2\left(\log\frac{\lambda v^2-m^2}{\mu^2}-\frac{3}{2}\right)+3(g^2v^2)^2\left(\log\frac{g^2v^2}{\mu^2}-\frac{5}{6}\right)\Bigg],\end{aligned} \tag{D.29}$$

where m^2 depends on parameters $\{v,\lambda\}$ via the one-loop stationarity condition (D.11)

$$\begin{aligned}m^2=\lambda v^2+\frac{1}{16\pi^2}\Bigg(&4\lambda m^2-10\lambda^2v^2-g^4v^2-3\lambda(m^2-3\lambda v^2)\log\left[\frac{3\lambda v^2-m^2}{\mu^2}\right]+\\&+\lambda(\lambda v^2-m^2)\log\left[\frac{\lambda v^2-m^2}{\mu^2}\right]+3g^4v^2\log\left[\frac{g^2v^2}{\mu^2}\right]\Bigg).\end{aligned} \tag{D.30}$$

The one-loop effective Higgs mass is calculated as

$$m^2_{H,eff}=\left.\frac{\partial^2\langle V_0\rangle}{\partial v^2}\right|_{\frac{\partial\langle V_0+V_1\rangle}{\partial v}=0}+\left.\frac{\partial^2\langle V_1\rangle}{\partial v^2}\right|_{\frac{\partial\langle V_0\rangle}{\partial_v}=0}, \tag{D.31}$$

which gives, after employing (D.6), (D.29) and (D.30), the final result

$$\begin{aligned}m^2_{H,eff}=&\,2\lambda v^2+\\&+\frac{v^2}{8\pi^2}\left(\lambda^2\log\left[\frac{0_{WGB}}{\mu^2}\right]+9\lambda^2\log\left[\frac{2\lambda v^2}{\mu^2}\right]+3g^4\log\left[\frac{g^2v^2}{\mu^2}\right]+2g^4\right),\end{aligned} \tag{D.32}$$

where 0_{WGB} stands for the would-be Goldstone mass. The effective Higgs mass is IR diverging due to the presence of the vanishing masses in the scalar mass spectrum and as such manifests its non-physicality.

Let us take a closer look at the renormalization scale dependence of the effective mass $m^2_{H,eff}$ calculated in (D.32). At one-loop,

$$\frac{d}{d\log\mu}m^2_{H,eff} = \frac{\partial m^2_{H,eff}}{\partial\log\mu} + \beta_\lambda\frac{\partial m^2_H}{\partial\lambda} + \beta_v\frac{\partial m^2_H}{\partial v} + \text{two-loop contributions}, \quad \text{(D.33)}$$

where m^2_H is tree-level Higgs mass (D.7), β_λ and β_v are one-loop beta functions (D.18) and (D.28), respectively. Explicitly,

$$\frac{\partial m^2_{H,eff}}{\partial\log\mu} = -\frac{v^2}{4\pi^2}\left(10\lambda^2 + 3g^4\right), \quad \text{(D.34)}$$

$$\frac{\partial m^2_H}{\partial\lambda} = 2v^2, \quad \text{(D.35)}$$

$$\frac{\partial m^2_H}{\partial v} = 4\lambda v. \quad \text{(D.36)}$$

Substituting relations (D.34)-(D.36) into (D.33), one obtains

$$\frac{d}{d\log\mu}m^2_{H,eff} = -\frac{v^2}{4\pi^2}\left(10\lambda^2 + 3g^4\right) + 2v^2\left(\frac{5\lambda^2}{4\pi^2} + \frac{3g^4}{8\pi^2} - \frac{3g^2\lambda}{4\pi^2}\right) + \\ + 4\lambda v\frac{3g^2 v}{16\pi^2} = -\frac{6g^2\lambda v^2}{4\pi^2} + \frac{6g^2\lambda v^2}{8\pi^2} = -\frac{6g^2\lambda v^2}{8\pi^2} \neq 0. \quad \text{(D.37)}$$

Thus the effective mass is renormalization scale dependent as it is not, in general, a physically measurable quantity.

D.4 The Higgs boson one-loop physical mass

We proceed to calculate the one-loop Higgs boson physical mass $m^2_{H,phys}$. In general [148, 164, 167],

$$m^2_{H,phys} = m^2_{H,eff} + \Sigma_{\overline{\text{MS}}}(p^2 = m^2_{H,phys}) - \Sigma_{\overline{\text{MS}}}(p^2 = 0), \quad \text{(D.38)}$$

where $\Sigma_{\overline{\text{MS}}}(p^2)$ is the Higgs field self-energy and we exploited the fact that the U(1) representation containing the H field has multiplicity equal to one. The difference $\Sigma_{\overline{\text{MS}}}(m^2_{H,phys}) - \Sigma_{\overline{\text{MS}}}(0)$ represents the shift from the effective mass to the physical mass and it can be approximated at one-loop as

$$\Sigma_{\overline{\text{MS}}}(p^2 = m^2_H) - \Sigma_{\overline{\text{MS}}}(p^2 = 0). \quad \text{(D.39)}$$

Only the p^2-dependent part of the self-energy can contribute to the mass shift (D.39), thus for all further purposes

$$\Sigma_{\overline{\text{MS}}}(p^2) \approx \Sigma^{bubbles}_{\overline{\text{MS}}}(p^2) \quad \text{(D.40)}$$

with $\Sigma^{bubbles}_{\overline{\text{MS}}}(p^2)$ calculated from bubble diagrams depicted in Figure D.1. Hence

$$\Sigma^{bubbles}_{\overline{\text{MS}}}(p^2) = \frac{9\lambda^2 v^2}{8\pi^2}\int_0^1 dx \log\left[\frac{2\lambda v^2 - p^2 x(1-x)}{\mu^2}\right] + \\ + \frac{\lambda^2 v^2}{8\pi^2}\int_0^1 dx \log\left[\frac{-p^2 x(1-x)}{\mu^2}\right] +$$

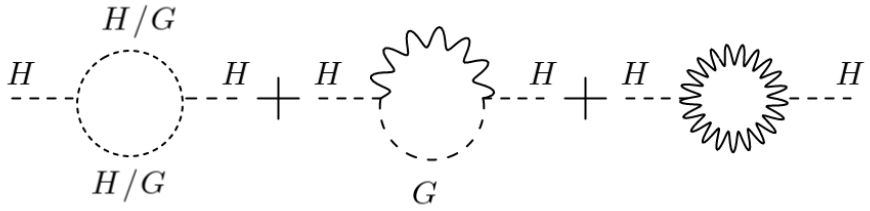

Figure D.1: Feynman diagrams contributing to the p^2-dependent part of the Higgs field self-energy $\Sigma^{bubbles}_{\overline{\rm MS}}(p^2)$.

$$
\begin{aligned}
&+\frac{g^4v^2}{4\pi^2}+\frac{g^4v^2}{4\pi^2}\int_0^1 dx\log\left[\frac{g^2v^2-p^2x(1-x)}{\mu^2}\right]+\\
&+\frac{g^4v^2}{8\pi^2}\int D^3(x)\log\left[\frac{g^2v^2-p^2\frac{(x+y)(1-x-y)}{(1-y)}}{\mu^2}\right]+\\
&+\frac{g^4v^2}{16\pi^2}\int D^3(x)\frac{p^2(x+y)^2}{g^2v^2(1-y)-p^2(x+y)(1-x-y)}-\\
&-\frac{g^4v^2}{8\pi^2}\int D^3(x)\frac{p^2(x+y)}{g^2v^2(1-y)-p^2(x+y)(1-x-y)}-\\
&-\frac{g^4v^2}{48\pi^2}\int D^4(x)\frac{p^4(x+z)^2}{(g^2v^2(y+x)-p^2(x+z)(1-x-z))^2}+\\
&+\frac{g^4v^2}{96\pi^2}\int D^4(x)\frac{p^2}{g^2v^2(y+x)-p^2(x+z)(1-x-z)}-\\
&-\frac{g^2p^2}{4\pi^2}\int_0^1 dx\log\left[\frac{g^2v^2(1-x)-p^2x(1-x)}{\mu^2}\right]-\\
&-\frac{g^2p^2}{32\pi^2}+\frac{g^2p^2}{16\pi^2}\int D^3(x)\log\left[\frac{g^2v^2-p^2y(1-y)}{\mu^2}\right]+\\
&+\frac{g^2p^2}{8\pi^2}\int D^3(x)\frac{p^2y^2}{g^2v^2x-p^2y(1-y)},
\end{aligned}
\tag{D.41}
$$

where

$$
\begin{aligned}
\int D^3(x)&=2!\int_0^1 dx\int_0^1 dy\int_0^1 dz\delta(1-x-y-z),\\
\int D^4(x)&=3!\int_0^1 dx\int_0^1 dy\int_0^1 dz\int_0^1 dw\delta(1-x-y-z-w).
\end{aligned}
$$

Computing the mass shift (D.39) from (D.41), one obtains the one-loop physical mass

$$
\begin{aligned}
m^2_{H,phys}=\;&2\lambda v^2+\frac{v^2}{8\pi^2}\left(\lambda^2\int_0^1 dx\log\left[\frac{2\lambda v^2x(1-x)}{\mu^2}\right]+\right.\\
&+9\lambda^2\int_0^1 dx\log\left[\frac{2\lambda v^2-2\lambda v^2x(1-x)}{\mu^2}\right]+\\
&+2g^4\int_0^1 dx\log\left[\frac{g^2v^2-2\lambda v^2x(1-x)}{\mu^2}\right]+\\
&\left.+g^4\int D^3(x)\log\left[\frac{g^2v^2-2\lambda v^2\frac{(x+y)(1-x-y)}{(1-y)}}{\mu^2}\right]+2g^4\right)+
\end{aligned}
$$

$$
\begin{aligned}
&+\frac{g^4v^2}{16\pi^2}\int D^3(x)\frac{2\lambda(x+y)^2}{g^2(1-y)-2\lambda(x+y)(1-x-y)}- \\
&-\frac{g^4v^2}{8\pi^2}\int D^3(x)\frac{2\lambda(x+y)}{g^2(1-y)-2\lambda(x+y)(1-x-y)}- \\
&-\frac{g^4v^2}{48\pi^2}\int D^4(x)\frac{4\lambda^2(x+z)^2}{(g^2(y+x)-2\lambda(x+z)(1-x-z))^2}+ \\
&+\frac{g^4v^2}{96\pi^2}\int D^4(x)\frac{2\lambda}{g^2(y+x)-2\lambda(x+z)(1-x-z)}\Bigg)- \\
&-\frac{8g^2\lambda v^2}{16\pi^2}\int_0^1 dx\log\left[\frac{g^2v^2(1-x)-2\lambda v^2x(1-x)}{\mu^2}\right]- \\
&-\frac{4g^2\lambda v^2}{64\pi^2}+\frac{8g^2\lambda v^2}{64\pi^2}\int D^3(x)\log\left[\frac{g^2v^2-2\lambda v^2y(1-y)}{\mu^2}\right]+ \\
&+\frac{8g^2\lambda v^2}{32\pi^2}\int D^3(x)\frac{2\lambda y^2}{g^2x-2\lambda y(1-y)}. \qquad \text{(D.42)}
\end{aligned}
$$

We immediately see that the one-loop physical mass does not suffer from IR divergences. These have been regularized by the shift (D.39), which replaces the logarithmic tree-level mass-dependent contributions according to the scheme

$$
\log\left[\frac{m^2_{tree}}{\mu^2}\right]\to\int_0^1 dx\log\left[\frac{m^2_{tree}-m^2_Hx(1-x)}{\mu^2}\right]+\ldots, \qquad \text{(D.43)}
$$

where m^2_{tree} is the tree-level mass of the field in the loop of a one-loop contribution. Thus the physical mass does not contain any diverging logarithmic contributions even for vanishing m^2_{tree}. We used the prescription (D.43) as the main inspiration behind the definition of the regularized effective mass in Sec. 3.1.1.

Finally, we explicitly demonstrate that the one-loop physical mass is renormalization scale independent. In analogy to the effective mass,

$$
\frac{d}{d\log\mu}m^2_{H,phys}=\frac{\partial m^2_{H,phys}}{\partial\log\mu}+\beta_\lambda\frac{\partial m^2_H}{\partial\lambda}+\beta_v\frac{\partial m^2_H}{\partial v}+\text{two-loop contributions} \qquad \text{(D.44)}
$$

at one loop, where m^2_H is the tree-level Higgs mass (D.7), β_λ and β_v are the one-loop beta functions (D.18) and (D.28), respectively. Inserting Eqns.(D.35)-(D.36) and

$$
\frac{\partial m^2_{H,phys}}{\partial\log\mu}=-\frac{v^2}{4\pi^2}\left(10\lambda^2+3g^4-3g^2\lambda\right) \qquad \text{(D.45)}
$$

into the RGE (D.44) we get

$$
\begin{aligned}
\frac{d}{d\log\mu}m^2_{H,eff}=-\frac{v^2}{4\pi^2}\left(10\lambda^2+3g^4-3g^2\lambda\right)+4\lambda v\frac{3g^2v}{16\pi^2}+ \\
+2v^2\left(\frac{5\lambda^2}{4\pi^2}+\frac{3g^4}{8\pi^2}-\frac{3g^2\lambda}{4\pi^2}\right)=0. \qquad \text{(D.46)}
\end{aligned}
$$

Thus the one-loop physical Higgs mass is indeed renormalization scale independent.

E. Tree-level scalar masses in the $45 \oplus 126$ Higgs model

E.1 Tree-level masses in the limiting cases

In this section we collect the analytical expressions for the tree-level masses of the scalar fields in the $\mathbf{45} \oplus \mathbf{126}$ SO(10) Higgs model in the $\omega_{BL} \to 0$ and $\omega_R \to 0$ limits of interest, and, for the sake of completeness, in the phenomenologically non-viable regime $\omega_R \to -\omega_{BL}$ for which the tree-level tachyonic instabilities in the scalar spectrum get resolved. The interested reader is deferred to [12, 15] for the general form of the tree-level scalar mass matrices in the $\mathbf{45} \oplus \mathbf{126}$ SO(10) Higgs model.

The scalar spectrum of the minimal SO(10) is dependent on the dimensionful parameter τ, whose value is given by the stationarity condition (2.36), implying implicit dependence of the mass spectrum on the VEV ratio

$$(\omega_{BL} + \omega_R)\frac{\omega_{BL}\omega_R}{|\sigma|^2}. \tag{E.1}$$

Since the perturbativity constraint $|\tau| \lesssim M_{GUT}$ prevents (E.1) from acquiring large values, the limits $\omega_{BL} \to 0$, $\omega_R \to 0$ and $\omega_R \to -\omega_{BL}$ should be properly understood as

$$|\omega_R| \gg |\sigma| \geq \sqrt{|\omega_R||\omega_{BL}|} \gg |\omega_{BL}|, \tag{E.2}$$

$$|\omega_{BL}| \gg |\sigma| \geq \sqrt{|\omega_R||\omega_{BL}|} \gg |\omega_R|, \tag{E.3}$$

and

$$|\omega_{BL}| \gg |\sigma| \geq \sqrt{|\omega_{BL}||\omega_{BL} + \omega_R|} \gg |\omega_R + \omega_{BL}|, \tag{E.4}$$

respectively. Hence it is worthwhile to present the tree-level masses as functions of the dimensionless scalar couplings and the set of parameters $\{\omega_R, \sigma, \chi\}$ for $\omega_{BL} \to 0$ case, $\{\omega_{BL}, \sigma, \chi\}$ in the $\omega_R \to 0$ regime and $\{\omega_R, \sigma, \chi_2\}$ in the $\omega_R \to -\omega_{BL}$ limit, where the universal VEV ratio χ is defined as in Eq. (2.37) and

$$\chi_2 := \frac{(\omega_{BL} + \omega_R)\omega_{BL}}{|\sigma|^2}. \tag{E.5}$$

The tree-level scalar mass-squared eigenvalues for all three limiting cases are compiled in Table E.1. We display only the dominant contributions, which are proportional either to the SO(10)-breaking VEVs ω_{BL} or ω_R, or the intermediate-symmetry-breaking scale σ.[1] Observe that the *heavy* scalars with mass-squared eigenvalues proportional to M^2_{GUT} belong to multiplets of the intermediate symmetry $\mathrm{SU}(4)_C \times \mathrm{SU}(2)_L \times \mathrm{U}(1)_R$ in the $\omega_{BL} \to 0$ limit, $\mathrm{SU}(3)_c \times \mathrm{SU}(2)_L \times \mathrm{SU}(2)_R \times \mathrm{U}(1)_{B-L}$ in the $\omega_R \to 0$ case and $\mathrm{SU}(5)' \times \mathrm{U}(1)_{Z'}$ in the $\omega_R \to -\omega_{BL}$ regime, c.f. Tables F.1-F.4 for representation decompositions.

[1] Note that the $|\sigma|^2$-proportional mass contributions cannot compete with the M^2_{GUT}-proportional ones due to the large hierarchy between the scales $\left(|\sigma|/\omega \sim 10^{-(4-10)}\right)$. Consequently, the one-loop mass contributions of the order $\sim M^2_{GUT}/16\pi^2$ also dominate over the subleading $|\sigma|^2$-proportional terms.

Table E.1: Dominant contributions to the tree-level scalar masses in all three scenarios $\omega_{BL} \to 0$, $\omega_R \to 0$ and $\omega_R \to -\omega_{BL}$.

Mass	$\omega_{BL} \to 0$	$\omega_R \to 0$	$\omega_R \to -\omega_{BL}$
$M_S^2(1,3,0)$	$+4a_2\omega_R^2$	$-2a_2\omega_{BL}^2$	$+4a_2\omega_{BL}^2$
$M_S^2(8,1,0)$	$-2a_2\omega_R^2$	$+4a_2\omega_{BL}^2$	$+4a_2\omega_{BL}^2$
$M_S^2(1,1,+2)$	$-4(4\beta_4' + a_2\chi)\omega_R^2$	$+4(2\lambda_2 + 2\lambda_4 + 8\lambda_4' - a_2\chi^2)\lvert\sigma\rvert^2$	$-4(4\beta_4' + a_2\chi_2)\omega_{BL}^2$
$M_S^2(1,3,-1)$	$-2(2\beta_4' + a_2\chi)\omega_R^2$	$-6(6\beta_4' + a_2\chi)\omega_{BL}^2$	$-4(4\beta_4' - a_2\chi_2)\omega_{BL}^2$
$M_S^2(\bar{3},1,+\frac{4}{3})$	$-4(4\beta_4' + a_2\chi)\omega_R^2$	$+2(\beta_4 - 2\beta_4' - a_2\chi)\omega_{BL}^2$	$+2(\beta_4 - 2\beta_4' + a_2\chi_2)\omega_{BL}^2$
$M_S^2(3,3,-\frac{1}{3})$	$-2(2\beta_4' + a_2\chi)\omega_R^2$	$+2(\beta_4 - 8\beta_4' - 2a_2\chi)\omega_{BL}^2$	$+2(\beta_4 - 2\beta_4' - a_2\chi_2)\omega_{BL}^2$
$M_S^2(6,3,+\frac{1}{3})$	$-2(2\beta_4' + a_2\chi)\omega_R^2$	$-2(2\beta_4' + a_2\chi)\omega_{BL}^2$	$+2(4\lambda_2 + 4\lambda_4 + 16\lambda_4' + a_2\chi_2^2)\lvert\sigma\rvert^2$
$M_S^2(\bar{6},1,-\frac{4}{3})$	$+4(2\lambda_2 + 2\lambda_4 + 8\lambda_4' - a_2\chi^2)\lvert\sigma\rvert^2$	$-4(4\beta_4' + a_2\chi)\omega_{BL}^2$	$-4(4\beta_4' - a_2\chi_2)\omega_{BL}^2$
$M_S^2(\bar{6},1,-\frac{1}{3})$	$+2(\beta_4 - 2\beta_4' - a_2\chi)\omega_R^2$	$-4(4\beta_4' + a_2\chi)\omega_{BL}^2$	$+2(\beta_4 - 2\beta_4' - a_2\chi_2)\omega_{BL}^2$
$M_S^2(\bar{6},1,+\frac{2}{3})$	$-4(4\beta_4' + a_2\chi)\omega_R^2$	$-4(4\beta_4' + a_2\chi)\omega_{BL}^2$	$+4(4\lambda_2 + 6\lambda_4 + 4\lambda_4' + a_2\chi_2^2)\lvert\sigma\rvert^2$
$M_S^2(1,2,+\frac{1}{2})_1$	$+\frac{1}{2}\left(\beta_4 - 10\beta_4' - 4a_2\chi - 2\sqrt{4\lvert\gamma_2\rvert^2 + (4\beta_4' + a_2\chi)^2}\right)\omega_R^2$	$+\frac{1}{2}(7\beta_4 - 18\beta_4' - 6a_2\chi - 4\lvert\gamma_2\rvert)\omega_{BL}^2$	$+2(\beta_4 - 2\beta_4' - a_2\chi_2)\omega_{BL}^2$
$M_S^2(1,2,+\frac{1}{2})_2$	$+\frac{1}{2}\left(\beta_4 - 10\beta_4' - 4a_2\chi + 2\sqrt{4\lvert\gamma_2\rvert^2 + (4\beta_4' + a_2\chi)^2}\right)\omega_R^2$	$+\frac{1}{2}(7\beta_4 - 18\beta_4' - 6a_2\chi + 4\lvert\gamma_2\rvert)\omega_{BL}^2$	$+6\beta_4\omega_{BL}^2$
$M_S^2(3,2,+\frac{7}{6})_1$	$+\frac{1}{2}\left(\beta_4 - 10\beta_4' - 4a_2\chi - 2\sqrt{4\lvert\gamma_2\rvert^2 + (4\beta_4' + a_2\chi)^2}\right)\omega_R^2$	$+\frac{1}{2}\left(\beta_4 - 26\beta_4' - 6a_2\chi - 4\sqrt{\lvert\gamma_2\rvert^2 + (6\beta_4' + a_2\chi)^2}\right)\omega_{BL}^2,$	$+2(\beta_4 - 2\beta_4' + a_2\chi_2)\omega_{BL}^2$
$M_S^2(3,2,+\frac{7}{6})_2$	$+\frac{1}{2}\left(\beta_4 - 10\beta_4' - 4a_2\chi + 2\sqrt{4\lvert\gamma_2\rvert^2 + (4\beta_4' + a_2\chi)^2}\right)\omega_R^2$	$+\frac{1}{2}\left(\beta_4 - 26\beta_4' - 6a_2\chi + 4\sqrt{\lvert\gamma_2\rvert^2 + (6\beta_4' + a_2\chi)^2}\right)\omega_{BL}^2$	$-4(4\beta_4' + a_2\chi_2)\omega_{BL}^2$
$M_S^2(8,2,+\frac{1}{2})_1$	$+\frac{1}{2}\left(\beta_4 - 10\beta_4' - 4a_2\chi - 2\sqrt{4\lvert\gamma_2\rvert^2 + (4\beta_4' + a_2\chi)^2}\right)\omega_R^2$	$+\frac{1}{2}(\beta_4 - 18\beta_4' - 6a_2\chi - 4\lvert\gamma_2\rvert)\omega_{BL}^2$	$+2(\beta_4 - 2\beta_4' - a_2\chi_2)\omega_{BL}^2$
$M_S^2(8,2,+\frac{1}{2})_2$	$+\frac{1}{2}\left(\beta_4 - 10\beta_4' - 4a_2\chi + 2\sqrt{4\lvert\gamma_2\rvert^2 + (4\beta_4' + a_2\chi)^2}\right)\omega_R^2$	$+\frac{1}{2}(\beta_4 - 18\beta_4' - 6a_2\chi + 4\lvert\gamma_2\rvert)\omega_{BL}^2$	$+(12\lambda_2 + 12\lambda_4 + 16\lambda_4' + 3a_2\chi_2^2)\lvert\sigma\rvert^2$
$M_S^2(\bar{3},1,+\frac{1}{3})_1$	$+(\beta_4 - 4\beta_4' - 2a_2\chi - 4\lvert\gamma_2\rvert)\omega_R^2$	$+\left(\beta_4 - 10\beta_4' - 3a_2\chi - \sqrt{16\lvert\gamma_2\rvert^2 + (6\beta_4' + a_2\chi)^2}\right)\omega_{BL}^2$	$+6\beta_4\omega_{BL}^2$
$M_S^2(\bar{3},1,+\frac{1}{3})_2$	$+2(\beta_4 - 2\beta_4' - a_2\chi)\omega_R^2$	$+2(\beta_4 - 2\beta_4' - a_2\chi)\omega_{BL}^2$	$+2(\beta_4 - 2\beta_4' - a_2\chi_2)\omega_{BL}^2$
$M_S^2(\bar{3},1,+\frac{1}{3})_3$	$+(\beta_4 - 4\beta_4' - 2a_2\chi + 4\lvert\gamma_2\rvert)\omega_R^2$	$+\left(\beta_4 - 10\beta_4' - 3a_2\chi + \sqrt{16\lvert\gamma_2\rvert^2 + (6\beta_4' + a_2\chi)^2}\right)\omega_{BL}^2$	$+2(4\lambda_2 + 4\lambda_4 - \frac{16}{3}\lambda_4' + a_2\chi_2^2)\lvert\sigma\rvert^2$
$M_S^2(1,1,+1)_2$	$+2(\beta_4 - 2\beta_4' - a_2\chi)\omega_R^2$	$-2a_2\omega_{BL}^2$	$+2(\beta_4 - 2\beta_4' + a_2\chi_2)\omega_{BL}^2$
$M_S^2(\bar{3},1,-\frac{2}{3})_2$	$-2a_2\omega_R^2$	$+2(\beta_4 - 2\beta_4' - a_2\chi)\omega_{BL}^2$	$+2(\beta_4 - 2\beta_4' - a_2\chi_2)\omega_{BL}^2$
$M_S^2(3,2,+\frac{1}{6})_2$	$+\frac{1}{2}\left(\beta_4 - 10\beta_4' - 4a_2\chi - 2\sqrt{4\lvert\gamma_2\rvert^2 + (4\beta_4' + a_2\chi)^2}\right)\omega_R^2$	$+\frac{1}{2}\left(\beta_4 - 26\beta_4' - 6a_2\chi - 4\sqrt{\lvert\gamma_2\rvert^2 + (6\beta_4' + a_2\chi)^2}\right)\omega_{BL}^2$	$+2(\beta_4 - 2\beta_4' - a_2\chi_2)\omega_{BL}^2$
$M_S^2(3,2,+\frac{1}{6})_3$	$+\frac{1}{2}\left(\beta_4 - 10\beta_4' - 4a_2\chi + 2\sqrt{4\lvert\gamma_2\rvert^2 + (4\beta_4' + a_2\chi)^2}\right)\omega_R^2$	$+\frac{1}{2}\left(\beta_4 - 26\beta_4' - 6a_2\chi + 4\sqrt{\lvert\gamma_2\rvert^2 + (6\beta_4' + a_2\chi)^2}\right)\omega_{BL}^2$	$+4a_2\omega_{BL}^2$
$M_S^2(1,1,0)_2$	$+\left(8\lambda_0 - \frac{8((\alpha+\beta_4')^2+(\alpha+\beta_4')a_2\chi)}{4a_0+a_2} + \frac{4(6a_0+a_2)a_2\chi^2}{4a_0+a_2}\right)\lvert\sigma\rvert^2$	$+\left(8\lambda_0 - \frac{12((\alpha+\beta_4')^2+(\alpha+\beta_4')a_2\chi)}{6a_0+a_2} + \frac{(24a_0+a_2)a_2\chi^2}{6a_0+a_2}\right)\lvert\sigma\rvert^2$	$+\left(8\lambda_0 - \frac{4(5(\alpha+\beta_4')^2-(\alpha+\beta_4')a_2\chi_2)}{10a_0+a_2} - \frac{(48a_0+5a_2)a_2\chi_2^2)}{10a_0+a_2}\right)\lvert\sigma\rvert^2$
$M_S^2(1,1,0)_3$	$-2a_2\omega_R^2$	$-2a_2\omega_{BL}^2$	$+4a_2\omega_{BL}^2$
$M_S^2(1,1,0)_4$	$+4(4a_0 + a_2)\omega_R^2$	$+4(6a_0 + a_2)\omega_{BL}^2$	$+4(10a_0 + a_2)\omega_{BL}^2$

Finally, note that the set of the scalar states is extended in the full version of the $\mathbf{45} \oplus \mathbf{126} \oplus \mathbf{10}_{\mathbb{C}}$ SO(10) model by two SM doublets $(1,2,+\frac{1}{2})$ and two SM triplets $(\bar{3},1,+\frac{1}{3})$. Thus, the mass-squares $M^2(1,2,+\frac{1}{2})_{1,2}$ and $M^2(\bar{3},1,+\frac{1}{3})_{1,2,3}$ are eigenvalues of the subparts of a larger mass matrix structure, c.f. full doublet and triplet mass matrices in Eqns. (3.58) and (3.61), respectively.

E.2 Decoupling issue for general case

Let us study the general combination of $\omega_{BL} \neq 0$, $\omega_R \neq 0$, where none of these VEVs is subject to any of the limits $\omega_{BL} \to 0$, $\omega_R \to 0$ or $\omega_R \to \pm\omega_{BL}$. We show

that in such a case, contrary to general expectation, the mass of the intermediate-symmetry-breaking Higgs $M_S^2(1,1,0)_2$, c.f. Table E.1 for the limiting cases, is not necessarily proportional to the σ scale.

The argument in [124] demonstrated that the mass of the Higgs boson is always proportional to its VEV. The proof uses the Appelquist-Carazzone theorem [168] to constrain the behaviour of the 1PI Green's functions. However, whenever the Appelquist-Carrazone theorem does not hold, the Higgs boson mass does not necessarily have to be proportional to its VEV. The manifestation of the aforementioned situation can be found in the minimal SO(10) model, where for the general ω-VEV configuration the intermediate stage $\mathrm{SU}(3)_c \times \mathrm{SU}(2)_L \times \mathrm{U}(1)_R \times \mathrm{U}(1)_{B-L}$ (broken by the non-zero σ VEV) and the full SO(10) (broken by the non-zero ω VEV) effective field theory cannot decouple in the sense of the Appelquist-Carrazone decoupling theorem.

First, it is instructive to recollect the ω-VEV-induced vacuum stationarity conditions (2.31)-(2.32) which lead to the $\tau-$dependent tree-level equation

$$(\omega_{BL}-\omega_R)|\sigma|^2\tau = a_2\omega_{BL}\omega_R(\omega_{BL}+\omega_R)(\omega_{BL}-\omega_R)+ \\ +2\beta_4'(3\omega_{BL}+2\omega_R)(\omega_{BL}-\omega_R)|\sigma|^2. \quad \text{(E.6)}$$

Outside the limiting cases $\omega_R \to 0$, $\omega_{BL} \to 0$ and $\omega_R \to \pm\omega_{BL}$, which are excluded from our current discussion, Eq. (E.6) is solved by

$$\tau = 2\beta_4'(3\omega_{BL}+2\omega_R) + a_2\frac{\omega_{BL}\omega_R(\omega_{BL}+\omega_R)}{|\sigma|^2} \quad \text{(E.7)}$$

and the condition (E.7) contains the VEV structure (E.1) with the σ-dependent denominator. The tree-level SM singlet mass-squared matrix then acquires the form

$$M_S^2(1,1,0) = \begin{pmatrix} \mathcal{M}_S^2(1,1,0) & 0 \\ 0 & 0 \end{pmatrix} \quad \text{(E.8)}$$

with the zero-eigenvalue subspace corresponding to the would-be Goldstone boson rotated out and

$$\mathcal{M}_S^2(1,1,0) = \begin{pmatrix} -2\left(6\beta_4'\sigma^2 - 12a_0 f[1,0,0] + a_2 f[-2,1,1]\right) & -4\sqrt{6}\left(\beta_4'\sigma^2 - 2a_0 f[0,1,0]\right) & 2\sqrt{6}\left(\iota_{BL}\sigma + \frac{a_2}{\sigma}\Upsilon\right) \\ -4\sqrt{6}\left(\beta_4'\sigma^2 - 2a_0 f[0,1,0]\right) & -2\left(4\beta_4'\sigma^2 - 8a_0 f[0,0,1] + a_2 f[1,-1,-2]\right) & 4\left(\iota_R\sigma + \frac{a_2}{\sigma}\Upsilon\right) \\ \sqrt{6}\left(\iota_{BL}\sigma + \frac{a_2}{\sigma}\Upsilon\right) & 2\left(\iota_R\sigma + \frac{a_2}{\sigma}\Upsilon\right) & 8\lambda_0\sigma^2 \end{pmatrix},$$

where

$$f[z_1,z_2,z_3] := z_1\omega_{BL}^2 + z_2\omega_{BL}\omega_R + z_3\omega_R^2, \quad \text{(E.9)}$$

$$\Upsilon := \omega_{BL}\omega_R(\omega_{BL}+\omega_R), \quad \text{(E.10)}$$

$$\iota_{R/BL} := 2(\alpha+\beta_4')\omega_{R/BL}. \quad \text{(E.11)}$$

For simplicity, the σ complex phase is absorbed into an overall phase of the representation **126**, so the preceding expressions assume real $\sigma > 0$.

In the decoupling limit $\left|\frac{\sigma}{\omega}\right| \to 0$, the $\frac{a_2}{\sigma}\Upsilon$-dependent singlet mass matrix elements, and consequently the tree-level mass of the intermediate-symmetry-breaking Higgs, diverge due to the presence of the $\frac{1}{|\sigma|^2}$-proportional term in the τ coupling from Eq. (E.7). In such a case, the Appelquist-Carrazone theorem does

not hold and the dynamics of the SO(10) effective field theory cannot decouple from the subsequent $\mathrm{SU}(3)_c \times \mathrm{SU}(2)_L \times \mathrm{U}(1)_R \times \mathrm{U}(1)_{B-L}$ intermediate effective theory stage. Hence, we have shown that the intermediate-symmetry-breaking Higgs does not have to obtain the $\sigma-$proportional mass outside the special VEV regimes $\omega_{BL} \to 0$, $\omega_R \to 0$ and $\omega_R \to \pm\omega_{BL}$.

The attentive reader can wonder if the validity of the Appelquist-Carazzone theorem is re-established in case of $a_2 = 0$, since the potentially problematic $\frac{1}{|\sigma|^2}$-proportional VEV structure (E.1) in (E.7) vanishes at the tree-level. Indeed, the stationarity conditions (2.31)-(2.32) at one-loop level with $a_2 \to 0$ lead to the equation

$$\tau_{1-loop} = 2\beta_4'(3\omega_{BL} + 2\omega_R) + \frac{\lambda\tilde{\lambda} + g^4}{16\pi^2}\frac{\omega_{BL}\omega_R(\omega_{BL} + \omega_R)}{|\sigma|^2} + \cdots , \tag{E.12}$$

where λ, $\tilde{\lambda}$ denote dimensionless scalar parameters and g is the gauge coupling, c.f. Eq. (3.8). Hence the presence of the $\frac{1}{|\sigma|^2}$-proportional VEV structure perseveres beyond tree-level and Appelquist-Carazzone theorem does not hold for general combination $\omega_{BL} \neq 0$, $\omega_R \neq 0$ even if $a_2 \to 0$.

Finally, we explicitly demonstrate that there is no σ-proportional singlet mass at the tree-level for general $\omega_{BL} \neq 0$, $\omega_R \neq 0$ VEVs. The mass matrix $\mathcal{M}_S^2(1,1,0)$ has three real eigenvalues, call them m_1, m_2, m_3, which can be obtained by finding three roots of the characteristic polynomial. As such a task can be rather cumbersome, we will employ easier-to-calculate principal invariants

$$I_1 := \mathrm{Tr}\left(\mathcal{M}^2\right) = m_1 + m_2 + m_3, \tag{E.13}$$

$$I_2 := \frac{1}{2}\left(\mathrm{Tr}\left(\mathcal{M}^2\right)^2 - \mathrm{Tr}\left(\mathcal{M}^4\right)\right) = m_1m_2 + m_1m_3 + m_2m_3, \tag{E.14}$$

$$I_3 := \det\left(\mathcal{M}^2\right) = m_1m_2m_3 \tag{E.15}$$

to show that no eigenvalue of $\mathcal{M}_S^2(1,1,0)$ can be σ^2-proportional. By inserting the singlet mass matrix, we find that

$$I_1 = \mathcal{O}(\sigma^0), \tag{E.16}$$

$$I_2 = \frac{x_{I_2}}{\sigma^2} + \mathcal{O}(\sigma^0), \tag{E.17}$$

$$I_3 = \frac{x_{I_3}}{\sigma^2} + \mathcal{O}(\sigma^0), \tag{E.18}$$

where

$$x_{I_2} = -20a_2^2\Upsilon^2, \tag{E.19}$$

$$x_{I_3} = -8a_2^2\Upsilon^2\left(24a_0 f[1,-2,1] + a_2 f[1,-5,4]\right). \tag{E.20}$$

Now, let us assume for a moment, that m_1 is the σ^2-proportional eigenvalue, i.e. $m_1 = b\sigma^2$ with b being a real dimensionless parameter. Then

$$I_2 = b\sigma^2 I_1 - b^2\sigma^4 + \lambda_2\lambda_3 \tag{E.21}$$

and Eqns. (E.16)-(E.17) imply

$$\lambda_2\lambda_3 = \frac{x_{I_2}}{\sigma^2} + \mathcal{O}(\sigma^0). \tag{E.22}$$

Consequently,

$$I_3 = b\sigma^2\lambda_2\lambda_3 = bx_{I_2} + \mathcal{O}(\sigma^2), \tag{E.23}$$

which is in complete contradiction with relation (E.18). Thus we conclude that no SM singlet has the tree-level σ-proportional mass in the minimal SO(10) model with the general combination of $\omega_{BL} \neq 0$, $\omega_R \neq 0$.

F. SO(10) group theory tidbits

Symmetry groups of Particle Physics models typically form Lie groups. Lie group is a group of continuous transformations whose group elements depend on at least one continuous parameter [169]. Every element g of a connected Lie group can be expressed via infinitesimal Lie group generators T^a by invoking exponential map

$$g(\alpha) = \exp\left(i\alpha^a T^a\right). \tag{F.1}$$

A complete set of infinitesimal Lie group generators forms the Lie algebra. Generators satisfy fundamental commutation relations

$$[T^a, T^b] = if^{abc}T^c, \tag{F.2}$$

where f^{abc} are called structure constants and they are specific to every Lie algebra. Rather than Lie groups, Lie algebras are usually of interest in the context of Particle Physics because the algebra generators act directly on quantum fields and the operators T^a are referred to as gauge symmetry generators.

The symmetry group governing gauge transformations of the SO(10) GUT is Spin(10), double cover of the SO(10) Lie group [170]. As corresponding Lie algebras, and consequently gauge symmetry generators, of both SO(10) and Spin(10) groups are isomorphic, there is no difference in the calculation of physical quantities between the two. Hence, for simplicity, we will claim that the gauge group of the model under study is SO(10).

F.1 Generators in defining representation

In the defining 10-dimensional vector representation [169], the SO(10) group elements act as rotations on the 10-dimensional Euclidean vector space and they can be represented by the 10×10 real matrices M which satisfy

$$M^T M = I_{10}, \qquad \det M = 1. \tag{F.3}$$

Henceforth we will not deal with the SO(10) symmetry transformations on the Lie group level but rather always focus on their infinitesimal generators that form the corresponding Lie algebra. Simultaneously we will adhere to the physicist's habit of sometimes using the term "group" even when talking about "algebra".

The SO(10) gauge symmetry generators form the set of all 10×10 purely imaginary Hermitian matrices $T_{(ij)}$ with zero trace, i.e.

$$T^\dagger_{(ij)} = T_{(ij)}, \qquad \mathrm{Tr}\; T_{(ij)} = 0, \tag{F.4}$$

where (ij) stands for 45 different ordered pairs of indices $i, j = 1, \ldots, 10$, and they satisfy commutation relations

$$[T_{(ij)}, T_{(kl)}] = \frac{i}{\sqrt{2}}\left(\delta_{jk}T_{(il)} - \delta_{ik}T_{(jk)} - \delta_{jl}T_{(ik)} + \delta_{il}T_{(jk)}\right). \tag{F.5}$$

The generators in the defining vector representation adopt the form of matrices with individual matrix elements

$$\left(T_{(ij)}\right)_{mn} = -\frac{i}{\sqrt{2}}\left(\delta_{im}\delta_{jn} - \delta_{jm}\delta_{in}\right). \tag{F.6}$$

Such a choice automatically guarantees proper normalization

$$\mathrm{Tr}\left(T_{(ij)}T_{(kl)}\right) = \delta_{ik}\delta_{jl} - \delta_{il}\delta_{jk}. \tag{F.7}$$

F.2 Generators in spinor representation

Apart from the vector and the tensorial representations, the SO(10) group has another type of representation called spinorial [11, 169]. The SO(10) gauge generators in the spinorial representation take the form of

$$\tilde{S}_{(ij)} = \frac{1}{4i}[\Gamma_i, \Gamma_j], \tag{F.8}$$

where Γ_i are basis operators of the Clifford algebra Cliff(10), $i, j = 1, \ldots, 10$ and Γ_i obey anticommutation relations

$$\{\Gamma_i, \Gamma_j\} = 2\delta_{ij}. \tag{F.9}$$

Operators Γ_i are direct generalizations of Dirac Gamma matrices well known from the spinor calculus of charged fermionic fields. They can be explicitly expressed by the 32×32 matrices

$$\Gamma_{2p+1} = \left(\bigotimes_{p} I_2\right) \otimes \sigma_2 \otimes \left(\bigotimes_{4-p} \sigma_3\right), \tag{F.10}$$

$$\Gamma_{2p+2} = -\left(\bigotimes_{p} I_2\right) \otimes \sigma_1 \otimes \left(\bigotimes_{4-p} \sigma_3\right), \tag{F.11}$$

$$\tag{F.12}$$

where $p = 0, \ldots, 4$ and σ_i are 2×2 Pauli matrices. Hence, gamma matrices Γ_i act on the 32-dimensional vector space. Spinorial 32-dimensional representation is reducible and we can construct chiral projectors $P_\pm = \frac{1}{2}\left(I_{32} + \Gamma_{11}\right)$ onto two irreducible 16-dimensional subspaces. Clifford algebra element Γ_{11} is defined as

$$\Gamma_{11} = -\Gamma_1\Gamma_2\cdots\Gamma_{10} \tag{F.13}$$

and it commutes with all the gauge generators $\tilde{S}_{(ij)}$.

F.3 Various SO(10) subgroups

While discussing the spontaneous symmetry breaking in Sec. 2.2, we mentioned several SO(10) subgroups. Hence we will have a look at the explicit form of their gauge symmetry generators in the vector representation.

The SU(4) subgroup has 15 generators which can be indentified with the SO(10) generators $T_{(ij)}$, $i,j \in \{1,\ldots,6\}$. Subset of 8 generators of the form

$$\begin{pmatrix} -\tilde{X} & 0 \\ 0 & 0_{4\times 4} \end{pmatrix}, \tag{F.14}$$

where

$$\tilde{X} = \begin{cases} -\frac{1}{2} I_2 \otimes \lambda_q & \text{if } q = 2,5,7 \\ -\frac{1}{2}\sigma_2 \otimes \lambda_q & \text{if } q = 1,3,4,6,8 \end{cases} \tag{F.15}$$

and λ_q are Gell-Mann matrices, constitute the subgroup SU(3) $\subset$ SU(4). Let us add that the following relation holds for the $\mathrm{U}(1)_{BL}$ charge generator T_{BL}:

$$\tilde{X}_{BL} = -\frac{2}{3}\sigma_2 \oplus I_3. \tag{F.16}$$

Generators of the $\mathrm{SU}(2)_L \times \mathrm{SU}(2)_R$ subgroup have the form

$$\begin{pmatrix} 0_{6\times 6} & 0 \\ 0 & -\frac{1}{2}\tilde{Y} \end{pmatrix} \tag{F.17}$$

and they commute with group generators of the SU(3) and the $\mathrm{U}(1)_{BL}$. Gauge symmetry generators of the $\mathrm{SU}(2)_L$ are defined by

$$\tilde{Y} \in \{I_2 \otimes \sigma_2, \sigma_2 \otimes \sigma_1, \sigma_2 \otimes \sigma_3\}, \tag{F.18}$$

and generators of the $\mathrm{SU}(2)_R$ are determined by

$$\tilde{Y} \in \{\sigma_2 \otimes I_2, \sigma_1 \otimes \sigma_2, \sigma_3 \otimes \sigma_2\}, \tag{F.19}$$

where the $\tilde{Y}_R := \sigma_2 \otimes I_2$ gives rise to the $\mathrm{U}(1)_R$ generator $T_R^{(3)}$. Consequently, the hypercharge $\mathrm{U}(1)_Y$ is generated by

$$T_Y = \tfrac{1}{2} T_{BL} + T_R^{(3)} = i \begin{pmatrix} \frac{1}{3}\sigma_2 \otimes I_3 & 0 \\ 0 & \frac{1}{2}\sigma_2 \otimes I_2 \end{pmatrix}. \tag{F.20}$$

The subgroup SU(5) has 24 generators, 11 out of which correspond to the SU(3) and the $\mathrm{SU}(2)_L$ generators introduced earlier. The remaining gauge group generators are proportional to

$$T_{(i7)} - T_{(j9)}, \tag{F.21}$$
$$T_{(i8)} - T_{(j10)}, \tag{F.22}$$
$$T_{(i9)} + T_{(j7)}, \tag{F.23}$$
$$T_{(i10)} + T_{(j8)} \tag{F.24}$$

and

$$T_{(14)} + T_{(25)} + T_{(36)}, \tag{F.25}$$

where pairs $(i,j) \in \{(1,4),(2,5),(3,6)\}$. If the $\mathrm{SU}(5) \times \mathrm{U}(1)_Z$ symmetry group is considered, additional U(1) generator is defined as [11]

$$T_Z = -4T_R^{(3)} + 3T_{BL}. \tag{F.26}$$

Let us note that there exists an alternative embedding of the $\mathrm{SU}(5)' \times \mathrm{U}(1)_{Z'}$ into the SO(10), commonly called as the flipped SU(5). In such a case, $\mathrm{SU}(5)'$ contains the subgroup $\mathrm{SU}(3) \times \mathrm{SU}(2)_L \times \mathrm{U}(1)_{Y'}$ with

$$T_{Y'} = \frac{1}{2} T_{BL} - T_R^{(3)} \tag{F.27}$$

and an additional U(1) factor generator is determined by

$$T_{Z'} = 4T_R^{(3)} + 3T_{BL}. \tag{F.28}$$

F.4 Representation decomposition

Decompositions of the SO(10) representations that accommodate fermion, scalar and gauge fields of the GUT model under consideration can be found in Tables F.1-F.4. We consider only the subgroups $\mathrm{SU}(3)_c \times \mathrm{SU}(2)_L \times \mathrm{SU}(2)_R \times \mathrm{U}(1)_{B-L}$ and $\mathrm{SU}(4)_C \times \mathrm{SU}(2)_L \times \mathrm{U}(1)_R$ corresponding to the potentially viable regimes $\omega_R \to 0$ and $\omega_{BL} \to 0$, respectively, and the flipped embedding $\mathrm{SU}(5)' \times \mathrm{U}(1)_{Z'}$ leading to the limiting case $\omega_R \to -\omega_{BL}$ which, although being phenomenologically non-viable, resolves the tachyonic mass instabilities in the tree-level scalar spectrum as discussed in Sec. 2.4.2.

All tables adhere to the same colour scheme which indicates whether given representation is *real* (**blue**), *complex* (**black**) or *complex conjugate* (**red**) of a different multiplet within the same SO(10) representation. The **45** and **10** are real and hence consist of real multiplets or complex-conjugated pairs; the **126** and **16** are complex and thus contain only complex multiplets.

Table F.1: Decomposition of the 10-dimensional defining representation of the SO(10) into the multiplets of $\mathrm{SU}(4)_C \times \mathrm{SU}(2)_L \times \mathrm{U}(1)_R$ (the left sub-table), $\mathrm{SU}(3)_c \times \mathrm{SU}(2)_L \times \mathrm{SU}(2)_R \times \mathrm{U}(1)_{B-L}$ (the middle sub-table) and $\mathrm{SU}(5)' \times \mathrm{U}(1)_{Z'}$ (the right sub-table) subgroups.

$4_C 2_L 1_R$	$3_c 2_L 1_Y$
$(6,1,0)$	$(3,1,-\frac{1}{3})$
	$(\bar{3},1,+\frac{1}{3})$
$(1,2,+\frac{1}{2})$	$(1,2,+\frac{1}{2})$
$(1,2,-\frac{1}{2})$	$(1,2,-\frac{1}{2})$

$3_c 2_L 2_R 1_{BL}$	$3_c 2_L 1_Y$
$(3,1,1,-\frac{2}{3})$	$(3,1,-\frac{1}{3})$
$(\bar{3},1,1,+\frac{2}{3})$	$(\bar{3},1,+\frac{1}{3})$
$(1,2,2,0)$	$(1,2,+\frac{1}{2})$
	$(1,2,-\frac{1}{2})$

$5'1_{Z'}$	$3_c 2_L 1_Y$
$(5,-2)$	$(3,1,-\frac{1}{3})$
	$(1,2,-\frac{1}{2})$
$(\bar{5},2)$	$(\bar{3},1,+\frac{1}{3})$
	$(1,2,+\frac{1}{2})$

Table F.2: Decomposition of the 16-dimensional spinorial representation of the SO(10) into the multiplets of $\mathrm{SU}(4)_C \times \mathrm{SU}(2)_L \times \mathrm{U}(1)_R$ (the left sub-table), $\mathrm{SU}(3)_c \times \mathrm{SU}(2)_L \times \mathrm{SU}(2)_R \times \mathrm{U}(1)_{B-L}$ (the middle sub-table) and $\mathrm{SU}(5)' \times \mathrm{U}(1)_{Z'}$ (the right sub-table) subgroups.

$4_C 2_L 1_R$	$3_c 2_L 1_Y$
$(4,2,0)$	$(3,2,+\frac{1}{6})$
	$(1,2,-\frac{1}{2})$
$(\bar{4},1,-\frac{1}{2})$	$(\bar{3},1,-\frac{2}{3})$
	$(1,1,0)$
$(\bar{4},1,+\frac{1}{2})$	$(\bar{3},1,+\frac{1}{3})$
	$(1,1,+1)$

$3_c 2_L 2_R 1_{BL}$	$3_c 2_L 1_Y$
$(3,2,1,+\frac{1}{3})$	$(3,2,+\frac{1}{6})$
$(\bar{3},1,2,-\frac{1}{3})$	$(\bar{3},1,-\frac{2}{3})$
	$(\bar{3},1,+\frac{1}{3})$
$(1,2,1,-1)$	$(1,2,-\frac{1}{2})$
$(1,1,2,1)$	$(1,1,0)$
	$(1,1,+1)$

$5'1_{Z'}$	$3_c 2_L 1_Y$
$(10,1)$	$(3,2,+\frac{1}{6})$
	$(\bar{3},1,+\frac{1}{3})$
	$(1,1,0)$
$(\bar{5},-3)$	$(1,2,-\frac{1}{2})$
	$(\bar{3},1,-\frac{2}{3})$
$(1,5)$	$(1,1,+1)$

Table F.3: Decomposition of the 45-dimensional adjoint representation of the SO(10) into the multiplets of $\mathrm{SU}(4)_C \times \mathrm{SU}(2)_L \times \mathrm{U}(1)_R$ (the left sub-table), $\mathrm{SU}(3)_c \times \mathrm{SU}(2)_L \times \mathrm{SU}(2)_R \times \mathrm{U}(1)_{B-L}$ (the middle sub-table) and $\mathrm{SU}(5)' \times \mathrm{U}(1)_{Z'}$ (the right sub-table) subgroups.

$4_C 2_L 1_R$	$3_c 2_L 1_Y$
$(1,3,0)$	$(1,3,0)$
$(15,1,0)$	$(8,1,0)$
	$(\bar{3},1,-\frac{2}{3})$
	$(3,1,+\frac{2}{3})$
	$(1,1,0)$
$(6,2,-\frac{1}{2})$	$(3,2,-\frac{5}{6})$
	$(\bar{3},2,-\frac{1}{6})$
$(6,2,+\frac{1}{2})$	$(\bar{3},2,+\frac{5}{6})$
	$(3,2,+\frac{1}{6})$
$(1,1,+1)$	$(1,1,+1)$
$(1,1,-1)$	$(1,1,-1)$
$(1,1,0)$	$(1,1,0)$

$3_c 2_L 2_R 1_{BL}$	$3_c 2_L 1_Y$
$(1,3,1,0)$	$(1,3,0)$
$(8,1,1,0)$	$(8,1,0)$
$(3,2,2,-\frac{2}{3})$	$(3,2,-\frac{5}{6})$
	$(3,2,+\frac{1}{6})$
$(\bar{3},2,2,+\frac{2}{3})$	$(\bar{3},2,+\frac{5}{6})$
	$(\bar{3},2,-\frac{1}{6})$
$(1,1,3,0)$	$(1,1,+1)$
	$(1,1,-1)$
	$(1,1,0)$
$(\bar{3},1,1,-\frac{4}{3})$	$(\bar{3},1,-\frac{2}{3})$
$(3,1,1,+\frac{4}{3})$	$(3,1,+\frac{2}{3})$
$(1,1,1,0)$	$(1,1,0)$

$5'1_{Z'}$	$3_c 2_L 1_Y$
$(24,0)$	$(1,3,0)$
	$(8,1,0)$
	$(3,2,+\frac{1}{6})$
	$(\bar{3},2,-\frac{1}{6})$
	$(1,1,0)$
$(10,-4)$	$(3,2,-\frac{5}{6})$
	$(\bar{3},1,-\frac{2}{3})$
	$(1,1,-1)$
$(\overline{10},4)$	$(\bar{3},2,+\frac{5}{6})$
	$(3,1,+\frac{2}{3})$
	$(1,1,+1)$
$(1,0)$	$(1,1,0)$

Table F.4: Decomposition of the 126-dimensional tensor representation of the SO(10) into the multiplets of $\mathrm{SU}(4)_C \times \mathrm{SU}(2)_L \times \mathrm{U}(1)_R$ (the left sub-table), $\mathrm{SU}(3)_c \times \mathrm{SU}(2)_L \times \mathrm{SU}(2)_R \times \mathrm{U}(1)_{B-L}$ (the middle sub-table) and $\mathrm{SU}(5)' \times \mathrm{U}(1)_{Z'}$ (the right sub-table) subgroups.

$4_C 2_L 1_R$	$3_c 2_L 1_Y$
$(\overline{10}, 1, +1)$	$(1, 1, +2)$
	$(\bar{3}, 1, +\frac{4}{3})$
	$(\bar{6}, 1, +\frac{2}{3})$
$(10, 3, 0)$	$(1, 3, -1)$
	$(3, 3, -\frac{1}{3})$
	$(6, 3, +\frac{1}{3})$
$(\overline{10}, 1, -1)$	$(\bar{6}, 1, -\frac{4}{3})$
	$(\bar{3}, 1, -\frac{2}{3})$
	$(1, 1, 0)$
$(\overline{10}, 1, 0)$	$(\bar{6}, 1, -\frac{1}{3})$
	$(\bar{3}, 1, +\frac{1}{3})$
	$(1, 1, +1)$
$(15, 2, +\frac{1}{2})$	$(1, 2, +\frac{1}{2})$
	$(3, 2, +\frac{7}{6})$
	$(8, 2, +\frac{1}{2})$
	$(\bar{3}, 2, -\frac{1}{6})$
$(15, 2, -\frac{1}{2})$	$(1, 2, -\frac{1}{2})$
	$(\bar{3}, 2, -\frac{7}{6})$
	$(8, 2, -\frac{1}{2})$
	$(3, 2, +\frac{1}{6})$
$(6, 1, 0)$	$(\bar{3}, 1, +\frac{1}{3})$
	$(3, 1, -\frac{1}{3})$

$3_c 2_L 2_R 1_{BL}$	$3_c 2_L 1_Y$
$(1, 1, 3, +2)$	$(1, 1, +2)$
	$(1, 1, +1)$
	$(1, 1, 0)$
$(1, 3, 1, -2)$	$(1, 3, -1)$
$(\bar{3}, 1, 3, +\frac{2}{3})$	$(\bar{3}, 1, +\frac{4}{3})$
	$(\bar{3}, 1, +\frac{1}{3})$
	$(\bar{3}, 1, -\frac{2}{3})$
$(3, 3, 1, -\frac{2}{3})$	$(3, 3, -\frac{1}{3})$
$(6, 3, 1, +\frac{2}{3})$	$(6, 3, +\frac{1}{3})$
$(\bar{6}, 1, 3, -\frac{2}{3})$	$(\bar{6}, 1, -\frac{4}{3})$
	$(\bar{6}, 1, -\frac{1}{3})$
	$(\bar{6}, 1, +\frac{2}{3})$
$(1, 2, 2, 0)$	$(1, 2, +\frac{1}{2})$
	$(1, 2, -\frac{1}{2})$
$(3, 2, 2, +\frac{4}{3})$	$(3, 2, +\frac{7}{6})$
	$(3, 2, +\frac{1}{6})$
$(\bar{3}, 2, 2, -\frac{4}{3})$	$(\bar{3}, 2, -\frac{7}{6})$
	$(\bar{3}, 2, -\frac{1}{6})$
$(8, 2, 2, 0)$	$(8, 2, +\frac{1}{2})$
	$(8, 2, -\frac{1}{2})$
$(\bar{3}, 1, 1, +\frac{2}{3})$	$(\bar{3}, 1, +\frac{1}{3})$
$(3, 1, 1, -\frac{2}{3})$	$(3, 1, -\frac{1}{3})$

$51'_{Z'}$	$3_c 2_L 1_Y$
$(\overline{50}, 2)$	$(6, 3, +\frac{1}{3})$
	$(\bar{3}, 1, +\frac{1}{3})$
	$(\bar{6}, 1, +\frac{2}{3})$
	$(1, 1, 0)$
	$(3, 2, +\frac{1}{6})$
	$(8, 2, +\frac{1}{2})$
$(45, -2)$	$(3, 3, -\frac{1}{3})$
	$(\bar{6}, 1 - \frac{1}{3})$
	$(\bar{3}, 1, -\frac{2}{3})$
	$(\bar{3}, 2, -\frac{1}{6})$
	$(1, 2, -\frac{1}{2})$
	$(8, 2, -\frac{1}{2})$
	$(3, 1, -\frac{1}{3})$
$(\overline{15}, -6)$	$(1, 3, -1)$
	$(\bar{6}, 1, -\frac{4}{3})$
	$(\bar{3}, 2, -\frac{7}{6})$
$(10, 6)$	$(1, 1, +1)$
	$(\bar{3}, 1, +\frac{4}{3}))$
	$(3, 2, \frac{7}{6})$
$(\bar{5}, 2)$	$(1, 2, +\frac{1}{2})$
	$(\bar{3}, 1, +\frac{1}{3})$
$(1, 10)$	$(1, 1, +2)$

Bibliography

[1] A. Abed Abud et al. Snowmass Neutrino Frontier: DUNE Physics Summary. 3 2022.

[2] Angel Abusleme et al. JUNO Sensitivity on Proton Decay $p \to \bar{\nu}K^+$ Searches. 12 2022.

[3] J. Bian et al. Hyper-Kamiokande Experiment: A Snowmass White Paper. In *Snowmass 2021*, 3 2022.

[4] M. Askins et al. Theia: Summary of physics program. Snowmass White Paper Submission. In *Snowmass 2021*, 2 2022.

[5] P. S. B. Dev et al. Searches for Baryon Number Violation in Neutrino Experiments: A White Paper. 3 2022.

[6] Helena Kolešová, Michal Malinský, and Timon Mede. Theoretical Uncertainties in Proton Lifetime Estimates. *AIP Conf. Proc.*, 1743(1):030006, 2016.

[7] Helena Kolešová and Michal Malinský. Flavor structure of GUTs and uncertainties in proton lifetime estimates. *Phys. Rev. D*, 99(3):035005, 2019.

[8] Masaki Yasue. Symmetry Breaking of SO(10) and Constraints on Higgs Potential. 1. Adjoint (45) and Spinorial (16). *Phys. Rev. D*, 24:1005, 1981.

[9] G. Anastaze, J. P. Derendinger, and F. Buccella. Intermediate symmetries in the SO(10) model with $16 \oplus \overline{16} \oplus 45$ Higgses. *Z. Phys. C*, 20:269–273, 1983.

[10] K. S. Babu and Ernest Ma. Symmetry Breaking in SO(10): Higgs Boson Structure. *Phys. Rev. D*, 31:2316, 1985.

[11] Stefano Bertolini, Luca Di Luzio, and Michal Malinsky. On the vacuum of the minimal nonsupersymmetric SO(10) unification. *Phys. Rev. D*, 81:035015, 2010.

[12] Stefano Bertolini, Luca Di Luzio, and Michal Malinsky. Seesaw Scale in the Minimal Renormalizable SO(10) Grand Unification. *Phys. Rev. D*, 85:095014, 2012.

[13] Stefano Bertolini, Luca Di Luzio, and Michal Malinsky. Light color octet scalars in the minimal SO(10) grand unification. *Phys. Rev. D*, 87(8):085020, 2013.

[14] Helena Kolešová and Michal Malinský. Proton lifetime in the minimal SO(10) GUT and its implications for the LHC. *Phys. Rev. D*, 90(11):115001, 2014.

[15] Lukáš Gráf, Michal Malinský, Timon Mede, and Vasja Susič. One-loop pseudo-Goldstone masses in the minimal $SO(10)$ Higgs model. *Phys. Rev. D*, 95(7):075007, 2017.

[16] Kateřina Jarkovská, Michal Malinský, Timon Mede, and Vasja Susič. Quantum nature of the minimal potentially realistic SO(10) Higgs model. *Phys. Rev. D*, 105(9):095003, 2022.

[17] Kateřina Jarkovská, Michal Malinský, and Vasja Susič. The trouble with the minimal renormalizable SO(10) GUT. 4 2023.

[18] John David Jackson and L. B. Okun. Historical roots of gauge invariance. *Rev. Mod. Phys.*, 73:663–680, 2001.

[19] H. Weyl. A New Extension of Relativity Theory. *Annalen Phys.*, 59:101–133, 1919.

[20] Norbert Straumann. Early history of gauge theories and weak interactions. In *Zuoz Summer School on Physics with Neutrinos*, pages 153–180, 8 1996.

[21] V. Fock. On the invariant form of the wave equation and the equations of motion for a charged point mass. (In German and English). *Z. Phys.*, 39:226–232, 1926.

[22] H. Weyl. Electron and Gravitation. 1. (In German). *Z. Phys.*, 56:330–352, 1929.

[23] Paul Adrien Maurice Dirac and Niels Henrik David Bohr. The quantum theory of the emission and absorption of radiation. *Proceedings of the Royal Society of London. Series A, Containing Papers of a Mathematical and Physical Character*, 114(767):243–265, 1927.

[24] S. Tomonaga. On a relativistically invariant formulation of the quantum theory of wave fields. *Prog. Theor. Phys.*, 1:27–42, 1946.

[25] Julian S. Schwinger. Quantum electrodynamics. I A covariant formulation. *Phys. Rev.*, 74:1439, 1948.

[26] R. P. Feynman. Space - time approach to quantum electrodynamics. *Phys. Rev.*, 76:769–789, 1949.

[27] R. P. Feynman. Mathematical formulation of the quantum theory of electromagnetic interaction. *Phys. Rev.*, 80:440–457, 1950.

[28] Tatsumi Aoyama, Masashi Hayakawa, Toichiro Kinoshita, and Makiko Nio. Tenth-Order QED Contribution to the Electron g-2 and an Improved Value of the Fine Structure Constant. *Phys. Rev. Lett.*, 109:111807, 2012.

[29] Chen-Ning Yang and Robert L. Mills. Conservation of Isotopic Spin and Isotopic Gauge Invariance. *Phys. Rev.*, 96:191–195, 1954.

[30] S. L. Glashow. Partial Symmetries of Weak Interactions. *Nucl. Phys.*, 22:579–588, 1961.

[31] Abdus Salam and John Clive Ward. Electromagnetic and weak interactions. *Phys. Lett.*, 13:168–171, 1964.

[32] Steven Weinberg. A Model of Leptons. *Phys. Rev. Lett.*, 19:1264–1266, 1967.

[33] H. Georgi and S. L. Glashow. Gauge theory of weak and electromagnetic interactions with han-nambu quarks. *Phys. Rev. D*, 7:561–563, 1973.

[34] Jeffrey Goldstone, Abdus Salam, and Steven Weinberg. Broken Symmetries. *Phys. Rev.*, 127:965–970, 1962.

[35] Philip W. Anderson. Plasmons, Gauge Invariance, and Mass. *Phys. Rev.*, 130:439–442, 1963.

[36] Peter W. Higgs. Broken symmetries, massless particles and gauge fields. *Phys. Lett.*, 12:132–133, 1964.

[37] F. Englert and R. Brout. Broken Symmetry and the Mass of Gauge Vector Mesons. *Phys. Rev. Lett.*, 13:321–323, 1964.

[38] G. S. Guralnik, C. R. Hagen, and T. W. B. Kibble. Global Conservation Laws and Massless Particles. *Phys. Rev. Lett.*, 13:585–587, 1964.

[39] R. Jackiw and K. Johnson. Dynamical Model of Spontaneously Broken Gauge Symmetries. *Phys. Rev. D*, 8:2386–2398, 1973.

[40] Steven Weinberg. Implications of Dynamical Symmetry Breaking. *Phys. Rev. D*, 13:974–996, 1976. [Addendum: Phys.Rev.D 19, 1277–1280 (1979)].

[41] Y. Fukuda et al. Measurement of the flux and zenith angle distribution of upward through going muons by Super-Kamiokande. *Phys. Rev. Lett.*, 82:2644–2648, 1999.

[42] Q. R. Ahmad et al. Direct evidence for neutrino flavor transformation from neutral current interactions in the Sudbury Neutrino Observatory. *Phys. Rev. Lett.*, 89:011301, 2002.

[43] K. Eguchi et al. First results from KamLAND: Evidence for reactor antineutrino disappearance. *Phys. Rev. Lett.*, 90:021802, 2003.

[44] Stephen L. Adler. Axial vector vertex in spinor electrodynamics. *Phys. Rev.*, 177:2426–2438, 1969.

[45] J. S. Bell and R. Jackiw. A pcac puzzle: $\pi_0 \to \gamma\gamma$ in the σ-model. *Il Nuovo Cimento A (1965-1970)*, 60:47–61, 1969.

[46] Paul Langacker. Grand Unified Theories and Proton Decay. *Phys. Rept.*, 72:185, 1981.

[47] J. A. Minahan, Pierre Ramond, and R. C. Warner. A Comment on Anomaly Cancellation in the Standard Model. *Phys. Rev. D*, 41:715, 1990.

[48] A. Abbas. Spontaneous symmetry breaking, quantization of the electric charge and the anomalies. *J. Phys. G*, 16:L163–L166, 1990.

[49] E. Golowich and P. B. Pal. Charge quantization from anomalies. *Phys. Rev. D*, 41:3537–3540, 1990.

[50] S. Rudaz. Electric charge quantization in the standard model. *Phys. Rev. D*, 41:2619–2621, 1990.

[51] Peter Minkowski. $\mu \to e\gamma$ at a Rate of One Out of 10^9 Muon Decays? *Phys. Lett. B*, 67:421–428, 1977.

[52] Tsutomu Yanagida. Horizontal gauge symmetry and masses of neutrinos. *Conf. Proc. C*, 7902131:95–99, 1979.

[53] Rabindra N. Mohapatra and Goran Senjanovic. Neutrino Mass and Spontaneous Parity Nonconservation. *Phys. Rev. Lett.*, 44:912, 1980.

[54] J. Schechter and J. W. F. Valle. Neutrino Masses in SU(2) x U(1) Theories. *Phys. Rev. D*, 22:2227, 1980.

[55] C. Q. Geng. Remarks on Charge Quantization of Fermions and Bosons. *Phys. Rev. D*, 41:1292, 1990.

[56] K. S. Babu and R. N. Mohapatra. Is There a Connection Between Quantization of Electric Charge and a Majorana Neutrino? *Phys. Rev. Lett.*, 63:938, 1989.

[57] J. Sladkowski and M. Zralek. Charge quantization in the standard model with the three generations of fermions. *Phys. Rev. D*, 45:1701–1707, 1992.

[58] Robert Foot, H. Lew, and R. R. Volkas. Electric charge quantization. *J. Phys. G*, 19:361–372, 1993. [Erratum: J.Phys.G 19, 1067 (1993)].

[59] Rabindra N. Mohapatra and Deepinder P. Sidhu. Gauge Theories of Weak Interactions with Left-Right Symmetry and the Structure of Neutral Currents. *Phys. Rev. D*, 16:2843, 1977.

[60] W. Grimus. Introduction to left-right symmetric models. In *4th Hellenic School on Elementary Particle Physics*, pages 619–632, 3 1993.

[61] Jogesh C. Pati and Abdus Salam. Lepton Number as the Fourth Color. *Phys. Rev. D*, 10:275–289, 1974. [Erratum: Phys.Rev.D 11, 703–703 (1975)].

[62] H. David Politzer. Reliable Perturbative Results for Strong Interactions? *Phys. Rev. Lett.*, 30:1346–1349, 1973.

[63] David J. Gross and Frank Wilczek. Ultraviolet Behavior of Nonabelian Gauge Theories. *Phys. Rev. Lett.*, 30:1343–1346, 1973.

[64] J. R. Alonso et al. Advanced Scintillator Detector Concept (ASDC): A Concept Paper on the Physics Potential of Water-Based Liquid Scintillator. 9 2014.

[65] Volodymyr Takhistov. Review of Nucleon Decay Searches at Super-Kamiokande. In *51st Rencontres de Moriond on EW Interactions and Unified Theories*, pages 437–444, 2016.

[66] H. Georgi and S. L. Glashow. Unity of All Elementary Particle Forces. *Phys. Rev. Lett.*, 32:438–441, 1974.

[67] G.'t Hooft. Magnetic monopoles in unified gauge theories. *Nuclear Physics B*, 79(2):276–284, 1974.

[68] Alexander M. Polyakov. Particle Spectrum in Quantum Field Theory. *JETP Lett.*, 20:194–195, 1974.

[69] V. A. Rubakov. Superheavy Magnetic Monopoles and Proton Decay. *JETP Lett.*, 33:644–646, 1981.

[70] Curtis G. Callan, Jr. Dyon-Fermion Dynamics. *Phys. Rev. D*, 26:2058–2068, 1982.

[71] V. A. Rubakov. Monopole Catalysis of Proton Decay. *Rept. Prog. Phys.*, 51:189–241, 1988.

[72] A.J. Buras, J. Ellis, M.K. Gaillard, and D.V. Nanopoulos. Aspects of the grand unification of strong, weak and electromagnetic interactions. *Nuclear Physics B*, 135(1):66–92, 1978.

[73] John Ellis and Mary K. Gaillard. Fermion masses and higgs representations in su(5). *Physics Letters B*, 88(3):315–319, 1979.

[74] George Lazarides, Q. Shafi, and C. Wetterich. Proton Lifetime and Fermion Masses in an SO(10) Model. *Nucl. Phys. B*, 181:287–300, 1981.

[75] M. Magg and C. Wetterich. Neutrino Mass Problem and Gauge Hierarchy. *Phys. Lett. B*, 94:61–64, 1980.

[76] Rabindra N. Mohapatra and Goran Senjanovic. Neutrino Masses and Mixings in Gauge Models with Spontaneous Parity Violation. *Phys. Rev. D*, 23:165, 1981.

[77] Robert Foot, H. Lew, X. G. He, and Girish C. Joshi. Seesaw Neutrino Masses Induced by a Triplet of Leptons. *Z. Phys. C*, 44:441, 1989.

[78] H. Georgi, Helen R. Quinn, and Steven Weinberg. Hierarchy of Interactions in Unified Gauge Theories. *Phys. Rev. Lett.*, 33:451–454, 1974.

[79] J. Alitti et al. An Improved determination of the ratio of W and Z masses at the CERN $\bar{p}p$ collider. *Phys. Lett. B*, 276:354–364, 1992.

[80] P. H. Frampton and S. L. Glashow. Staying Alive With SU(5). *Phys. Lett. B*, 131:340, 1983. [Erratum: Phys.Lett.B 135, 515 (1984)].

[81] Tristan Hubsch, S. Meljanac, and S. Pallua. A nonminimal SU(5) model. *Phys. Rev. D*, 31:2958, 1985.

[82] Ugo Amaldi, Wim de Boer, Paul H. Frampton, Hermann Furstenau, and James T. Liu. Consistency checks of grand unified theories. *Phys. Lett. B*, 281:374–382, 1992.

[83] N. V. Krasnikov. (Non)supersymmetric SU(5) grand unified models with light colored octets and electroweak triplets. *Phys. Lett. B*, 306:283–287, 1993.

[84] Ilja Dorsner and Pavel Fileviez Perez. Upper Bound on the Mass of the Type III Seesaw Triplet in an SU(5) Model. *JHEP*, 06:029, 2007.

[85] Ilja Dorsner. Minimal realistic SU(5) scenario. In *41st Rencontres de Moriond on Electroweak Interactions and Unified Theories*, pages 167–172, 6 2006.

[86] Bartosz Fornal and Benjamín Grinstein. Grand Unified Theory with a Stable Proton. *Int. J. Mod. Phys. A*, 33(31):1844013, 2018.

[87] Stefan Antusch and Kevin Hinze. Nucleon decay in a minimal non-SUSY GUT with predicted quark-lepton Yukawa ratios. *Nucl. Phys. B*, 976:115719, 2022.

[88] Lorenzo Calibbi and Xiyuan Gao. Lepton flavor violation in minimal grand unified type II seesaw models. *Phys. Rev. D*, 106(9):095036, 2022.

[89] Stefan Antusch, Kevin Hinze, and Shaikh Saad. Viable quark-lepton Yukawa ratios and nucleon decay predictions in SU(5) GUTs with type-II seesaw. *Nucl. Phys. B*, 986:116049, 2023.

[90] M. Fukugita, T. Yanagida, and M. Yoshimura. $N\overline{N}$ Oscillation without Left-Right Symmetry. *Phys. Lett. B*, 109:369–372, 1982.

[91] Parthasarathi Majumdar. $N\bar{N}$ Oscillations in a an SU(6) GUT: With and Without Supersymmetry. *Phys. Lett. B*, 121:25–29, 1983.

[92] A. Hartanto and L. T. Handoko. Grand unified theory based on the SU(6) symmetry. *Phys. Rev. D*, 71:095013, 2005.

[93] Harald Fritzsch and Peter Minkowski. Unified Interactions of Leptons and Hadrons. *Annals Phys.*, 93:193–266, 1975.

[94] F. Gursey, Pierre Ramond, and P. Sikivie. A Universal Gauge Theory Model Based on E6. *Phys. Lett. B*, 60:177–180, 1976.

[95] O. K. Kalashnikov and S. E. Konshtein. Hierarchy of Interactions and Mass Relations in Asymptotically Free E6 Model of Unified Interaction. *Nucl. Phys. B*, 166:507–524, 1980.

[96] Feza Gursey and Meral Serdaroglu. Basic Fermion Masses and Mixings in the $E(6)$ Model. *Lett. Nuovo Cim.*, 21:28, 1978.

[97] Yoav Achiman and Berthold Stech. Quark Lepton Symmetry and Mass Scales in an E6 Unified Gauge Model. *Phys. Lett. B*, 77:389–393, 1978.

[98] Q. Shafi. E(6) as a Unifying Gauge Symmetry. *Phys. Lett. B*, 79:301–303, 1978.

[99] H. Ruegg and Thomas Schucker. Masses for Fermions in a Unified Gauge Model Based on E6. *Nucl. Phys. B*, 161:388–396, 1979.

[100] Riccardo Barbieri and Dimitri V. Nanopoulos. An Exceptional Model for Grand Unification. *Phys. Lett. B*, 91:369–375, 1980.

[101] F. Buccella and G. Miele. SO(10) From Supersymmetric $E(6)$. *Phys. Lett. B*, 189:115–117, 1987.

[102] K. S. Babu, Borut Bajc, and Vasja Susič. A minimal supersymmetric E_6 unified theory. *JHEP*, 05:108, 2015.

[103] R. Slansky. Group Theory for Unified Model Building. *Phys. Rept.*, 79:1–128, 1981.

[104] Stefano Bertolini, Luca Di Luzio, and Michal Malinsky. Intermediate mass scales in the non-supersymmetric SO(10) grand unification: A Reappraisal. *Phys. Rev. D*, 80:015013, 2009.

[105] Sacha Ferrari, Thomas Hambye, Julian Heeck, and Michel H. G. Tytgat. SO(10) paths to dark matter. *Phys. Rev. D*, 99(5):055032, 2019.

[106] K. S. Babu and S. Khan. Minimal nonsupersymmetric $SO(10)$ model: Gauge coupling unification, proton decay, and fermion masses. *Phys. Rev. D*, 92(7):075018, 2015.

[107] K. S. Babu and R. N. Mohapatra. Predictive neutrino spectrum in minimal SO(10) grand unification. *Phys. Rev. Lett.*, 70:2845–2848, 1993.

[108] Borut Bajc, Alejandra Melfo, Goran Senjanovic, and Francesco Vissani. Yukawa sector in non-supersymmetric renormalizable SO(10). *Phys. Rev. D*, 73:055001, 2006.

[109] Anjan S. Joshipura and Ketan M. Patel. Fermion Masses in SO(10) Models. *Phys. Rev. D*, 83:095002, 2011.

[110] Guido Altarelli and Davide Meloni. A non supersymmetric SO(10) grand unified model for all the physics below M_{GUT}. *JHEP*, 08:021, 2013.

[111] Alexander Dueck and Werner Rodejohann. Fits to SO(10) Grand Unified Models. *JHEP*, 09:024, 2013.

[112] Sofiane M. Boucenna, Tommy Ohlsson, and Marcus Pernow. A minimal non-supersymmetric SO(10) model with Peccei–Quinn symmetry. *Phys. Lett. B*, 792:251–257, 2019. [Erratum: Phys.Lett.B 797, 134902 (2019)].

[113] Tommy Ohlsson and Marcus Pernow. Fits to Non-Supersymmetric SO(10) Models with Type I and II Seesaw Mechanisms Using Renormalization Group Evolution. *JHEP*, 06:085, 2019.

[114] V. Suryanarayana Mummidi and Ketan M. Patel. Leptogenesis and fermion mass fit in a renormalizable SO(10) model. *JHEP*, 12:042, 2021.

[115] Davide Meloni, Tommy Ohlsson, and Stella Riad. Effects of intermediate scales on renormalization group running of fermion observables in an SO(10) model. *JHEP*, 12:052, 2014.

[116] K. S. Babu, Borut Bajc, and Shaikh Saad. Yukawa Sector of Minimal SO(10) Unification. *JHEP*, 02:136, 2017.

[117] Davide Meloni, Tommy Ohlsson, and Stella Riad. Renormalization Group Running of Fermion Observables in an Extended Non-Supersymmetric SO(10) Model. *JHEP*, 03:045, 2017.

[118] Tommy Ohlsson and Marcus Pernow. Running of Fermion Observables in Non-Supersymmetric SO(10) Models. *JHEP*, 11:028, 2018.

[119] Takeshi Fukuyama, Nobuchika Okada, and Hieu Minh Tran. Alternative renormalizable $SO(10)$ GUTs and data fitting. *Nucl. Phys. B*, 954:114992, 2020.

[120] Stefan Antusch, Christian Hohl, and Vasja Susič. Yukawa ratio predictions in non-renormalizable SO(10) GUT models. *JHEP*, 02:086, 2020.

[121] Stephen M. Barr. A New Symmetry Breaking Pattern for SO(10) and Proton Decay. *Phys. Lett. B*, 112:219–222, 1982.

[122] J. P. Derendinger, Jihn E. Kim, and Dimitri V. Nanopoulos. Anti-SU(5). *Phys. Lett. B*, 139:170–176, 1984.

[123] N. G. Deshpande, E. Keith, and Palash B. Pal. Implications of LEP results for SO(10) grand unification with two intermediate stages. *Phys. Rev. D*, 47:2892–2896, 1993.

[124] Matěj Hudec and Michal Malinský. Hierarchy and decoupling. *J. Phys. G*, 47(1):015004, 2020.

[125] M. Fukugita and T. Yanagida. Barygenesis without grand unification. *Physics Letters B*, 174(1):45–47, 1986.

[126] Jiří Hořejší. *Fundamentals of electroweak theory*. The Karolinum Press, 2002.

[127] R. L. Workman et al. Review of Particle Physics. *PTEP*, 2022:083C01, 2022.

[128] H. Arason, D. J. Castano, E. J. Piard, and Pierre Ramond. Mass and mixing angle patterns in the standard model and its minimal supersymmetric extension. *Phys. Rev. D*, 47:232–240, 1993.

[129] Henry Primakoff and Peter S. Rosen. Baryon number and lepton number conservation laws. *Ann. Rev. Nucl. Part. Sci.*, 31:145–192, 1981.

[130] Frank Wilczek and A. Zee. Operator Analysis of Nucleon Decay. *Phys. Rev. Lett.*, 43:1571–1573, 1979.

[131] Steven Weinberg. Varieties of Baryon and Lepton Nonconservation. *Phys. Rev. D*, 22:1694, 1980.

[132] W. Buchmuller and D. Wyler. Effective Lagrangian Analysis of New Interactions and Flavor Conservation. *Nucl. Phys. B*, 268:621–653, 1986.

[133] B. Grzadkowski, M. Iskrzynski, M. Misiak, and J. Rosiek. Dimension-Six Terms in the Standard Model Lagrangian. *JHEP*, 10:085, 2010.

[134] K. Kobayashi et al. Search for nucleon decay via modes favored by supersymmetric grand unification models in Super-Kamiokande-I. *Phys. Rev. D*, 72:052007, 2005.

[135] K. Abe et al. Search for Nucleon Decay via $n \to \bar{\nu}\pi^0$ and $p \to \bar{\nu}\pi^+$ in Super-Kamiokande. *Phys. Rev. Lett.*, 113(12):121802, 2014.

[136] S. Mine. Recent nucleon decay results from Super Kamiokande. *J. Phys. Conf. Ser.*, 718(6):062044, 2016.

[137] K. Abe et al. Search for nucleon decay into charged antilepton plus meson in 0.316 megaton·years exposure of the Super-Kamiokande water Cherenkov detector. *Phys. Rev. D*, 96(1):012003, 2017.

[138] A. Takenaka et al. Search for proton decay via $p \to e^+\pi^0$ and $p \to \mu^+\pi^0$ with an enlarged fiducial volume in Super-Kamiokande I-IV. *Phys. Rev. D*, 102(11):112011, 2020.

[139] R. Matsumoto et al. Search for proton decay via $p \to \mu^+K^0$ in 0.37 megaton-years exposure of Super-Kamiokande. *Phys. Rev. D*, 106(7):072003, 2022.

[140] Pavel Fileviez Perez. Fermion mixings versus d = 6 proton decay. *Phys. Lett. B*, 595:476–483, 2004.

[141] Pran Nath and Pavel Fileviez Perez. Proton stability in grand unified theories, in strings and in branes. *Phys. Rept.*, 441:191–317, 2007.

[142] Helena Kolešová and Michal Malinský. Minimal SO(10) grand unification at next-to-leading order. In *37th International Conference on High Energy Physics*, 10 2014.

[143] Ben Gripaios and Dave Sutherland. An operator basis for the Standard Model with an added scalar singlet. *JHEP*, 08:103, 2016.

[144] Jun-Sik Yoo, Yasumichi Aoki, Peter Boyle, Taku Izubuchi, Amarjit Soni, and Sergey Syritsyn. Proton decay matrix elements on the lattice at physical pion mass. *Phys. Rev. D*, 105(7):074501, 2022.

[145] Yasuo Hara, Satoshi Itoh, Yoichi Iwasaki, and Tomoteru Yoshie. Proton Decay and Lattice QCD. *Phys. Rev. D*, 34:3399, 1986.

[146] Y. Aoki, E. Shintani, and A. Soni. Proton decay matrix elements on the lattice. *Phys. Rev. D*, 89(1):014505, 2014.

[147] John E. Prussing. The principal minor test for semidefinite matrices. *Journal of Guidance, Control, and Dynamics*, 9(1):121–122, 1986.

[148] Sidney R. Coleman and Erick J. Weinberg. Radiative Corrections as the Origin of Spontaneous Symmetry Breaking. *Phys. Rev. D*, 7:1888–1910, 1973.

[149] William J. Marciano. Quantitative tests of the standard model of electroweak interactions. *Ann. Rev. Nucl. Part. Sci.*, 41:469–509, 1991.

[150] Johann H. Kuhn and M. Steinhauser. A Theory driven analysis of the effective QED coupling at M(Z). *Phys. Lett. B*, 437:425–431, 1998.

[151] W. Martens, L. Mihaila, J. Salomon, and M. Steinhauser. Minimal Supersymmetric SU(5) and Gauge Coupling Unification at Three Loops. *Phys. Rev. D*, 82:095013, 2010.

[152] Christian Sturm. Leptonic contributions to the effective electromagnetic coupling at four-loop order in QED. *Nucl. Phys. B*, 874:698–719, 2013.

[153] P. A. Zyla et al. Review of Particle Physics. *PTEP*, 2020(8):083C01, 2020.

[154] Manolis Georgioudakis and Vagelis Plevris. A comparative study of differential evolution variants in constrained structural optimization. *Frontiers in Built Environment*, 6, 2020.

[155] N. G. Deshpande, E. Keith, and Palash B. Pal. Implications of LEP results for SO(10) grand unification. *Phys. Rev. D*, 46:2261–2264, 1993.

[156] F. del Aguila and Luis E. Ibanez. Higgs Bosons in SO(10) and Partial Unification. *Nucl. Phys. B*, 177:60–86, 1981.

[157] Rabindra N. Mohapatra and Goran Senjanovic. Higgs Boson Effects in Grand Unified Theories. *Phys. Rev. D*, 27:1601, 1983.

[158] Sacha Davidson and Alejandro Ibarra. A Lower bound on the right-handed neutrino mass from leptogenesis. *Phys. Lett. B*, 535:25–32, 2002.

[159] K. Jarkovská. *Pseudo-Goldstone bosons in grand unified theories.* Master thesis, Charles University, http://hdl.handle.net/20.500.11956/99155, 2018.

[160] P. A. Zyla et al. Review of Particle Physics. *PTEP*, 2020(8):083C01, 2020.

[161] Steven Weinberg. Effective Gauge Theories. *Phys. Lett. B*, 91:51–55, 1980.

[162] Lawrence J. Hall. Grand Unification of Effective Gauge Theories. *Nucl. Phys. B*, 178:75–124, 1981.

[163] Sebastian A. R. Ellis and James D. Wells. Visualizing gauge unification with high-scale thresholds. *Phys. Rev. D*, 91(7):075016, 2015.

[164] M.E. Peskin and D.V. Schroeder. *An Introduction To Quantum Field Theory.* Frontiers in Physics. Avalon Publishing, 1995.

[165] L. F. Abbott and Mark B. Wise. The Effective Hamiltonian for Nucleon Decay. *Phys. Rev. D*, 22:2208, 1980.

[166] Ilja Dorsner, Svjetlana Fajfer, Jernej F. Kamenik, and Nejc Kosnik. Light colored scalars from grand unification and the forward-backward asymmetry in t t-bar production. *Phys. Rev. D*, 81:055009, 2010.

[167] Michal Malinsky. Fun with the Abelian Higgs Model. *Eur. Phys. J. C*, 73:2415, 2013.

[168] Thomas Appelquist and J. Carazzone. Infrared Singularities and Massive Fields. *Phys. Rev. D*, 11:2856, 1975.

[169] H. Georgi. *Lie algebras in Particle Physics: from Isospin To Unified Theories*, volume 54. 1982.

[170] John C. Baez and John Huerta. The Algebra of Grand Unified Theories. *Bull. Am. Math. Soc.*, 47:483–552, 2010.

[171] Katerina Jarkovska. New advances in the minimal potentially realistic $SO(10)$. *PoS*, EPS-HEP2021:652, 2022.

[172] Katerina Jarkovska. Proton decay in the minimal realistic $SO(10)$ GUT. *PoS*, ICHEP2020:667, 2021.

List of publications

Regular articles:

[17] Kateřina Jarkovská, Michal Malinský, and Vasja Susič. The trouble with the minimal renormalizable SO(10) GUT. Submitted to *Phys. Rev. D* in May 2023.

[16] Kateřina Jarkovská, Michal Malinský, Timon Mede, and Vasja Susič. Quantum nature of the minimal potentially realistic SO(10) Higgs model. *Phys. Rev. D*, 105(9):095003, 2022.

Conference proceedings:

[171] Kateřina Jarkovská. New advances in the minimal potentially realistic SO(10). *PoS*, EPS-HEP2021:652, 2022.

[172] Kateřina Jarkovská. Proton decay in the minimal realistic SO(10) GUT. *PoS*, ICHEP2020:667, 2021.

The results presented in this thesis are based on studies [16, 17], which we also include in the attachments.

G. Attachments

G.1 Quantum nature of the minimal potentially realistic SO(10) Higgs model

Authors: Kateřina Jarkovská, Michal Malinský, Timon Mede, and Vasja Susič

Published in: Phys. Rev. D 105 (2022) 9, 095003

e-Print: https://arxiv.org/abs/2109.06784

Published version:
https://link.aps.org/doi/10.1103/PhysRevD.105.095003

The author of the thesis was one of the main authors of this paper and she contributed to the vast majority of the calculations and writing of the text. In particular:

- She worked on the one-loop mass calculations for the scalar spectrum (except technical details from Appendix A 1 and A 2), including devising the notion of the regularized one-loop masses and its connection to the physical mass based on the Abelian Higgs model case-study she carried out.
- She derived the full set of one-loop beta functions for all dimensionless scalar couplings of the minimal SO(10) Higgs model.
- She studied semi-analytical aspects of non-tachyonicity and performed the numerical parameter space scans at the one-loop level (except writing the core of the differential evolution algorithm used in parameter-space scanning) in the minimal SO(10) Higgs model, including proper implementation of the penalization function. She contributed to the discussion of all the results.

G.2 The trouble with the minimal renormalizable SO(10) GUT

Authors: Kateřina Jarkovská, Michal Malinský, and Vasja Susič

Submitted to : Phys. Rev. D, May 2023

e-Print: `https://arxiv.org/abs/2304.14227`

The author of the thesis was one of the main authors of this paper and she contributed to the vast majority of the calculations and writing of the text. In particular:

- She derived the full set of the one-loop beta functions for all dimensionless scalar couplings of the minimal SO(10) GUT.
- She analytically studied doublet fine-tuning at the tree-level.
- She performed the numerical parameter space scans at the one-loop level (except writing the core of the differential evolution algorithm used in parameter-space scanning) in the minimal SO(10) GUT, including proper implementation of the penalization function. She contributed to the discussion of all the results.